Aus dem Bereich Molekulare Zellbiologie

Theoretische Medizin und Biowissenschaften

Der Medizinischen Fakultät

Der Universität des Saarlandes, Homburg/Saar

Structural and Functional Characterisation of TRP channels

Dissertation zur Erlangung des Grades eines

Doktors der Naturwissenschaften

Der Medizinischen Fakultät

Der Universität des Saarlandes

2018

vorgelegt von: Wenying Xian

geb. am: 02.01.1988 in Chongqing, China

To my dear and loving parents

致我亲爱的父母！

Zusammenfassung

Die Familie der TRP-Rezeptorkanäle (TRP= ''transient receptor potential") umfasst in Säugergewebe 28 Mitglieder, welche in 6 Subfamilien untergliedert sind: TRPC, TRPM, TRPV, TRPA, TRPP und TRPML. TRP-Kanäle spielen in verschiedenen physiologischen, sowie pathologischen Prozessen eine wichtige Rolle. In dieser Arbeit lag der Fokus zum einen auf dem TRPM4-Kanal, welcher zu der TRPM Subfamilie gehört und zum anderen auf den TRPC1- und TRPC4- Kanäle, welche der TRPC Familie zugeordnet werden können.

TRPM4 ist ein Kalzium-aktivierter, nichtselektiver Kationen-Kanal. Jüngste Studien legen nahe, dass TRPM4 als potentielles therapeutisches Ziel für eine Reihe erblich bedingter Herzrhythmusstörungen dienen kann. Mutationen im *TRM4*-Gen sind mit atrioventrikulärem (AV) Block im Kindesalter, familiärer progressiver kardialer Reizleitungsstörungen (Typ I) sowie dem Brugada-Syndrom assoziiert. Allerdings sind bis heute nur wenige dieser Mutationen gut untersucht und der zugrundeliegende Pathomechanismus ist nach wie vor unklar. Im ersten Teil dieser Arbeit wurden zum einen UV-Blitzlicht-Photolyse von „*caged*" Kalzium und quantitatives Kalzium-, sowie elektrophysiologische Messungen durchgeführt, um die Eigenschaften von TRPM4-Kanälen detailliert zu analysieren. Die Ergebnisse zeigen, dass die TRPM4^{A432T} Mutation, welche mit einer erblichen Herzrhythmusstörung assoziiert ist, mit einer zweifach höheren Stromdichte und einer vierfach verlangsamten Kalzium-abhängige Deaktivierung einhergeht. Diese Veränderungen scheinen für die pathologische Aktionspotenzialform verantwortlich zu sein. In dieser Arbeit konnte ich im Zusammenspiel von Experiment und molekularer Modellierung erstmalig aufzeigen, dass die Größe der Aminosäure an Position 432 eine substanzielle Determinante für das Deaktivierungsverhalten des TRPM4 Kanals ist. Weiterhin habe ich mit Hilfe der UV-Blitzlicht Analyse systematisch 9 weitere humane TRPM4-Mutationen untersucht. Dabei konnte gezeigt werden, dass 5 Mutationen veränderte TRPM4-Eigenschaften auswiesen (Kalzium-Empfindlichkeit, Aktivierung und Deaktivierung, veränderte Membranströme). 4 TRPM4-Mutationen hatten keinen Einfluss auf die von mir untersuchten TRPM4-Eigenschaften.

TRPC-Kanäle besitzen die Fähigkeit, Homo-, oder Heterotetramere-Kanalstrukturen zu bilden. Das TRPC4/TRPC1-Heterotetramer wurde bereits ausführlich beschrieben und weist im Vergleich zu TRPC1 oder TRPC4 Homomeren sehr unterschiedliche biophysikalische Eigenschaften auf. Durch die Mangan-Quench und Patch-Clamp Methoden konnten im zweiten Teil der Arbeit gezeigt werden, dass das TRPC1-Homotetramer keine Rezeptor-aktivierten Kanäle bilden. Im Gegensatz dazu kann TRPC1 mit TRPC4 interagieren und bildet dann einen heteromeren Kanal (TRPC4/TRPC1-Kanal). Dieser zeigte allerdings im Gegensatz zum TRPC1 Homomer einen verringerten Kalzium-Einstrom. Um die molekularen Hintergründe für dieses charakteristische Merkmal von TRPC4/TRPC1 weiter zu untersuchen, wurden chimäre Kanalproteine, $TRPC1C4_{Pore}$ und der $TRPC4C1_{Pore}$ erzeugt. Dieser Ansatz wurde gewählt um zu zeigen, dass die Porenregion von TRPC1 entscheidend für die physikalischen Eigenschaften des TRPC4/TRPC1-Heteromerkanals ist (z.B. Stromstärke, Kalzium-Permeation). Zudem konnte ich in dieser Arbeit darlegen, dass die G-S-Mutation im S4-S5-Linker von TRPC1 den Kalzium-Einstrom des TRPC4/TRPC1-Kanal-Komplexes erhöhen kann.

Zusammenfassend liefern die in dieser Arbeit gewonnenen Ergebnisse nicht nur neue Einblicke in den Pathomechanismus von mutierten TRPM4-Kanals bei erblich bedingter Herzleitungsblockade, sondern deckten neue Ätiologien für humane Herzrhythmusstörungen auf. Diese neuen Ätiologien stellen potenzielle Zielmechanismen für neuartige Medikamente zur Behandlung dieser erblichen Herzrhythmusstörungen dar. Die hier von mir vorgestellten neuen Ergebnisse zum TRPC4/TRPC1 Kanal tragen zum Verständnis der Porenregion sowie des S4-S5-Linkers von TRPC1 im TRPC4/TRPC1-Heteromer bei.

Abstract

The transient receptor potential (TRP) family includes 28 mammalian members, which have been categorized into six subfamilies: TRPC, TRPM, TRPV, TRPA, TRPP and TRPML. TRP channels play an important role in various physiological and pathological process. In this study, I focused on the TRPM4 channel a membrane of the TRPM subfamily and TRPC1 and TRPC4 channels from the TRPC subfamily.

The TRPM4 channel is a Ca^{2+} activated, non-selective cation channel. Recently, studies suggested that TRPM4 could be a potential target for inherited human cardiac conduction blocks. Childhood atrioventricular block, isolated cardiac conduction disease and progressive familial heart block type I as well as the Brugada syndrome are associated with mutations in *TRPM4* gene. However, only a few of these mutations have been well studied and the underlying pathological mechanism is still not understood. In the first part of my thesis, I used UV-flash photolysis of caged Ca^{2+}, quantitative Ca^{2+} and electrophysiological measurements to investigate the properties of such TRPM4 channels. My results showed that the TRPM4^{A432T} mutation, associated with isolated cardiac conduction disease, caused a two-fold increased current density and a four-fold slower deactivation which are most likely responsible for the increased membrane currents during human cardiac action potentials. Furthermore, I found that it is the bulkiness of the amino acid at position 432 that rendered TRPM4's aberrant gating. Moreover, using the UV-flash approach, I systematically studied nine additional identified human TRPM4 mutations and revealed that five of them altered TRPM4's properties including Ca^{2+} sensitivity, activation and deactivation gating as well as the maximal membrane current density, while four of them exhibited no apparent influence on TRPM4's properties.

TRPC channels are known to form tetrameric structures, such as homotetramers or heterotetramers. The TRPC4/TRPC1 heterotetramer has been widely reported and displays totally different biophysical properties when compared to TRPC1 or TRPC4 homotetramers. In the second part of my thesis, using the Mn^{2+} quench and patch-clamp, I found that TRPC1 homotetramers failed to form receptor-activated channels, while TRPC1 could interact with TRPC4 to form a heteromeric channel TRPC4/TRPC1, that displayed less Ca^{2+} influx in comparison to TRPC4 homotetramers. To further

investigate the molecular determinants for these distinctive characteristics of TRPC4/TRPC1, I used the chimeras TRPC1C4$_{Pore}$ and TRPC4C1$_{Pore}$ demonstrating that the pore region of TRPC1 is crucial for preserving the TRPC4/TRPC1 heteromeric channel's physical properties such as its current amplitude, I-V relationship and Ca^{2+} permeation. Moreover, I found that the G-S mutation in the S4-S5 linker of TRPC1 could increase the Ca^{2+} permeation of the TRPC4/TRPC1 channel complex.

In summary, these results from TRPM4 channels not only provide new insights into the pathological mechanisms of TRPM4 mutants in hereditary cardiac conduction blocks, but also reveal new etiologies for human cardiac arrhythmia. These new etiologies could be potential targets for novel drugs to treat these hereditary cardiac arrhythmias. These new results from the TRPC4/TRPC1 channels presented here make a contribution to understand roles of the pore region and the S4-S5 linker of TRPC1 in the TRPC4/TRPC1 heterotetramer.

List of Figures

List of Tables

List of Abbreviations

TRP	Transient receptor potential
TRPC	Transient receptor potential Canonical subfamily
TRPM	Transient receptor potential Melastatin subfamily
TRPV	Transient receptor potential Vanilloid subfamily
TRPP	Transient receptor potential Polycastin subfamily
TRPA	Transient receptor potential Ankyrin subfamily
TRPML	Transient receptor potential Mucolipin subfamily
ER	Endoplasmic reticulum
TRPM4	Transient receptor potential Melastatin subfamily member 4
MHRs	TRPM high homology region
ATP	Adenosine triphosphate
PKA	Protein kinase A
PKC	Protein kinase C
PIP_2	Phosphatidylinositol 4,5-bisphosphate
HG	Highly-glycosylation
CG	Core-glycosylation
PLC	Phospholipase C
PH	Pleckstrin homology
Sur1	Sulfonylurea receptor1
DD	Diastolic depolarizations
NSC_{Ca}	Ca^{2+}-activated nonselective cation channel
SAN	Sino-atrial node
CCS	Cardiac conduction system
SCN5A	Sodium voltage-gated channel alpha subunit 5
SCN1B	Sodium voltage-gated channel beta subunit 1
KCNK17	Potassium two pore domain channel subfamily K member 17
PFHBI	Progressive familial heart block type I
ICCD	Isolated cardiac conduction disease
BrS	Brugada syndrome
TRPC1	Transient receptor potential canonical subfamily member 1

TRPC4	Transient receptor potential canonical subfamily member 4
STIM1	Stromal interacting molecule 1
SOCE	Store operated calcium entry
CRAC	Calcium release activated calcium entry
IP$_3$	Inositol 1,4,5- triphosphate
CaCC	Calcium-activated chloride channel
DAG	Diacylglycerol
PHA	Pulmonary arterial hypertension
NP-EGTA	o-Nitrophenyl ethylene glycol tetra acetic acid
HEK293	Human Embryonic Kidney 293 cells
hiPS-CM	Human induced pluripotent stem cell derived cardiac myocytes
Fura-2 AM	Fura-2-acetoxymethyl ester
EDTA	Ethylenediaminetetraacetic acid
EGTA	Ethylene glycol tetraacetic acid
ECG	Electrocardiogram
NFAT	Nuclear factor of activated T-cells
SESTD	SEC14-like and spectrin-type domains
M$_2$R	Muscarinic acetylcholine receptor M2
PHA	Pulmonary arterial hypertension
GABA	Gamma-aminobutyric acid
cPKC	Conventional protein kinase C
DMSO	Dimethylglycerol
SR	Sarcoplasmic reticulum
RBBB	Right-bundle block
LAHB	Left anterior hemiblock
AVB	Atrioventricular block
Carb	Carbachol
wt	Wild type
FRET	Forster resonance energy transfer

Contents

xii

1 Introduction

1.1 General information on TRP channels

The transient receptor potential (*TRP*) gene was first cloned from the *Drosophila* fly in 1989, the form " transient receptor potential" results from the observation of a mutant in this gene showing a transient light response to continuous light[1]. Since then, more and more TRP channels have been identified and extensively investigated to determine the properties and functions of these channels in physiological and pathological processes. To date, 28 mammalian TRP channels have been identified and categorized into six subfamilies based on their amino acid sequence homology and functional relationship: TRPC(canonical), TRPM(melastatin), TRPV(vanilloid), TRPA(ankyrin), TRPP(polycastin) and TRPML(mucolipin)[2].
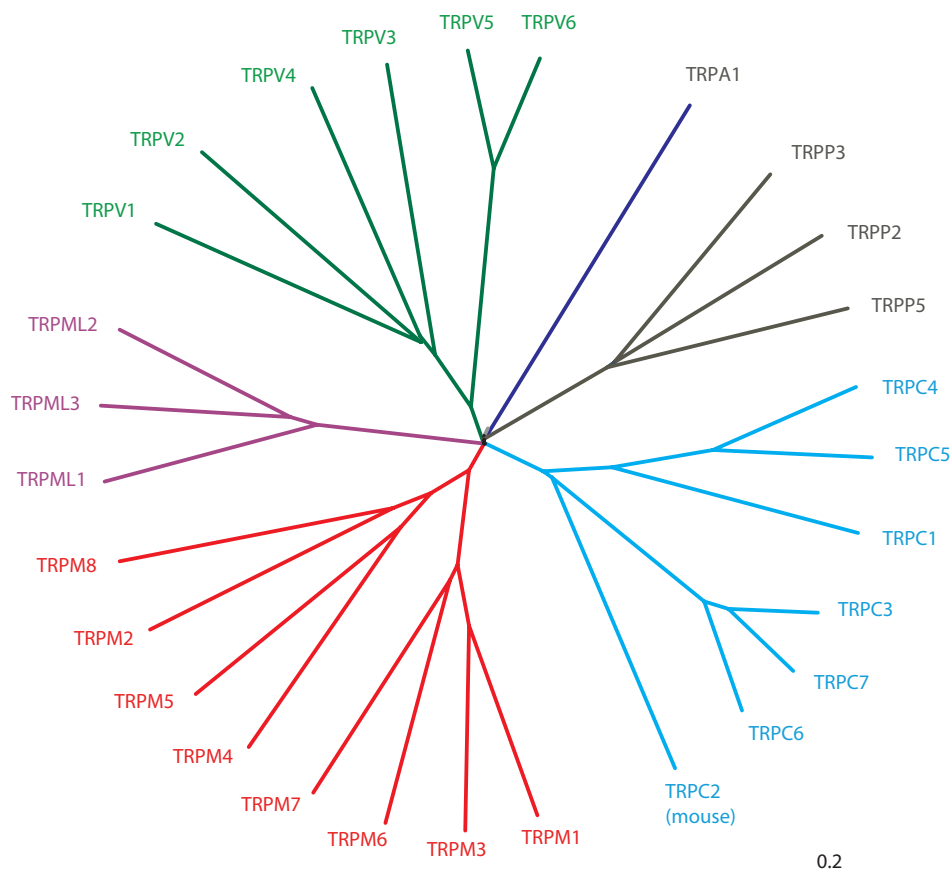
Figure 1.1 The phylogenetic tree of the TRP family.

Different colors represent different TRP subfamilies[3].

As illustrated in Figure 1.2, TRP channels comprise six putative transmembrane spanning domains (S1-S6) and the cytosolic amino (N-) and carboxyl (C-) terminus.

Similar to other ion channels with six transmembrane domains such as voltage-gated potassium channels, four subunits are required to form the basic tetrameric architecture of TRP channels. The cation-permeable pore region is a short hydrophobic stretch located between S5 and S6. The length and characteristic of the intracellular N- and C-terminus varies in the different TRP subfamilies. These cytoplasmic regions take part in the regulation and modulation of TRP channel's functions[4]. Some common structural features are shared between different TRP subfamilies. Channels from the TRPV, TRPA and TRPC subfamilies contain variable numbers of Ankyrin repeats, which may play a role in protein-protein interactions and serve as ligand binding sites[5]. In their C-terminus, TRPV, TRPM and TRPC channels share a conserved region-the TRP box, which is believed to be involved in channel gating[6-8]. A few unique motifs are also included in these TRP proteins, such as a coiled-coil domain, an endoplasmic reticulum (ER) retention domain[9], a calmodulin binding site[10] and a kinase domain[11].
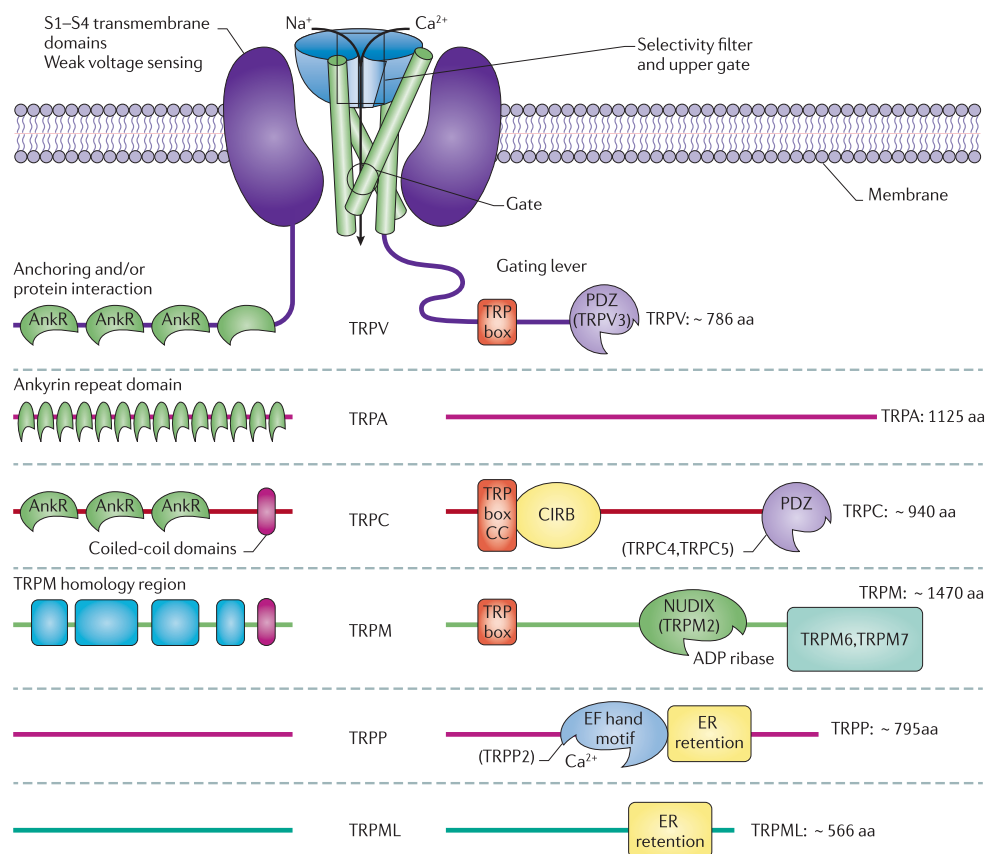
Figure 1.2 Structure of different human TRP subfamilies.

CIRB: calmodulin/inositol-1, 4, 5-trisphosphate (IP3) receptor binding domain; NUDIX: nucleoside diphosphate-linked moiety X; PDZ: acronym for postsynaptic density protein 95 (PSD95), Drosophila disc large tumor suppressor (DLGA) and zonula occludens protein1 (ZO1)[9].

TRP channels are ubiquitously expressed in diverse tissues and different cell types, where they modulate physiological and pathological functions[3]. TRP channels are regarded as the vanguard of sensory systems detecting chemical and physical stimulis on both intracellular and extracellular sides[12]. The TRPM5 channel is involved in sweet and bitter taste transduction but not in sour or salty taste[13,14]. Moreover, some TRP channels underlie the perception of pain and temperature, which have drawn great attentions as potential drug targets[15,16]. Apart from sensory perception, TRP channels were also demonstrated to participate in many other processes, including inflammation[17,18], cardiovascular regulation[19-21], regulation of myogenic tone[22], lysosomal function[23], neurotransmitter release[24], cell adhesion, control of growth and differentiation of cells and cell death[25-27].

1.2 The TRPM4 channel

The melastatin-related transient receptor potential (TRPM) subfamily is named according to its first member melastatin 1 (TRPM1), which has been linked to melanoma metastasis[28]. There are eight members in the TRPM channel subfamily (TRPM1-8), which have been categorized into four subsets based on their similarities in amino acid sequences and unique features: TRPM1/TRPM3, TRPM6/TRPM7, TRPM4/TRPM5, TRPM2/TRPM8[29,30]. The evolutionary relationships of TRPM proteins are depicted in Figure 1.3[31].
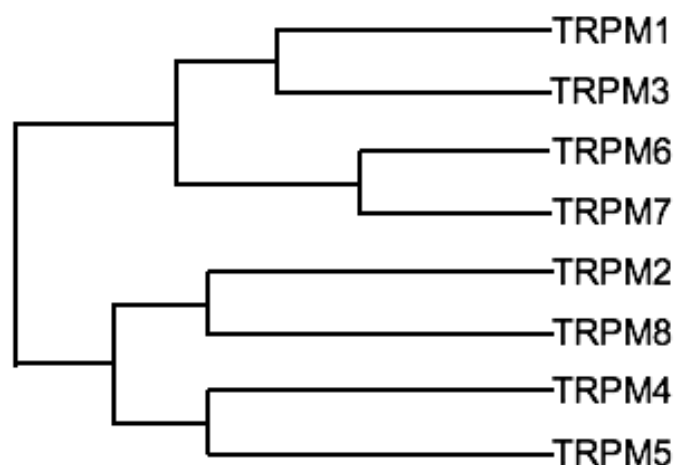
Figure 1.3 Phylogenetic tree of the TRPM subfamily.

Unlike the TRPC, TRPA and TRPV channels, TRPM channels contain a considerably longer N-terminus and lack ankyrin repeats[32]. Instead, based on sequence similarity, they share four TRPM high homology regions (MHR1-4)[12]. More and more attention has been focused on the TRPM subfamily over the past decades and increasing evidences support the notion that TRPMs play an important role in performing a multitude of physiological functions and are involved in numerous pathophysiological process as well[31,33-35]. Among the TRPMs, TRPM4 and TRPM5 are closely related with an approximately 50% homologous sequence and exhibit salient features with the unique properties of being Ca^{2+}-activated and permeable to monovalent cations but impermeable to Ca^{2+}[36].

1.2.1 TRPM4 gene cloning, expression and protein structure

The *TRPM4* gene locates in chromosome 19q13.33 of the human genome and encodes a non-selective cation channel-transient receptor potential melastatin 4 (TRPM4)[37]. In

humans there are two splice variants of the *TRPM4* gene, the full-length protein is referred to as TRPM4b, and the short variant is known as TRPM4a with 174 amino acids lacking at the N-terminus[31]. The majority of functional characterizations of the TRPM4 protein has been performed with the full-length clone (TRPM4b)[38].

Like other TRP channels, the TRPM4 protein contains six transmembrane segments (S1-S6) with a pore region between S5 and S6 as well as the cytoplasmic N- and C-termini. Four subunits are required to form a functional channel[39]. In the cytoplasmic N- and C-terminus, the TRPM4 channel contains several binding domains, which could modulate the channel's function. Five putative calmodulin binding sites are identified at both N- and C- termini while only three of them located at the C-terminus were shown to impair current activation by altering the Ca^{2+} sensitivity and voltage dependence[40]. The ATP-binding cassette (ABC) transporter-like signature motifs and Waller B motifs are predicted in the TRPM4 protein and mutations within these sites caused a fast and complete decay of TRPM4 current by affecting ATP binding[40]. Phosphorylation sites for protein kinase A (PKA) and protein kinase C (PKC)[40] and a phosphatidylinositol 4,5-bisphosphate (PIP_2) binding site with homology to a pleckstrin homology domain (PH)[41] are identified in the TRPM4 protein, as well as a coiled-coil domain at the C-terminus[38].

1.2.2 Regulation of TRPM4 channels

1.2.2.1 N-glycosylation of TRPM4

Glycosylation is an important post-translational modification, which participates in the process of correct protein folding, functional channel complex forming, and proteins' surface translocation[42-44]. In vitro studies showed that N-glycosylation is a principal form of post-translational modification for the TRPM4 protein and a N-glycosylation consensus sequence has been identified[45]. A mutation Asn988Gln of the TRPM4 protein located in the pore-forming loop between S5 and S6, prevents channel's glycosylation[45]. Two forms of N-glycosylation are detected in TRPM4, the complex, highly-glycosylation (HG) and the high mannose, core-glycosylation (CG)[46]. The HG plays an important role in stabilizing the expression of TRPM4 protein on the surface membrane[46].

1.2.2.2 Phosphorylation of TRPM4

Phosphorylation of proteins on serine, threonine and tyrosine residues is a major mechanism to regulate their activity[47]. The human TRPM4 contains numerous tyrosine, serine and threonine residues[48]. The predicated PKC phosphorylation sites of TRPM4 are Ser^{1145} and Ser^{1152} at the C-terminus and Thr^{68} and Thr^{356} at the N terminus[40]. PKC-dependent phosphorylation at Ser^{1145} and Ser^{1152} has been shown to increase the Ca^{2+} sensitivity of TRPM4 channels[40]. In vascular smooth muscle, PKCδ activation increased the transportation of TRPM4 to the plasma membrane, causing membrane depolarization and vasoconstrictions[49]. A casein kinase 1 (CK1) phosphorylation site was identified at Ser^{839} which is responsible for the basolateral localization of TRPM4[48]. In pancreatic islets, PKC-dependent TRPM4 and TRPM5 activation is reported to play a role in insulin secretion stimulated by glucagon-like peptide1 (GLP-1)[50].

1.2.2.3 Regulation of TRPM4 by Phosphatidylinositol 4,5-biphophate

Phosphatidylinositol 4,5-biphophate (PIP_2), a minor phospholipid component of the cell membrane, serves as a substrate for phospholipase C (PLC) to generate the second messengers inositol 1,4,5-trisphosphate (IP_3) and diacylglycerol (DAG). PIP_2 was firstly reported to rescue TRPM4 channels from desensitization in 2005 by Zhang *et al.*[51]. Bernd and coworkers' results showed a comparable observation[41]. They reported that PIP_2 counteracted Ca^{2+} desensitization of the TRPM4 channel in inside-out patches and also overcame the rundown of TRPM4 currents in whole-cell patch-clamp. They further demonstrated that the pleckstrin homology (PH) domain at the C-terminal of TRPM4 was the putative PIP_2 binding site[41]. By biophysical and molecular modeling methods, two specific positions R755 and R767 at the N-terminus of TRPM4 are putative binding sites for PIP_2 and its structural analogue PIP_3[52]. Mutations within these two positions caused a loss of PIP_2/PIP_3 binding specificity[52].

1.2.2.4 Interaction of TRPM4 with other proteins

Hetero-association between TRPM4 and TRPC3 was confirmed by immunoprecipitation and confocal microscopic analysis. Overexpression of TRPM4 negatively regulated the activity of the TRPC3 channel and inhibited the store-operated Ca^{2+} entry through

TRPC3[53]. In COSm6 cells expressing both TRPM4 and the Sulfonylurea receptor1 (Sur1), Rabanal and coworkers did not observe any functional or structural association between TRPM4 and Sur1 by electrophysiological and FRET studies[54]. However, in a later study, Sur1 and TRPM4 were reported to form the unique Sur1-TRPM4 channels when overexpressed in COS-7 and HEK293 cells[55]. The interaction between Sur1 and TRPM4 changed the biophysical properties of TRPM4, including the affinity for calmodulin, and sensitivity to intracellular Ca^{2+}[55].

1.2.3 The role of the TRPM4 channel in the cardiovascular system

TRPM4 mRNA can be identified in a large variety of tissues from human, mouse and rat. The physiological roles of TRPM4 in the cardiovascular system have been widely discussed[37,56-58]. Several studies have investigated TRPM4 mRNA and protein expression in tissues[37,56,59,60], indicating a higher expression of TRPM4 mRNA and protein in the cardiac conductive system, such as the sinoatrial node of the mouse and the bundle branch in bovine[61,62]. Quantitative RT-PCR was used to quantify the relative expression of TRPM4 transcripts in the human heart and found that TRPM4 was prominently expressed in Purkinje fibers, when compared to the septum, the atrium, and the right and left ventricles[59].

Sinoatrial node (SAN) is the pacemaker of the heart and responsible for generation and modulation of the cardiac automaticity[63]. A sinus rhythm is necessary for the normal activity of the heart. It arises from the SAN pacemaker cells. These cells have a specific expression pattern of ion channels and transporters, which generate spontaneous diastolic depolarizations (DD) for activation of T-type and L-type Ca^{2+} channels. Two components, the hyperpolarization-activated cyclic nucleotide-gated ion channel (HCN)[64] and Ca^{2+}-activated inward current[65], may participate to mediate the DD. The main component of the Ca^{2+}-activated current is mediated by the Na^+/Ca^{2+} exchanger, and an additional component is attributed to TRPM4, which was identified in isolated mouse SNA cells by Marie and coworkers[62]. They found a Ca^{2+}-activated nonselective cation channel (NSC_{Ca}), which was activated by the increasing intracellular Ca^{2+} concentration and displayed an equal permeability for Na^+ and K^+, but did not conduct Ca^{2+}. The channel was voltage dependent with a conductance of 20.9±0.5 pS, which could be reversibly inhibited by Flufenamic acid and Glibenclamide, showing

hallmarks of the TRPM4 current. They confirmed the expression of TRPM4 in SAN cells by Western blot and RT-PCR[62]. Hof and coworkers further demonstrated the importance of TRPM4 for action potential generation in the SAN in a TRPM4 deficient ($Trpm4^{-/-}$) mouse model[66]. The TRPM4 inhibitor 9-phenanthrol was used to unmask potential contributions of the TRPM4 channel to action potentials[66]. Application of 9-phenanthrol decreased spontaneous activity in wild-type SNA, but had no effect on the SAN activity in TRPM4 deficient ($Trpm4^{-/-}$) mice[66]. A similar 9-phenanthrol dependent reduction was also observed in the rat SAN. Moreover, in rabbit sinus node cells, by treatment with 9-phenanthrol, a significant reduction in the slope of diastolic depolarization was detected[66]. The authors provided strong evidences for the contribution of TRPM4 in maintaining SAN automaticity and heart beating.

TRPM4 channels are reported to modulate the atrial action potentials as well. Guinamard and colleagues characterized the property of a Ca^{2+}-activated non-selective cation channel (NSC_{Ca}) in freshly dissociated human atrial cardiomyocytes by excised inside-out patches[60]. The channel's open probability increased following a rise of the Ca^{2+} with a $K_{D,Ca}$ of 20.8 µM and showed the established properties of TRPM4, such as poor discrimination between Na^+ and K^+, a conductance of 19±0.4 pS and inhibition by ATP[60]. Intracellular microelectrodes were used to record the transmembrane potential of mouse atrium to investigate TRPM4's implication in action potentials[67]. Flufenamic acid and 9-phenanthrol reversibly reduced the duration of action potentials in $Trpm4^{+/+}$ mice while this phenomenon was absent in $Trpm4^{-/-}$ mice[67]. In isolated atrial cardiomyocytes, a typical TRPM4 current was recorded from $Trpm4^{+/+}$ but not from $Trpm4^{-/-}$ cells[67]. Moreover, the atrial action potential recorded from $Trpm4^{-/-}$ mouse was 20% shorter than that from littermate controls[67]. This shortening of atrial action potentials in $Trpm4^{-/-}$ mice was further confirmed by Demion and coworkers by patch clamp measurement with isolated atrial cardiomyocytes[68].

The role of TRPM4 in ventricular cardiac myocytes is still controversial. An inward current activated by Ca^{2+} was first recorded in cultured rat ventricular muscle cells by single channel recording[69]. In 2006, Guinamard and coworkers reported the expression of TRPM4 current in ventricular cardiomyocytes from spontaneously hypertensive rats[70]. They recorded a Ca^{2+}-activated current in inside-out patches, and this current depicted the fingerprint of the TRPM4 channel[70]. Later on, Mathar's

results demonstrated that TRPM4 proteins were expressed in mouse ventricular myocytes[21]. In Trpm4$^{-/-}$ mice, the duration of action potentials in ventricular myocytes showed significantly decrease of both, 50% and 90% repolarization[21]. Whole-cell recording indicated a Ca^{2+}-activated current in Trpm4$^{+/+}$, which was absent in Trpm4$^{-/-}$ cells[21]. Western blot showed the expression of TRPM4 both in isolated rat atrial and ventricular myocytes[71]. However, other studies failed to detect TRPM4 channels in ventricular myocytes. TRPM4 inhibitor 9-phenanhol reduced the atrial action potential, while had no effects on ventricular action potential[67]. Moreover, action potentials recorded from left ventricular cardiomyocytes of Trpm4$^{+/+}$ mice showed no significant difference when compared to those of Trpm4$^{-/-}$ cells[67]. In rabbits, ventricular action potentials were recorded by intracellular microelectrodes and application of 9-phenanthrol did not change ventricular action potentials[72]. Moreover, a 9-phenanthrol sensitive current was not detected in ventricular cells but in isolated Purkinje fibers[72]. It seems that the role of TRPM4 for action potentials in ventricular cardiomyocytes is still unclear[68].

1.2.4 Cardiac conduction disorders

During live, the human heart beats billions of times to maintain the supply of nutrients, exchange of gases, remove of waste products and circulation of hormones and antibodies for the whole body. This process is accomplished by direct cell-cell coupling of cardiac muscle cells and proper generation and conduction of the cardiac electrical impulse in the cardiac conduction system (CCS). Electrical signals generated in the sinoatrial node, propagate through right atrium into the atrioventricular node, which also represents a secondary pacemaker that acts as a backup for the sinoatrial node. The impulse propagates further along the Bundle of His and bundle branches to eventually evoke contraction of the ventricle[73]. Cardiac conduction block represents a condition in which the pace-making signal initiated in the sinoatrial node is slowed down or even blocked on the way to the whole heart muscle. Based on the location where the block occurs these are classified as sinoatrial block, atrioventricular block or Intraventricular block. In some cases, heart blocks may not cause any symptoms, or only occasionally missed heartbeats. But in severe cases when the heart loses its ability to control and trigger the heartbeat reliably, implantation of an artificial pacemaker is required to provide correct electrical impulses for maintaining the normal function of the

heart[74,75].

A lot of factors are to be considered in CCS dysfunctions, primarily attributed to acquired conditions like myocardial ischemia, age-related degeneration, procedural complication and drug toxicity[76]. However, a subset of CCS disorders, without any underlying structural disease, is caused by genetic defects, which provides invaluable insight into the mechanisms of CCS development and function. Inherited defects in cardiac conduction have been linked to several genes of ion channels[76,77].

The *SCN5A* gene, encoding the human cardiac sodium voltage-gated channel α-subunit 5, plays a key role in cardiac electrophysiology in maintaining excitability of cardiomyocytes and propagation of the electrical signals through the cardiac-conduction system[77]. Mutations in the *SCN5A* gene cause a variety of rhythm and conduction disorders[77,78]. A progressive cardiac conduction defect, also known as Lev-Lenègre disease, is characterized by age-rated, fibro sclerotic degeneration of the His-Purkinje system[79]. *SCN5A* gene mutations are identified in inherited forms of Lev-Lenègre disease[79]. A mutation of the SCN5A protein was found and predicted to cause a switch from glycine to arginine (G1406R) in a family with Brugada syndrome or isolated cardiac conduction defects[80]. Thirteen of forty-five family members carried this mutation[80]. Patch-clamp studies indicated no detectable sodium current despite normal protein trafficking[80]. The mutation (R376H) located in the first pore segment of the SCN5A protein was associated with cardiac conduction disease[81]. An electrophysiological analysis demonstrated a loss of function with a significant current reduction in this mutant[81]. Mutations W156X and R225W in the *SCN5A* gene were associated with severe cardiac conduction defects[82]. No current was detected in Xenopus oocytes injected with cRNA encoding the W156 mutation[82]. The R225W mutation induced a significant reduction in the current and also affected gating of the sodium channel[82]. Moreover, in myotonic dystrophy alterations of *SCN5A* splicing also participated in the observed cardiac conduction defects[83].

SCN1B encodes the voltage-gated sodium channel β subunit 1, which can increase sodium channel expression at the plasma membrane, modulate its gating and voltage dependence, and also plays a role in cell adhesion and recruitment of cytosolic proteins[84]. Watanabe *et al.* identified three mutations in the *SCN1B* gene in patients with cardiac conduction abnormalities[85]. Two of these mutations located in β1B, a

new alternately processed transcript[85]. Watanabe and coworkers also provided evidence indicating that β1 and β1B transcripts varied in different region of the heart with a higher expression in Purkinje fibers than ventricular cells, which is consistent with the phenotype described in mutation carriers with a cardiac conduction defect[85]. Co-expression of Nav1.5 with the β1 or the β1B transcript mutations reduced the Nav1.5 current compared to the wide type[85]. These results demonstrate that SCN1B could be a potential target for the treatment of human cardiac conduction defects.

The *KCNK17* gene encodes the potassium two-pore domain channel subfamily K member 17, also known as TASK-4[86,87]. A mutation G88R, located in the first extracellular pore loop of the TASK-4 protein, was identified in a patient with progressive and severe cardiac conduction disorder together with idiopathic ventricular fibrillation[88]. The G88R mutant caused gain-of-function of the TASK-4 channel with an approximately three-fold increase in the current when compared to the wild-type channel, while cell surface expressions were similar. Further studies demonstrated that the G88R mutants stabilized the membrane potential and slowed down the upstroke velocity of spontaneous beating in the cardiac HL-1 cell line (spontaneously beating sinoatrial node like cardiomyocytes[89]). Furthermore, TASK-4 showed a strong expression in atrioventricular node and Purkinje fibers[88]. These published results support the possibility that TASK-4 is functionally involved in cardiac conduction disorders.

1.2.5 The involvement of TRPM4 in cardiac conduction defects

Progressive familial heart block type I (PFHBI) is an autosomal dominant inherited cardiac bundle branch disease in the His-Purkinje system[90]. Disease progression in PFHBI is characterized by the occurrence of right bundle branch block(RBBB), followed by bi-fascicular blocks[91]. A missense mutation c.19G>A with an amino acid substitution of Glu7Lys in the N-terminus of the TRPM4 channel was identified as a potential reason for PFHBI in 3 branches of a large South African pedigree[59]. Cellular expression studies depicted that the Glu7Lys mutation increased the amplitude of the TRPM4 current[59]. The proposed underlying mechanism is an attenuated deSUMOylation of the channel, that impairs endocytosis of the TRPM4 protein followed by an accumulation of TRPM4 channel in the plasma membrane[59]. Daumy *et al.*

identified a new gain-of-function mutation (I376T) of TRPM4 in one large family with 10 members diagnosed with PFHBI[92], supporting the notion that TRPM4 channels may play a crucial role in PFHBI.

In three families with autosomal dominant isolated cardiac conduction disease (ICCD), heterozygous missense mutations in TRPM4 gene were found in each family (Arg164Trp, Ala432Thr and Gly844Asp)[61]. All of these mutations were identified as gain-of-function mutations putatively increasing membrane currents through the same mechanism as suggested in TRPM4^{E7K}[61]. While in the study carried out by Syam *et al.*, the Ala432Thr variant showed a decreased expression of the TRPM4 protein at the plasma membrane and a reduced current density in whole-cell patch clamp recordings[93]. The discrepancy between these reports is still unsolved and requires more work to uncover the mechanism underlying the Ala432Thr mutation in diseases.

Stallmeyer *et al.* assessed the relative frequency of TRPM4 mutations and associated phenotypes in a cohort of 160 unrelated patients with various types of inherited cardiac arrhythmic syndromes to clarify the role of TRPM4 gene' variations in cardiac conduction disturbances[94]. A total of six novel (Gln131His, Gly582Ser, Pro970Ser, Gln293Arg, Tyr790His and Lys914Arg) and two published (Ala432Thr and Gly844Asp) TRPM4 mutations were identified[94], but the functional analyses of these novel mutants are still absent and needs to be explored experimentally.

Brugada syndrome (BrS) is a condition defined by ST-segment alterations in the right precordial leads of the electrocardiogram (ECG) and is often associated with right bundle branch block. 15-25% of BrS cases are linked to mutations in the *SCN5A* gene[95]. Several other genes are also correlated to BrS such as *CACNA2D1* (calcium voltage-gated channel auxiliary subunit alpha-2/delta-1)[96], *KCND3* (potassium voltage-gated channel subfamily D member 3)[97] and *SCN2B* (sodium voltage-gated channel beta subunit 2)[98]. Liu and co-workers screened for alterations in the *TRPM4* gene in a cohort of 248 BrS cases without *SCN5A* mutations and found 11 *TRPM4* mutations in 20 unrelated patients[99]. Functional and biochemical studies of 4 selected mutations indicated that mutations (Pro779Arg and Lys914X) caused a significant decrease in both current density and membrane expression[99]. Two variants (Thr873Ile and Leu1075Pro) were associated with an increased expression of TRPM4 proteins, no difference in the whole-cell current, single channel properties, and TRPM4

channel regulation compared to the wide-type[99]. They also mentioned that the TRPM4 mutations in BrS accounts for 2.7% to 6%[99].

1.3 TRPC subfamily

The transient receptor potential canonical (TRPC) channels-with the highest homology to *Drosophila trp*, are regarded as calcium-permeable cation channels[100]. Seven members (TRPC1-7) have been identified based on their sequence similarity, these channels are further subdivided into four subgroups: TRPC1, TRPC2, TRPC4/TRPC5, TRPC3/TRPC6/TRPC7[100]. TRPC1 is closed to TRPC4 and TRPC5, and in some case has been considered to oligomerise with them. TRPC2 is a pseudogene in humans, which has been reported to be a store-operated channel in sperm[101] and may be involved in vomeronasal function[102].

Table 1.1 Tissue distribution of TRPC channels

Subtype	Species	Method	Tissue distribution
TRPC1	Human	MTN	Heart, brain, testis, ovary, intestine
		MTN	Ubiquitous
	Rat	RT-PCR	Ubiquitous
		RT-PCR	Heart, brain, kidney, intestine, adrenal gland
TRPC2	Cattle	MTN	Testis, liver, spleen
		ISH	Late spermatogenic cells
	Mouse	MTN	Testis, cerebrum, cerebellum, heart
	Rat	ISH	Vomeronasal organ sensory epithelium
TRPC3	Human	MTN	Brain
	Mouse	ISH	Cerebellar Purkinje cells
		MTN	Brain
	Rat	RT-PCR	Ubiquitous
		RT-PCR	Cerebellum, midbrain, olfactory bulb, cortex
TRPC4	Cattle	MTN	Adrenal gland, testis, retina, heart, brain
	Mouse	MTN	Cerebrum, adrenal gland, cerebellum, ubiquitous
		ISH	Dentate gyrus granule cells, ca1 pyramidal neurons, cortex
	Rat	RT-PCR	Olfactory bulb, hippocampus, cortex
		RT-PCR	Cerebrum, nodose ganglion, testis, ovary, heart, lung
TRPC5	Mouse	MTN	Brain
		RT-PCR	Brain, testis, kidney, uterus
	Rat	RT-PCR	Cerebrum, cerebellum, ovary, adrenal gland, testis, ovary, nodose ganglion, kidney
	Rabbit	MTN	Brain
TRPC6	Human	MTN	Lung, placenta, ovary, spleen, ubiquitous
	Mouse	MTN	Lung, brain
	Rat	RT-PCR	Lung, cerebrum, ovary, ubiquitous
		RT-PCR	Cerebral cortex, hippocampus, heart, kidney, lung, adrenal gland
		ISH	Dentate gyrus granule cells, cerebral cortical neurons
TRPC7	Mouse	MTN	Heart, lung, eye, hindbrain, spleen, testis
		ISH	Cerebellar Purkinje cells, olfactory bulb, hippocampus

Modified from reference[103], MTN: multiple tissue northern blotting; RT-PCR: reverse transcriptase polymerase chain reaction; ISH: in situ hybridization.

Tissue distribution of TRPCs has been determined by various method such as multiple tissue northern blotting (MTN), reverse transcriptase polymerase chain reaction (RT-PCR) and in situ hybridization (ISH), showing a broad expression pattern from neuronal

tissues like hippocampus to peripheral tissues like heart and liver[103].

1.3.1 The TRPC1 channel

TRPC1 is the first member of the TRP channel family, purported to form a functional ion channel[104,105]. The human *TRPC1* gene locates at chromosome 3q22-3q24[29] generating four splices variants in humans (α-ε), the two splicing variants, long TRPC1α channel and short TRPC1β channel (lacking 34 amino acids in the third Ankyrin repeat), have been functionally validated[32]. The TRPC1 channel protein has six predicted transmembrane spanning domains flanked by intracellular N- and C-terminus. The pore-forming region is located between S5 and S6 and contains the LFW motif (conserved in the putative hydrophobic pore region).

Within the N- and C-terminus of TRPC1, several functional motifs have been identified. In the C-terminus a putative calmodulin binding site was described, which could mediate the Ca^{2+} dependent inactivation of store-operated calcium entry by binding of Ca^{2+}-calmodulin to the TRPC1 channel[106]. Two negatively charged aspartate residues in TRPC1 interact with positively charged lysine in Stromal interacting molecule 1 (STIM1) regulating the gating of TRPC1 channel[107]. Atomic force microscopy imaging revealed that TRPC1 forms tetramers[108]. The homomeric interaction between the TRPC1 proteins may be mediated by coiled-coil domains in the N-terminus[109]. Three Ankyrin repeats within the C-terminus may be involved in the heteromeric interaction between TRPC1 and TRPC3[110]. Neutralizing negatively charged residues in the hypothetic pore region reduced Ca^{2+} but not Na^+ permeability demonstrating the idea that this region contributes to the ionic selectivity[111].

1.3.1.1 Activation mechanism of TRPC1

Store-operated activation

Store operated calcium entry (SOCE) is activated by the depletion of the endoplasmic reticulum (ER) Ca^{2+} store. Inositol 1,4,5- triphosphate (IP_3) interacts with IP_3 receptors in the ER membrane and triggers Ca^{2+} release from the Ca^{2+} store thereby depleting it. Inhibition of TRPC1 leads to a decrease of plasma membrane Ca^{2+} influx in response to Ca^{2+} depletion of the ER, therefore, it seems that TRPC1 is a key subunit of SOCE channels[112]. One type of its functional correlate was described as a calcium release

activated calcium (CRAC) channel in mast and T lymphocytes[113]. The primary pore-forming component of CRAC is a four-transmembrane protein named Orai1, which locates at the plasma membrane[114]. STIM1 is an ER protein with an EF hand motif as a Ca^{2+} sensor facing the lumen of the ER[115]. Under resting conditions, STIM1 locates along microtubules, while after store depletion, STIM1 recruits Orai1 into specific ER-plasma membrane junctions and activates Orai1 by the Orai1 Activating Region (SOAR) in the C-terminus of STIM1[114,116]. Even though TRPC1 is involved in SOCE, the electrophysiological characteristics of TRPC1 do not resemble CRAC. Therefore, the TRPC1-associated current was named store-operated calcium current (I_{SOC}) to distinguish it from I_{CRAC}[111]. It is still unclear whether CRAC and SCOE are different channels or whether the SOCE channel is an alternative form of the CRAC channel containing TRPC1. The TRPC1 protein is reported to aggregate within ER-plasma membrane junctions[107]. The activation of TRPC1 is more complicated, besides STIM1 it also requires the participation of Orai1, which mediates Ca^{2+} entry and triggers recruitment of TRPC1 to the ER-plasma membrane junctions[117-119]. One explanation for this is that in cells only expressing STIM1 and Orai1 protein; the dominant store-operated current could be I_{CRAC}, while in cells expressing STIM1, Orai1 and TRPC1, the store-operated current could be a combination of I_{CRAC} and I_{SOC}[120].

Receptor-operated activation

TRPC1 has been shown to form receptor operated channel complexes with other TRP channels[20,121,122]. TRPC1 associates with TRPP2 to constitute a channel complex TRPC1/TRPP2 showing biophysical properties that are distinct from the homomeric channels[123]. The TRPC1/TRPP2 channel complex is activated by G-protein-coupled receptor stimulation and displays a distinct single-channel conductance of 40±5 pS. The amiloride sensitivity as well as ion permeability is different from TRPC1 or TRPP2 alone[123]. Native TRPC1/TRPP2 activity was detected in kidney cells by complementary gain- and loss-of-function experiments[123]. The existence of TRPC1/TRPP2 heterotetramers under physiological conditions was confirmed by co-localization and co-immunoprecipitation experiments[123]. TRPC1 and TRPC5 were suggested to form a heteromeric neuronal channel in the hippocampus[124]. Following co-expression of TRPC1 and TRPC5 in HEK293 cells, a novel Gq-coupled nonselective cation current was recorded with a voltage dependence, resembling that mediated by

NMDA receptor channels[124]. TRPC1 has also been reported to form a heteromeric channel complex with TRPC4[125]. $G_{q/11}$-coupled receptor stimulation increased TRPC1/TRPC4 current, while Gi/o-coupled receptor stimulation induced a current with a current-voltage relation distinct from TRPC4 alone[125]. In freshly isolated smooth muscle cells, TRPC1 and TRPC3 formed a channel complex TRPC1/TRPC3. This channel complex was activated by UTP, an activator of endogenous Gq-coupled receptors, and inhibited by protein kinase G (PGK), which contributed to the nitric oxide-mediated vasorelaxation in smooth muscle cells[126].

Mechanical activation

Interestingly, TRPC1 can also be activated by mechanical stimulation indicating a stretch-activated current[127]. In Xenopus laevis oocytes, TRPC1 was reported to represent the mechanosensitive cation channel[127], which has also been found in Xenopus neuronal cones to regulate the extension and direction of spinal axon outgrowth[128] and in Madin-Darby canine kidney cells to impact their migration[129].

1.3.1.2 Physiological functions of TRPC1

Based on its role as a store-, receptor- and mechanically activated channel, TRPC1 has been shown to play important roles in physiological and pathological processes in various native cells, organ systems and organisms.

Cardiac hypertrophy is a phenomenon during which cardiac myocytes respond to pressure or mechanical stimulation by increasing their cell size[130]. The importance of Ca^{2+} entry in the cardiac hypertrophic response is well established. The expression of TRPC1, a Ca^{2+} influx channel, is significantly increased during cardiac hypertrophy and it has been suggested to contribute to the signal pathway of cardiac hypertrophy[130]. Using a Trpc1^{-/-} mice model, a nonselective cation current found in wild type cells was absent in Trpc1^{-/-} myocytes[131]. Consistently, Trpc1^{-/-} mice failed to show maladaptive cardiac hypertrophy in response to hemodynamic stress and neuro-hormonal stimulation[131]. Furthermore, TRPC1 has been reported to mediate the activation of the NFAT signal pathway, which is required for cardiac hypertrophy[132]. In a recently study, a background Ca^{2+} entry pathway in cardiomyocytes mediated by TRPC1/TRPC4 has been identified and TRPC1/TRPC4 double knock out mice were reportedly protected from cardiac hypertrophy[20].

Skeletal muscle exhibits high plasticity in response to mechanical stimulation[133]. The TRPC1 channels are suggested to be involved in Ca^{2+} influx stimulated by store depletion[112] or membrane stretch[127]. Using an overexpressing strategy, TRPC1 revealed an expression pattern that matched the distribution of the sarcoplasmic reticulum (SR) Ca^{2+} pump in adult mouse muscle fibers. Ca^{2+} imaging data indicated that TRPC1 may serve as a SR Ca^{2+} leak channel in skeletal muscle, which is deeply involved in intracellular Ca^{2+} homeostasis[134]. In another study, the possible involvement of TRPC1 in the entry of Ca^{2+} and its possible role in muscle function has been investigated[135]. A small conductance Ca^{2+} current was completely absent in $Trpc1^{-/-}$ mouse fibers and these mice displayed a substantial decrease in the endurance of physical activity. These data suggested that TRPC1 mediates the entry of Ca^{2+} and helps maintaining skeletal muscles' force function especially during muscle fatigue[135]. TRPC1 also participated in the process of myoblast differentiation and muscle regeneration through a Ca^{2+} dependent activation of the PI3K/Akt/mTOR/p70S6K pathway[136].

Ca^{2+} entry via store operated Ca^{2+} (SOCE) channel is suggested to regulate salivary gland fluid secretion[137]. The SOCE current underlying salivary gland dysfunction is decreased in mice lacking TRPC1, which is consistent with the attenuation of neurotransmitter-regulated salivary gland fluid secretion[137], demonstrating that TRPC1 may be an important component of SOCE and thus essential for the regulation of fluid secretion in salivary gland cells[137]. Calcium-activated chloride channel (CaCC) are also important in modulating fluid secretion in salivary tissues. Interestingly, the Ca^{2+} required for activation of CaCC is supplied by TRPC1 channel[138].

1.3.2 The TRPC4 channel

The full-length TRPC4 cDNA was initially cloned from bovine adrenal glands[139]. Since then more and more TRPC4 orthologues were isolated from other species[140,141]. The most abundantly expressed transcripts of TRPC4 are TRPC4α and TRPC4β. The TRPC4β variant lacks a region containing 84 amino acids at the C-terminus when compared to TRPC4α[142]. Like other TRP channels, four TRPC4 subunits are required to form a functional tetramer and each subunit includes a six-transmembrane segment with a putative pore region located between the fifth and sixth transmembrane segment

and an intracellular N- and C- terminus[36]. In the cytoplasmic N-terminus of TRPC4, there are different domains such as ankyrin-like repeats, calmodulin binding site, coiled-coil domains and caveolin-binding sites[36,143]. A TRP box motif (a conserved six residues located in TRP domain), a shared binding site for calmodulin and inositol 1, 4, 5-trisphosphate, a conserved protein 4.1-binding domain and a second coiled-coil domain have been identified in the cytoplasmic C-terminus[144-146]. The last three C-terminal amino acids of TRPC4 might comprise a PDZ-interacting domain that binds to the scaffold protein ezrin/moesin/radixin-binding phosphoprotein 50 (EBP50) to control the localization and surface expression of TRPC4 in HEK293 cells[147]. Deletion of the PDZ motif significantly reduced the expression of TRPC4 in the plasma membrane[147]. A recent study showed that the N-terminus residues 23-29 (VRAETEL) of TRPC4 represent an important domain for TRPC4's translocation to the cell membrane, and the interaction between the N-terminus 98-124 amino acids and C-terminus 700-728 amino acids was essential for the formation of TRPC4 tetrameric complexes[148].

1.3.2.1 Activation mechanism of TRPC4 channel

Almost all studies on TRPC4 channels indicate that G-protein coupled receptors are involved in the activation of recombinant channels[124,139,142,149]. Using heterologously expressed murine TRPC4 channel in HEK293 cells, one study demonstrated that stimulation of G_q-coupled receptors, especially those coupled to PLCβ, evoked a large, nonselective cation current, which was independent of the depletion of intracellular Ca^{2+} stores[149]. The underlying mechanism remains elusive. Diacylglycerol (DAG), the product of PLC activity can directly activate TRPC3, TRPC6 and TRPC7[150,151], but was unable to activate TRPC4[142,149]. This notion was challenged by a recent study, in which the authors presented a DAG-mediated activation mechanism for TRPC4[152]. When PIP_2 and the Na^+/K^+ exchanger regulatory factor (NHERF) occupied the C-terminus of TRPC4, the channel was in a DAG-insensitive conformation. PIP_2 depletion evoked a conformational change in the C-terminus of TRPC4 leading to the dissociation of NHERF and an increased DAG sensitivity[152]. PIP_2 applied intracellularly has been reported to inhibit the activation of TRPM4α but not TRPC4β, and PIP_2 depletion might be involved in TRPC4 channel's activation[153] while we should notice that PIP_2 breakdown is essential but insufficient for TRPC4 channel fully opening, which still requires other components such as Ca^{2+}

and $G_{i/o}$ protein[153].

As a nonselective cation channel, TRPC4 can be activated by muscarinic stimulation[154,155]. Further studies suggested that it is the Gαi protein that participates in the activation of TRPC4. A blocker of the Gαi protein, PTX, inhibited M_2 muscarinic receptor activated currents recorded in HEK293 cells co-expressing the M_2 muscarinic receptor and TRPC4[156]. $Gα_i$ proteins comprise $Gα_{i1}$ $Gα_{i2}$ and $Gα_{i3}$. TRPC4 could be activated by several Gαi subunits, most prominently by $Gα_{i2}$ through direct interaction of its conserved C-terminal SEC14-like and spectrin-type domains (SESTD) with $Gα_{i2}$[157,158]. Thakur and coworkers revealed that TRPC4 activation requires coincident stimulation of $Gα_i$ and PLCδ, suggesting an integrative mechanism through TRPC4[159].

The store-operated activation mode has also been reported for TRPC4-containing channels[139,160,161]. STIM1, the endoplasmic reticulum Ca^{2+}-content sensor[115], has been reported to interact with TRPC4 in store-operated channels[162,163]. In contrast, in endothelial cell, knockdown of either TRPC1 or TRPC4 had no effect on store-operated Ca^{2+} entry[164]. Overexpression experiments also demonstrated that receptor activated current of TRPC4 was independent of the depletion of the Ca^{2+} store[149,165]. One possibility is that the level of endogenous STIM1 in a given cell type determines the operation of TRPC4 as a store-operated vs. receptor-activated channel, which may rationalize why in some studies TRPC4 did not contribute to store-operated channels[166].

1.3.2.2 TRPC4 physiological function

Many studies report the expression of TRPC4 in different cell types, in which TRPC4 contributes to Ca^{2+} entry pathways. In adult ventricular cardiomyocytes, a background Ca^{2+} entry pathway has been identified that relied on TRPC1/TRPC4 expression[20]. In TRPC1/TRPC4 but not TRPC3/TRPC6 double knockout mice this background Ca^{2+} entry was reduced and both diastolic and systolic Ca^{2+} concentrations were lower when compared with wild type[20]. A study in HEK293 cells revealed that overexpression of TRPC4 resulted in a gain of sensitivity towards pH-dependent capacitative Ca^{2+} entry[167]. In rat aortic and mesenteric smooth cells, stretch stimulation reduced TRPC4 expression and capacitative Ca^{2+} entry[168]. In human gingival keratinocytes,

knockdown of TRPC4 significantly reduced the raising of intracellular Ca^{2+} when exposed to high external Ca^{2+} solutions[169]. TRPC4 was also identified as the molecular component of store-operated Ca^{2+} channel in mouse mesangial[170] and endothelial cells[171]. Due to the lack of specific inhibitors for TRPC4, genetic approaches are widely used to explore the physiological and pathological functions of TRPC4 in native tissue.

By overexpression of TRPC dominant-negative (dn) variants, one study showed that cardiac hypertrophic responses induced by neuroendocrine agonist infusion or pressure overload were reduced in dnTRPC4, dnTRPC3 and dnTRPC6 transgenic mice[132]. More importantly, dnTRPC4 was found to inhibit the activity of TRPC3/TRPC6/TRPC7 channels[132]. Moreover, the activity of the well-known Ca^{2+} dependent hypertrophy-inducing pathways was significantly decreased when the expression of TRPC channels was downregulated[132]. In cardiac myocytes, a store-depletion operated Ca^{2+} influx was detected in hypertrophic wild type but not in dnTRPC4, dnTRPC3 and dnTRPC6 mice[132]. These results suggested that TRPC4, TRPC3 and TRPC6 may play an important role in the development of pathological cardiac hypertrophy[132]. In another independent study using TRPC1/TRPC4 double knockout mice the role of TRPC4 in the development of cardiac hypertrophy pathogenesis was described as well[20]. In TRPC1/TRPC4 double knockout but not in TRPC1- or TRPC4-single knockout mice cardiac hypertrophy and fetal gene expression were both reduced. These results indicated that TRPC1 and TRPC4 gene silencing could display a protective role in cardiac hypertrophy[20].

TRPC4 was also reported to contribute to cardiac pathologies following myocardial infarction (MI)[172]. Transgenic mice with overexpression of dnTRPC4 showed less cardiac dysfunction and reduced pathological remodeling[172]. TRPC-mediated Ca^{2+} entry after MI was recorded in wild type but did not in dnTRPC4 mice. The latter also showed less pathological hypertrophy and heart failure with better cardiac performance and survival rate, indicating that loss of TRPC4 function was protective against cardiac dysfunction after MI[172].

Pulmonary arterial hypertension (PHA) is defined by an increased pulmonary arterial pressure, TRPC4 inactivation was identified as a survival benefit in severe PAH[173]. In a following study, the authors revealed that TRPC4 as an endothelial store-operated

Ca^{2+} entry channel provides a Ca^{2+} source to regulate vascular permeability in PHA[174].

In native endothelial cells of wide type mice a store-operated Ca^{2+} current was described in wild type but absent in TRPC4 deficient mice, in which, as a consequence, vasorelaxation was markedly reduced, suggesting that TRPC4 functions as a Ca^{2+} entry pathway regulated blood vessel tone[160]. In mouse lung vascular endothelial cells the TRPC4-dependent Ca^{2+} entry was a key determinant to modulate the permeability of the microvasculature[161].

Besides the cardio vascular system, TRPC4 channels are also widely expressed and play vital roles in other organ systems. In lateral septal neurons, TRPC1 and TRPC4, as heteromeric channels, were essential components in mediating the plateau potential, which underlay the epileptiform burst firing induced by metabotropic glutamate receptor agonists[175]. One study identified TRPC4 as a critical factor for regulating γ-aminobutyric acid (GABA) release from dendrites in thalamic interneurons[176].

1.3.3 TRPCs heterotetramers

The oligomerization of TRPC channels has been investigated by different approaches such as sub-cellular trafficking of TRPC subunits, differential functional suppression by dominant-negative subunits, fluorescence resonance energy transfer between labeled TRPC subunits and co-immunoprecipitation[177,178]. TRPC channels have the ability to form tetrameric structures[178]. If all four TRPC subunits are the same, channels form homotetramers, otherwise heterotetramers[124,179-181]. TRPC1, TRPC3, TRPC4, TRPC5, TRPC6, TRPC7 are ubiquitous expressed in human tissues with varying heteromerizing ability.

1.3.3.1 TRPC1 containing channels

TRPC1 is promiscuous in terms of hetero-multimerization with other TRPC channels. In human parotid gland ductal cells, TRPC1 and TRPC3 co-assembled by N-terminal interaction to form a store-operated heteromeric channel[182]. In a recent study, a TRPC1/TRPC3 channel complex was reported in human coronary artery smooth muscles cells and mediate lysophosphatidylcholine-induced apoptosis[183]. A store-operated channel formed by endogenous TRPC1, TRPC3 and TRPC7 in HEK293 cells

was identified and supported by the evidence from co-immunoprecipitation experiment[181]. In cardiac myocytes, TRPC1/TRPC4 heteromeric channel mediated a background Ca^{2+} entry which participates in the development of pathological cardiac remodeling[20]. The combination of TRPC1 and TRPC5 was detected in mammalian brain as a novel nonselective cation channel triggered by Gq-coupled receptors in the hippocampus[124]. A heteromeric channel comprising TRPC1, TRPC4 and TRPC5 was reported in mouse brain and hippocampus and contributed to the efficiency of synaptic plasticity and neuronal network communication[184]. TRPC1 was shown to form functional heteromeric channel complex with TRPC6 in an exogenous expression experiment to modulate the Ca^{2+} permeability of the TRPCs channel complexes[110].

TRPC1 reportedly also interacts with members of other TRP subfamilies. In vascular endothelial cells, TRPC1 was reported to physically interact with TRPV4 to form heteromeric TRPV4/TRPC1 channel mediating flow-induced Ca^{2+} influx[185]. Another cross-family interaction between TRPC1 and TRPV6 was studied by two independent groups. In HEK293 cells, TRPV6 and TRPC1 associated and co-localized with each other, and TRPC1 inhibited TRPV6 expression in the plasma membrane, hence negatively regulating TRPV6-induced Ca^{2+} influx[121]. Similar results were obtained in oocytes depicting the interaction between TRPV6 and TRPC1 to inhibit TRPV6 current[186]. TRPP2, relating to polycystic kidney disease, belongs to the TRPP family and has been reported to interact with TRPC1 as well[123]. A continuing study further indicated a 2:2 stoichiometry in heterotetramer of TRPP2/TRPC1 channel complex[187]. Moreover, evidences for heteromeric TRP channel complex TRPV4/TRPC1/TRPP2, functionally mediating the flow-induced Ca^{2+} increase, were presented in primary cultured rat mesenteric artery endothelial cells[122].

Within the TRPC subfamily, besides TRPC1, identified heteromerizing channels also include: the redox-sensitive cation channel formed by TRPC3/TRPC4[188]; the direct protein-protein interaction between TRPC3 and TRPC6, which was identified as a native receptor-operated non-selective cation channel in vascular smooth muscle cells[178,189] and a TRPC6/TRPC7 channel complex, which contributes to the receptor-activated, nonselective cation current induced by arginine vasopressin[190].

1.3.3.2 The interaction between TRPC1 and TRPC4

Among all heterotetramers, those comprising TRPC1 and TRPC4 have been widely reported[124,175,180,191]. TRPC1 homotetramers failed to form functional receptor-operated channels in heterologous expression systems[110], mostly due to its detainment in the endoplasmic reticulum (ER) lacking further translocation to plasma membrane[191]. TRPC4 homotetramers could be activated by direct interaction of its conserved C-terminal SESTD with $G\alpha_{i2}$ subunits[157]. The I-V curve of TRPC4 homomeric channels depicts a double rectifying shape with a reversal potential at 0 mV. Following co-expression of TRPC4 and TRPC1 in HEK293 cell, TRPC4 channel brought ER retained TRPC1 channels to plasma membrane forming TRPC4/TRPC1 channel complexes[191]. The biophysical properties of TRPC4/TRPC1 channels are rather different from TRPC4 alone, showing an outward rectifying shape with larger outward and smaller inward currents[124,180]. TRPC1 may be involved in the formation of channel pores instead of acting as an accessory subunit to decrease the calcium permeability in heteromeric channel complexes[110]. A recent study revealed more detailed information about domains involving in the formation of TRPC4/TRPC1 heterotrimeric channel. The N-terminal coiled-coil domain and the C-terminal 725-745 region of TRPC1 participated in the formation of TRPC1/TRPC4 channel complex by interacting with the N-terminal coiled-coil domain and C-terminal 700-728 region of TRPC4, respectively[191].

1.4 Aims of my study

1.4.1 TRPM4 channel

Mutations in the Ca^{2+} activated cation channel-TRPM4, have been directly linked to inherited life-threatening cardiac arrhythmias, such as progressive familial heart block (PFHB) or isolated cardiac conduction disease (ICCD), but the underlying etiologies of the diseases are largely unknown. A human gain-of-function mutation, TRPM4^{A432T}, is linked to cardiac conduction disturbance. My goal was to employ photolysis of caged Ca^{2+}, quantitative Ca^{2+} and electrophysiological measurements to investigate the underlying disease mechanism.

Recently, a plethora of mutations in the *TRPM4* gene have been identified[93,99,192]. But not all of these have been studied in great details. Taking the advantage of the UV-flash approach, I systematically investigated nine mutations and their effects on TRPM4's properties to further elucidate the correlations between *TRPM4* gene mutations and inherited cardiac conduction diseases.

1.4.2 TRPC4/TRPC1 channel complex

The localization of TRPC1 can be changed from the ER membrane to the plasma membrane when co-expressed with other TRPCs such as TRPC4 or TRPC5. Moreover, the currents recorded from heteromeric TRPC1/TRPC4 and TRPC1/TRPC5 channels showed altered biophysical properties from double rectifying in TRPC4 or TRPC5 alone to outwardly rectifying when stimulated by Carbachol[125]. TRPC1 could reduce the Ca^{2+} permeability in heteromeric channel complexes when co-expressed with TRPC3, TRPC4, TRPC5, TRPC6 and TRPC7, but the underlying mechanism is unknown[110]. In my experiments, I concentrated on the pore region of TRPC1 to clarify the role of TRPC1 in modulating the electrophysiological properties and Ca^{2+} influx of the TRPC4/TRPC1 channel complex.

The substitution of conserved glycine residue by serine residue located in the cytosolic S4-S5 linker of TRPC4 or TRPC5 forced channels into a consecutive open state and rendered them insensitive to receptor agonist stimulation[8]. Due to the high homology of TRPC1 and TRPC4/TRPC5, I wonder whether a similar position exists in TRPC1 as

well? Alignment of *TRPC1* and *TRPC4* or *TRPC5* gene revealed that the glycine residue mentioned above is also conserved in TRPC1 at position 623, I thus wanted to further address whether the glycine residue to serine residue substitution in TRPC1 also alters the property of the TRPC4/TRPC1 channel complex.

2. Material and Methods

2.1 Material

2.1.1 Compounds and solutions

Chemical compound U37122, was purchased from Sigma-Aldrich (Munich, Germany). GÖ6983 was purchased from TOCRIS (Bristol, United Kingdom). NP-EGTA/Salt, Fluo-4/Salt, Fluo-4FF/Salt and Fura-2/AM were purchased from Life Technologies (Darmstadt, Germany). Dulbecco's modified Eagle's medium (DMEM), Dulbecco's Modified Eagle Medium: Nutrient Mixture F-12 (DMEM/F-12), Fetal bovine serum (FBS) and Pen-Strep (containing 10,000 U/ml penicillin and 10,000 µg/ml streptomycin) were purchased from Life Technologies (Darmstadt, Germany). Transfection reagent NanoJuice® and Lipofectamine 2000® were purchased from EMD Millipore (Darmstadt, Germany) and Life Technologies (Darmstadt, Germany), respectively.

External solution for TRPM4 current recording contained (mM): 140 NaCl, 1 $MgCl_2$, 1.8 $CaCl_2$, 10 HEPES and 10 Glucose, pH was adjusted to 7.35 with NaOH and the internal solution contained (mM): 140 CsCl, 1 $MgCl_2$, 10 HEPES, 1 NP-EGTA, 0.5 $CaCl_2$, and 0.15 Fluo-4FF, pH was adjusted to 7.2 with CsOH.

External solution for action potential recording contained (mM): 137 NaCl, 5.4 KCl, 10 HEPES, 10 Glucose, 1 $MgCl_2$, 1.8 $CaCl_2$, pH was set to 7.35 with NaOH and the internal solution contained (mM): 135 KCl, 10 NaCl, 2 $MgCl_2$, 1 EGTA, 10 HEPES, 3 MgATP, pH was adjusted to 7.2 with KOH.

External solution for TRPC current recording contained (mM): 140 NaCl, 2 $MgCl_2$, 1 $CaCl_2$, 10 HEPES and 10 Glucose, pH was adjusted to 7.35 with NaOH and the internal solution contained (mM): 120 Cesium glutamate, 8 NaCl, 1 $MgCl_2$, 10 HEPES, 10 BAPTA, 3.1 $CaCl_2$, pH was adjusted to 7.2 with CsOH.

2.1.2 Enzymes and kits for molecular cloning

The restriction endonucleases (EcoRI, HindIII BamHI EcoRV, BglII, KpnI, MluI, XbaI, NheI and XhoI), T4 ligase and the high-fidelity DNA polymerase Phusion® Hot Start II were purchased from Thermo Fisher Scientific (Bremen, Germany). The DH5α

competent cells were provided by Ms. Tanja Kuhn for the transformation and amplification of plasmids. The DNA gel extraction kit QIAquick® and plasmid Mini- and Maxi-preparation kits were purchased from QIAGEN (Hilden, Germany).

2.1.3 Primers

All DNA primers were synthesized by Invitrogen of Thermo Fisher Scientific and diluted with RNase free water to 100 µM stored at -20°C. All primers for this thesis are listed below (FW donates forward primer and RV means reverse primer):

Table 2.1 The list of primers for TRPM4 construction

Name	Sequence 5'-3'
hM4b Fu TagRFP FW	CTAGCTAGCATGGTGGTGCCGGAGAAG
hM4b Fu TagRFP RV	CGACGCGTCGGTCTTTGGACCCAGGCAG
TagRFPT E7K FW XL	CTAGCTAGCATGGTGGTGCCGGAGAAGAAGCAGAGC
A432T 1st sequence1 RV	TCAGCAGGGTGTCCATGAGG
A432T 1st sequence2 FW	CCTCATGGACACCCTGCTGA
A432D 1st sequence1 RV	CATTCAGCAGGTCGTCCATGAG
A432D 1st sequence2 FW	CTCATGGACGACCTGCTGAATG
A432K 1st sequence1 RV	CGGTCATTCAGCAGCTTGTCCATGAGGGAA
A432K 1st sequence2 FW	TTCCCTCATGGACAAGCTGCTGAATGACCG
A432V 1st sequence1 RV	ATTCAGCAGGACGTCCATGAGG
A432V 1st sequence2 FW	CCTCATGGACGTCCTGCTGAAT
A432G 1st sequence1 RV	ATTCAGCAGGCCGTCCATGAG
A432G 1st sequence2 FW	CTCATGGACGGCCTGCTGAAT
TagRFPT virus FW	GATATCATGGTGGTGCCGGAGAAGGAG
TagRFPT virus RV	TGCTCTAGATTACTTGTACAGCTCGTCCATGCC
Q131H 1st sequence1 RV	TGCAGCCAGGTGTGGAGGAC
Q131H 1st sequence2 FW	GTCCTCCACACCTGGCTGCA
Y790H 1st sequence1 RV	CAGCAGGTGGCTGACCACGT
Y790H 1st sequence2 FW	ACGTGGTCAGCCACCTGCTG
P970S 1st sequence1 RV	TGCAGGTAGGAACGGTAGAAGACG
P970S 1st sequence2 FW	CGTCTTCTACCGTTCCTACCTGCA
G737R 1st sequence1 RV	GGTCCGCCGTCCTGACAGGCCCTT
G737R 1st sequence2 FW	AAGGGCCTGTCAGGACGGCGGACC
R892C 1st sequence1 RV	GAGGACAGTGCAGCCCAGGTGGTA
R892C 1st sequence2 FW	GTACCACCTGGGCTGCACTGTCCTC
D561A 1st sequence1 RV	AAAGAAGCAGGGCGCTCCAGGGGGCCT
D561A 1st sequence2 FW	AGGCCCCCTGGAGCGCCCTGCTTCTTT
T677I 1st sequence1 RV	CCACCACTTCTGTATCAGCAGAGACTG

T677I 1st sequence2 FW	CAGTCTCTGCTGATACAGAAGTGGTGGG
G844D 1st sequence1 RV	AGGCCCGGGGTCCCCGCTGGC
G844D 1st sequence2 FW	GCCAGCGGGGACCCCGGGCCT
K914R 1st sequence1 RV	TTGGGCCCCAGCTGTCTGTTGACCGTGAAG
K914R 1st sequence1 FW	CTTCACGGTCAACAGACAGCTGGGGCCCAA

2.1.4 Expression vectors

The pCR259 vector (MP biomedical, Eschwege, Germany) containing TagRFPT was designed by Dr. Anke Scholz in my lab. To generate the adenovirus for infecting hiPS-CMs, I used the RAPAD$^®$ CMV adenoviral expression system (Cell Biolabs, Inc., America) containing a backbone plasmid vector and a shuttle vector for carrying the gene of interest. To enable cardiac myocyte-specific expression of the carried gene, the original CMV promoter was substituted by a cardiac specific promoter MLC2v under a CMV enhancer amplified by PCR from plasmid pUFCMV$_{enh}$/MLC2v0.8-luciferase by PhD candidate Jia Guo in my lab.

2.1.5 Antibodies

Primary antibodies

Name	Catalog Number and working dilution
Anti-tagRFPT	Cat. #AB234, Evrogen (1:5000)
Anti-Na/K+ ATPase α-1 N-15	Cat. #sc-16041, Santa Cruz Biotechnology (1:100)
Anti-actin	Cat. #sc-1616, Santa Cruz Biotechnology (1:1000)

Secondary antibodies

Name	Catalog Number and working condition
Goat anti-rabbit IgG-HRP	Cat. #sc-2004, Santa Cruz Biotechnology (1:5000)
Donkey anti-goat IgG-HRP	Cat. #sc-2056, Santa Cruz Biotechnology (1:5000)

2.2 Methods

2.2.1 Molecular biological methods

2.2.1.1 TRPM4 expression plasmid constructs

The full-length wild type TRPM4α sequence without stop code were amplified by PCR from a plasmid devoted by Prof. Dr. Flockerzi (Pharmacology and Toxicology, Medical

Faculty, Saarland University) with a pair of primers in which the forward primer contains NheI recognition site, and reverse one contains MluI recognition site.

The reaction mixture:

Component	Amout
H_2O	Add to 50 µL
5X Phusion HF Buffer	10 µL
10 mM dNTPs	1 µL
Primer A	2.5 µL
Primer B	2.5 µL
Template DNA	0.5 µL
DMSO	1.5 µL
Phusion Hot Start II DNA Polymerase	0.5 µL

The PCR program:

	Temperature	Time	Cycles
Initial denaturation	98°C	30 s	1
Denaturation	98°C	10 s	25
Annealing	X °C	30 s	25
Extention	72°C	120 s	25
Final Extension	72°C	10 min	1
Hold	4°C		1

1%(g/v) agrose gels were used for electrophoresis and the interested PCR products were retrieved by QIAquick Gel Extraction Kit (cat. 28706) according to the manufacturer's instructions. The purified fragments were then double-digested by restriction endonucleases NheI and MluI following the guide from online Thermo scientific double digested calculator. The pCR259 expression vector fused with TagRFPT was digested by the same restriction endonucleases. The digested fragments were inserted into the expression vector by a DNA ligation kit (cat. EL0012). Afterwards, the product was transformed into competent bacteria for purification and amplification.

The TRPM4-TagRFPT fusion protein fragment was amplified by PCR as described before from the well-constructed pCR259 expression vector with two restriction enzyme sites (EcoRV and XbaI). After digestion, the fragment was inserted into the adenoviral pacAd5 CMVK-NpA shuttle vector for virus generation.

2.2.1.2 TRPCs constructs

The plasmids containing TRPC1, TRPC1C4$_{Pore}$, TRPC4C1$_{Pore}$ and TRPC1$_{G-S}$ were constructed by Prof. Dr. Flockerzi's lab (Pharmacology and Toxicology, Medical Faculty, Saarland University)

2.2.1.3 TRPM4 mutagenesis

The p.E7K mutation in TRPM4 was obtained by using a long forward primer which includes the specific mutation. The other sited-direct mutations were obtained by a two-step PCR protocol. Mutations were made using the standard PCR overlap extension technique. Primers containing specific mutations were synthesized as designed. In the first PCR, the Forward primer (hM4b Fu TagRFP FW) paired with the reversed version of mutation oligo and the forward version of mutation oligo paired with the Reverse primer (hM4b Fu TagRFP RV), amplified the 5'-half and 3'-half TRPM4, respectively. Taking advantage of the sequence overlapping around the mutation site, the two fragments working as templates can be linked by a second round of PCR with the Forward and Reverse primers. In the PCR process, the annealing temperature of each reaction was set to the lowest melting temperature of the primers. Following similar steps as described above (chapter 2.2.1.1), the DNA fragment of the point mutated TRPM4 was inserted into the pCR259 TagRFP vectors.

2.2.1.4 Purification of plasmid DNA

LB medium containing selective antibiotics (50 µg/ml ampicillin) was inoculated with a positively colony and incubated overnight at 37 °C. The plasmid was isolated with the purification Kit from QIAGEN (Hilden, Germany).

2.2.2 Generation of the adenovirus

Virus generation was undertaken according to the instructions of RAPAD$^{®}$ CMV adenoviral expression system (Cell Biolabs, Inc, cat. VPK-252). Both the pacAd5 9.2-100 Ad backbone and the pacAd5 CMVK-NpA shuttle vector containing interested genes were digested with PacI for 4 hours. Both digested and undigested vectors were run on a 1% agarose gel to confirm the completion of the PacI digestion (after complete digestion, the pacAd5 9.2-100 Ad backbone yielded two bands at ~33 kb and ~2.0 kb). The purification kit was used to remove buffer and enzyme from the remainder of the

restriction reactions. The PacI digested vectors were re-suspended in sterile dH$_2$O and stored at -20°C.

HEK293 cells were seeded on 6-well plates and co-transfected with the digested backbone and shutter vector in a ratio of 2:1 by Polyethylenimine (PEI) when the cells were 50-70% confluence. The culture medium containing transfection reagents was changed in next day. Cells were transferred to T75 flasks when the cells' confluence became 95-100%. 7-10 days after transfection, the presence of plaques could be observed. Culturing for another 3-5 days until >80% of cell lifted, the crude viral lysates were harvested. For amplification, the crude virus lysates were added to cells with 70-80% confluence in T75 flasks. Cells were cultured for another 2-4 days and harvested when 80-90% of cells were round but not detached. The harvested virus-containing cells were centrifuged at 1000g for 5 minutes. The cell pellets were re-suspended in 0.5 ml PBS. With three freeze/thaw cycles, the supernatants were collected by centrifugation at 3000g for 10 minutes and aliquoted as viral stocks, which were saved at -80 °C.

2.2.3 Cell culture

2.2.3.1 HEK293 cell culture and transfection

The human embryonic kidney 293 (HEK293) cells were cultured in DMEM medium with 5%(v/v) FBS, 100 U/ml penicilin and 100 µg/ml streptomycin and maintained at 37°C with 5% CO$_2$ in an air humidified incubator. Before transfection, cells were seeded on 20 mm diameter glass coverslips in a 12-well plate with 30% confluence. 24 hour later, the plasmids were transfected into the cells by NanoJuice®, comprising two components, Core transfection reagent and Booster. The protocol is listed below:

1) Prepare the mixture for desired wells, for each well of a 12-well plate:

<div align="center">

50 µl DMEM (without antibiotics)

0.5 µl Core transfection reagent

l µl Booster

</div>

   and mix it thoroughly

2) Incubate the mixture at room temperature for 5 min;

3) 1 µg of DNA plasmid per well was added to the mixture and mixed gently;

4) After incubation at room temperature for 20 min, 50 µl of the final cocktail was added to each well;

5) Cells were then maintained in the incubator at 37 °C with 5% CO_2 for 72 hours.

The HEK293 cells stably expressing the M_2 receptor and the M_2R receptor plus the TRPC4 channel were kindly provided by Prof. Dr. Flockerzi's lab and were cultured in DMEM medium with 5%(v/v) FBS, 100 U/ml penicillin and 100 µg/ml streptomycin. 100 µg/ml Hygromycin B (cat. 10687010, Thermo Fisher) and 400 µg/ml Geneticin (cat. 10131035, Thermo Fisher) were used for M_2 receptor and TRPC4 channel selection, respectively.

2.2.3.2 hiPS-CM culture, dissociation and virus infection

Human induced pluripotent stem cell derived cardiac myocytes (hiPS-CM) explants from Prof. Dr. Alessandra Moretti's lab (Department of Medicine, Klinikum Rechts der Isar, Technische University München) were maintained in EB2 medium: DMEM/F-12 supplemented with 2% FCS, 2 mM Glutamine, 0.1 mM MEM-NEAA, 50 U/ml penicillin, 50 µg/ml streptomycin, 0.1mM ß-mercaptoethanol. Explants were dissociated by collagenase type Ⅱ (Worthington) in 4-6 repeats of 30 min incubation with 900 r/min shaking at 37°C. The dissociated cells were seeded on 20 mm glass coverslips coated with fibronectin in a 12-well plate. Virus infection was performed at day 2 after dissociation. The virus-containing medium was refreshed after 24 hours. Cells were cultured for another 48 hours prior to experiments.

2.2.4 Protein biochemistry

2.2.4.1 Cell surface biotinylation

Following 72-hour incubation after transient transfection, HEK293 cells were washed twice with ice-cold PBS. Biotinylation was initiated by adding 1mg/ml Sulfo-NHS-LC Biotin and the cells were incubated on a shaker for 30 min at 4°C. Cells were washed twice with ice-cold PBSB+0.1%BSA to inactivate and remove excess biotin. After washing twice with ice-cold PBS, cells were harvested and centrifuged at 8000 rpm for 5 min at 4 °C. The supernatants were discarded, the pellets were re-suspended with lysis buffer and incubated on ice for 30 minutes. Cell lysates were centrifuged at 13000 rpm for 30 min at 4 °C and the supernatants were collected. The Bio-Rad protein assay

kit (Bio-Rad, USA) was used to determinate the protein concentration. Then the supernatants were separated into two parts. In the first part as the total expression of TRPM4 was analyzed. To precipitate the biotinylated proteins, the second part was incubated with 50 µl Pierce Streptavidin Magnetic Beads (cat. 65001, Themo Fisher) for 30 min at room temperature with gentle rotation. The protein-coated beads were separated by DynaMag^{TM}-2 (cat.12321D, Thermo Fisher) and washed with lysis buffer for 4-5 times. The beads were then re-suspended in the desired volume of lysis buffer plus 1x NuPAGE LDS sample buffer (cat. NP0008, Thermo Fisher) and 1x NuPAGE reducing agent (cat. NP0009, Thermo Fisher). The biotinylated proteins were dissociated by incubating the beads at 72 °C for 10 min.

2.2.4.2 Western blot analysis

Proteins were separated by NuPAGE™ 3-8% Tris-Acetate Gels (cat. EA03755BOX, Thermo Fisher) using an Xcell SureLock Mini-Cell gel running tank (cat. EI0001, Thermo Fisher). Samples were loaded on the gel with PageRuler™ Prestained Protein Ladder (cat. 26616, Thermo Fisher). 40 mL of NuPAGE® Tris-Acetate SDS Running Buffer 20X (cat. LA0041) was added to 860 ml of deionized water to prepare 1X running buffer. The upper buffer chamber was filled with 200 mL 1X running buffer containing 500 µl NuPAGE® Antioxidant (cat. NP0005) to keep proteins in a reduced state during gel electrophoresis. The lower buffer chamber was filled with 600 ml 1X running buffer. The voltage for running gels was set to 150 V for 1 hour.

Proteins were then transferred from the gel onto Nitrocellulose membranes (cat. 88018 Thermo Fisher) using a Mini Trans Blot® Cell (Bio-Rad Inc, USA). 1X transfer buffer was prepared as following:

NuPAGE® Transfer Buffer (20X)	50 mL
NuPAGE® Antioxidant	1 mL
Methanol	100 mL
Deionized Water	849 mL
Total Volume	1000 mL

A blotting 'sandwich' was assembled and the transfer was undertaken at a constant voltage of 100 V for 1 hour.

After electrophoretic transfer, the nitrocellulose membrane was stained with Ponceau S to confirm sufficient transfer. The membrane was washed with deionized water and subsequently blocked for 1 hour in blocking buffer while gently shaking at room temperature. Antibodies were diluted in blocking buffer to the given dilutions (see 2.1.5). Incubation with the appropriate primary antibodies was performed for 1-2 hour at room temperature on a shaking platform. The primary antibody solution was removed and membranes were washed with PBST for 3×5 minutes under constant shaking. The appropriate horseradish peroxidase (HRP)-conjugated secondary antibody was applied for 1 hour at room temperature, followed by washing steps with PBST for 3×5 minutes. Immunoreactivity was visualized by ECL™ Western Blotting Detection Reagents (GE Healthcare). An equal volume of detection solution 1 was mixed with detection solution 2 to cover the membrane sufficiently and incubated for 5 minutes at room temperature. The membrane was immediately imaged by Fusion FX (Vilber, Germany). Chemiluminescence was quantified by Image J software and the quantified data was analyzed by Prism (6.0, GraphPad Software Inc., USA).

2.2.5 Electrophysiology and Imaging

2.2.5.1 Patch-clamp recording

A manual patch clamp set up was used to record electrophysiological signals. Patch pipettes were made from Clark borosilicate standard wall capillaries with filament (GC150F-7.5, Harvard Apparatus, USA) and pulled using a puller (DMZ-Universal Puller, Zeitz Instruments, Martinsried, Germany) to a final resistance of 3-5 MΩ when filled with the internal solution. Cells seeded on glass coverslips were mounted on the stage of an inverted microscope (TE2000-U, Nikon, Japan). Experimental recording and data acquisition were controlled by the EPC-10 amplifier (HEKA Electronic, Germany) combined with the Patch Master software (2.40, HEKA Electronic, Germany). The whole-cell configuration was obtained by applying additional negative pressure after attaining high quality of Gohm seals. Capacitance and access resistance were monitored continuously and cell membrane capacitance values were used to calculate current density. Data analysis was carried out in Matlab (R2014a, MathWorks, Germany) and Prism (6.0, GraphPad Software Inc., USA).

For TRPM4, whole cell membrane currents were measured in the whole-cell configuration. Generally the holding potential was set to -60 mV while during the acute recording of TRPM4 membrane currents the cells were clamped at +80 mV, a membrane potential at which TRPM4 currents were reportedly larger than that at negative potentials[38,59].

hiPS-CMs were differentiated and dissociated as described in 2.2.3.2. Spontaneous action potentials were record by whole-cell patch clamp in the current-clamp mode in normal Tyrode solution. For the experiments in HEK293 cells, typical ventricular-like action potential waveform from hiPS-CMs was selected as the voltage command for action potential playback experiments in voltage-clamp recording mode. This protocol also included triggering of UV-flashes and simultaneous Ca^{2+} recording as described below (2.2.5.2). Patch Master software was used for protocol editing and data acquisition.

For the TRPC4/TRPC1 studies, transiently transfected cells were continuously perfused with normal Tyrode solution. The resting potential was set to -60 mV. After formation of the whole-cell configuration a ramp protocol from -100 mV to +100 mV for 250 ms was applied every 3 seconds. Firstly, cells were perfused with Tyrode for 1 minute to obtain a steady control condition. To activate the muscarinic receptor, cells were sequentially perfused with Carbachol (25 μM) for 20 seconds. After that Tyrode was applied again to wash out the effects of Carbachol.

2.2.5.2 Ca^{2+} uncaging and Ca^{2+} measurement

Ca^{2+} uncaging was obtained by brief high-intensity flashes from a UV-flash lamp (RAPP OptoElectronic GmbH, Germany) coupled into the microscope via a light guide and reflection from a 420 nm long-pass dichroic mirror. For experiments using a single uncaging event I employed a UV-flash energy of 135J, while for trains of uncaging events the flash energy was set between 35J and 75J. Fluo-4FF was excited at 480 nm ($\pm$5 nm) with a monochromator (PolyChrome V, TILL, Photonics, Germany), and the emission was collected through a 515 nm long-pass filter onto an Avalanche photodiode based epifluorescence setup (TILL, Photonics, Germany). The Ca^{2+} concentration was calculated as described previously[193]: $[Ca^{2+}]=KR[(K/[Ca^{2+}]_0+1)-R]$. R is the fluorescence ratio and K is the dissociation constant for Fluo-4FF. $[Ca^{2+}]_0$ is the Ca^{2+}

concentration of the pipette solution that was determined in independent experiments in small aliquots in vitro as described as below.

Because of the overlapping of Fura-2 excitation wavelength and NP-EGTA's absorption spectra, the Ca^{2+} concentration of NP-EGTA containing pipette solution can't be measured directly by Fura-2, therefore I provided an alternative to quantify the Ca^{2+} concentration indirectly by using Fluo-4 and Fura-2. The TRPM4 pipette solution without NP-EGTA and Ca^{2+} was aliquots into 100 μL with 5 mM EGTA. Then different amount of Ca^{2+} was added to the solution for the final concentrations(mM): 0.1, 0.3, 0.5 and 0.7. Then these solutions were measured separately by Fura-2 and Fluo-4, from which I could know the Fluo-4 fluorescence intensity of these solutions as well the corresponding free Ca^{2+} concentrations. Based on these results I got two stand curves as shown in Figure 2.2.1, by which if the Fluo-4 fluorescence intensity of given solution was known, then the free Ca^{2+} concentration could be estimated. The fluorescence intensities of TRPM4 pipette solution with NP-EGTA (1 mM) and Ca^{2+} (0.5 mM) concentrations were measured by Fluo-4 (Figure 2.2.1 A horizontal dashed line). According to the Fluo-4 fluorescence intensity curve, the corresponding Ca^{2+} was 0.31 mM (showing in Figure 2.2.1 A vertical dashed line), which was also depicted in the Figure 2.2.1 B (vertical dashed line), then the free Ca^{2+} concentration was estimated according to the Fura-2 stand curve (showing in Figure 2.2.1 B horizontal dashed line), that was about 100 nM.
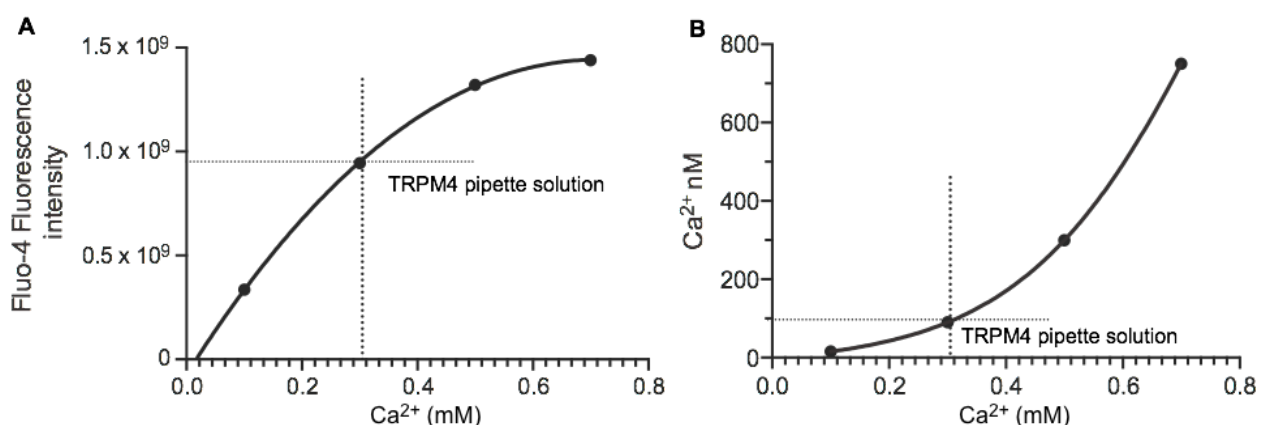
Figure 2.2.1 Free Ca^{2+} concentration measurement of TRPM4 pipette solution.
(A) Standard curve of Fluo-4 fluorescence intensity, the horizontal dashed line indicated the Fluo-4 fluorescence intensity of TRPM4 pipette solution and the vertical dashed line presented the corresponding Ca^{2+} (0.31 mM). (B) Standard curve of free Ca^{2+} concentration. The vertical dashed line exhibited the corresponding Ca^{2+} (0.31 mM) got from (A) and the horizontal dashed line showed the corresponding free Ca^{2+} concentration of TRPM4 pipette solution (99.51 nM)

The activation periods of the membrane currents were fitted in Prism 6.0 by the function $Y=Y0+(plateau-Y0)*(1-e^{-X/\tau})$, Y0 is the Y value when X (time) is zero, plateau is the Y value at infinite times, τ is the time constant for activation.

The deactivation time constant was determined by the function $Y=plateau+(Y0-plateau)*e^{-(X-X0)/\tau}$), X0 is the time at which the decay starts, Y0 is the average Y value to time X0, plateau is the Y value at infinite times. τ is the time constant for deactivation.

2.2.5.3 Confocal

The Leica TCS SP5 II (Leica Microsystems, Wetzlar, Germany) was based on an inverted microscope with a high-speed resonating X-scanner (8000 Hz). A 561 nm laser was employed for the excitation of TagRFPT. The Leica Application Suite software (ver. 2.4) was used to control the entire confocal system for image acquisition.

2.2.5.4 Mn^{2+} quenching

Transfected HEK293 cells were loaded with Fura-2-acetoxymethyl ester (Fura-2/AM) for 30 minutes in Tyrode solution without Ca^{2+}. The Fura-2 loaded cells were excited at 358 nm (the isosbestic wavelength in my set up) and the emitted fluorescence was collected at wavelength >515 nm. Cells were in continuous perfusion with Tyrode solution without Ca^{2+}. In Mn^{2+} quench experiments, 1 mmol/L $MnCl_2$ or 1 mmol/L $MnCl_2$ plus 25 µmol/L Carbachol were applied. The bleaching rate (BR) was the background bleaching of fluorescence without Mn^{2+} treatment, and fluorescence decrease during Mn^{2+} application (FDM) was the slop of Mn^{2+} application. Mn^{2+} quench rate was calculated as the difference between FDM and BR (FDM-BR).

2.2.6 Data Analysis

Results are presented as mean ± SEM. All resulting data were initially tested for normal distribution in Prism 6.0 software (GraphPad Software Inc., USA) using the D'Agostino & Pearson normality test. All data in this dissertation passed the normality test unless otherwise stated. The unpaired 2-tailed Student's t test was used to evaluate statistical differences. Significances were characterized by the particular p-values: (*) for $p<0.05$, (**) for $p<0.01$ and (***) for $p<0.005$. "n"-numbers are given as the number of investigated cells considering that the data were collected from at least 2 independent

set of experiments. For Western blot analysis, the "n" number represents the number of repetitive transfections.

3. Results

3.1 TRPM4

3.1.1 Expression of TRPM4 fusion proteins

To visualize the expressed TRPM4 protein in transfected HEK293 cells for the patch-clamp experiments and to quantify TRPM4's expression by Western blot, an expression vector with a fluorescent protein (TagRFPT) tag was constructed. I inserted the fluorescent protein either at the N- or the C-terminus of TRPM4. As shown in Figure 3.1.1 A, the TagRFPT-TRPM4 fusion proteins (TagRFPT located at the N-terminus of TRPM4) were mainly accumulated in possibly Golgi-like vesicles and failed to reach the plasma membrane. However, the TRPM4-TagRFPT fusion protein (TagRFPT located at the C-terminus of TRPM4) located correctly to the plasma membrane (Figure 3.1.1 B). These results indicated that the fluorescent protein TagFRPT influenced TRPM4's subcellular location when attached to the N-terminus. Thus in my studies, I solely used TagRFPT fluorescent proteins fused to the C-terminus of TRPM4 proteins.
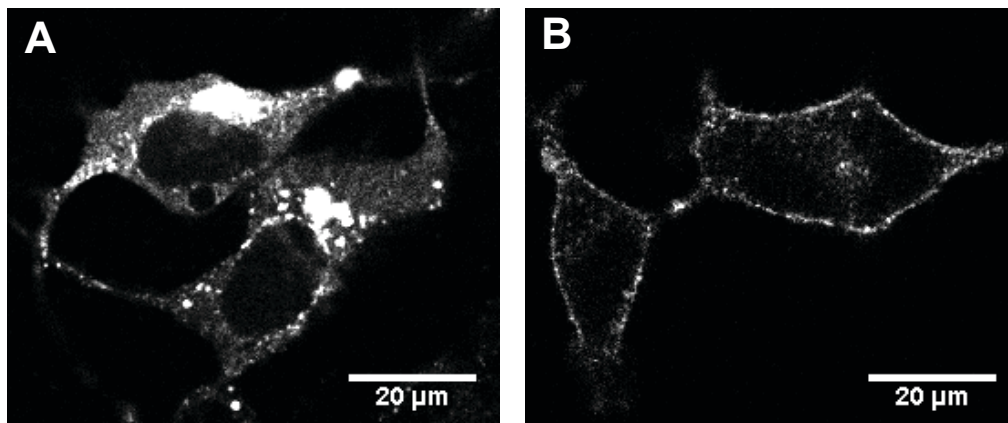
Figure 3.1.1 Subcellular localization of TRPM4 fusion proteins.
Panel (A) indicates an impaired membrane location of the TagRFPT-TRPM4 fusion protein. Panel (B) depicts a proper localizations of TRPM4-TagRFPT fusion proteins at the plasma membrane.

3.1.2 Establishment of the UV-flash approach

3.1.2.1 TRPM4 current activates by UV-flash

TRPM4 is a channel activated by Ca^{2+} and the reported and established approach to study the electrophysiological properties of the TRPM4 channel is to control the

intracellular Ca^{2+} concentration through the pipette solution[59]. Precise Ca^{2+} concentrations can be adjusted between 100 nM and 5 µM or higher by adding appropriate amounts of CaCl$_2$ to a solution of 5 mM EGTA as calculated by the 'CaBuf' program (http://maxchelator.stanford.edu/downloads.htm)[41,194] or by direct measurement of the Ca^{2+} concentration by the Ca^{2+} sensitive dye[59,61]. In these ways, cells are exposed to excessively high Ca^{2+} concentrations for extended periods of time, which most likely affects the physiological status of cells. Moreover, during cellular dialysis, it is rather difficult to determine the absolute Ca^{2+} concentration exactly and controlled changes of the intracellular Ca^{2+} concentration during a whole-cell recording have been reported to be challenging[195]. Furthermore, it was shown previously that the rate of rise in Ca^{2+} might affect TRPM5 channel's activation[196], suggesting that the temporal dynamics of intracellular Ca^{2+} may also be important for TRPM4's activation.

To provide controlled changes in Ca^{2+} with more 'physiological' kinetics, the methodology of caged-Ca^{2+} compounds using photolabile Ca^{2+} chelators such as 2-nitro-4,5-dimethoxyphenyl-EDTA[197] or o-nitrophenyl-EGTA (NP-EGTA)[198] offers better experimental strategies for studying TRPM4´s properties and more closely resembles the kinetics of cardiac Ca^{2+} transient. UV-flash mediated uncaging of caged-Ca^{2+} compounds has proven to be spatially homogeneous[199]. The combination of Ca^{2+}-uncaging and electrophysiological measurement has been used in adrenal chromaffin cells[200], mast cells[201] and neurons[202]. My group and others have applied this approach successfully in cardiac myocytes[199,203-205].

To investigate the electrophysiological properties of TRPM4, I performed experiments in a condition in which TRPM4 current was activated by the immediate Ca^{2+} release from the caged compound NP-EGTA following UV-flashes. In cardiac myocytes, the TRPM4 protein is exposed to fast and dynamic changes in the intracellular Ca^{2+} concentration during each cardiac cycle. In order to resemble such dynamicity and cover a wide range of Ca^{2+} concentrations I established two different experimental approaches employing UV-flash photolysis of caged Ca^{2+} while simultaneously measuring the intracellular Ca^{2+} concentration and the membrane current[206].
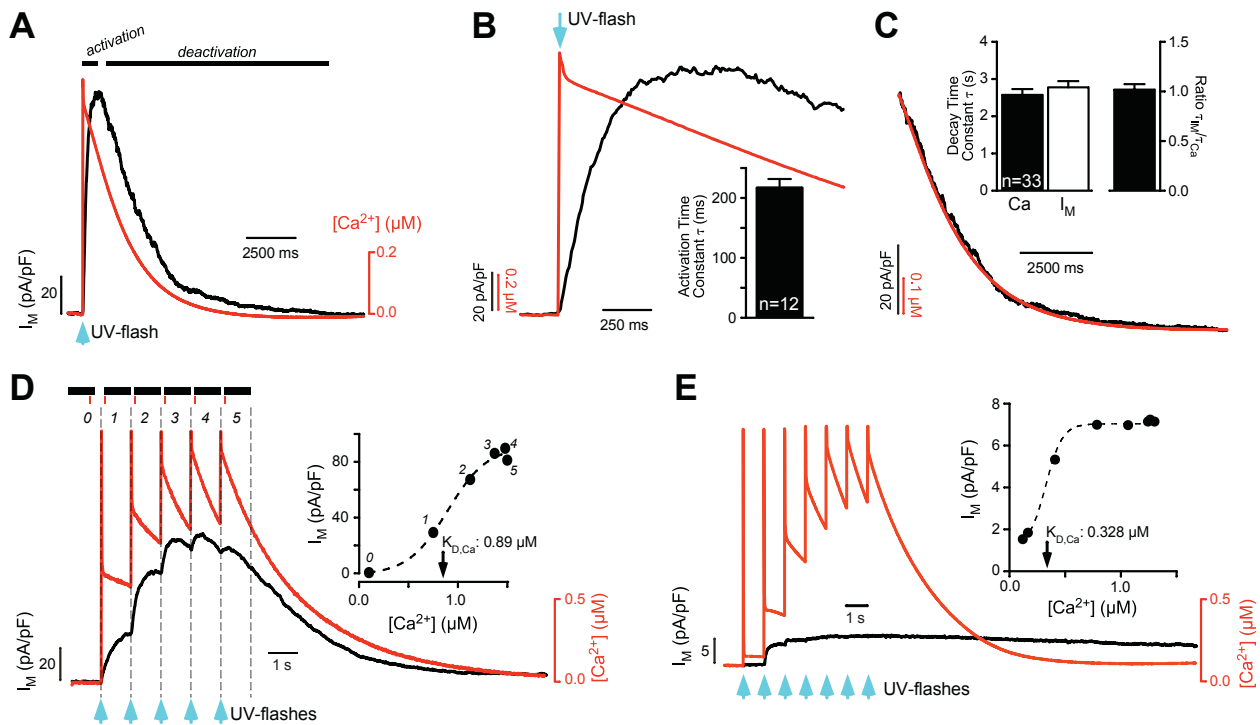
Figure 3.1.2 UV-flash assay for characterizing properties of heterologous expressed TRPM4 proteins.

(A) Time course of membrane current following a single UV-flash (at +80 mV) in TRPM4[wt]-TagRFPT expressing HEK293 cells. (Red traces - TRPM4 current, black traces - Ca^{2+} concentration). (B) Activation phase and (C) deactivation phase of the membrane current and Ca^{2+} transient from (A) at a magnified time scale together with the respective statistical analysis as insets. (D) A train of 5 consecutive UV-flashes results in a staircase like increase in the Ca^{2+} concentration (red) evoking a series of membrane current increases (black) in the TRPM4[wt]-TagRFPT expressing HEK293 cells. Membrane current vs. Ca^{2+} concentration plot from the data as inset depicting the apparent $K_{D,Ca}$. (E) Similar experiments as in (D) performed in non-transfected HEK293 cells. Note the 4-fold lower current scale (black). Taken form [206].

TRPM4[wt] was transiently expressed in HEK293 cells. Ca^{2+} increases generated substantial membrane currents at a holding potential of +80 mV (Figure 3.1.2 A). From this experiment, the activation and deactivation kinetics of TRPM4 channel could be derived as displayed in Figure 3.1.2 B and C, respectively. Trains of repetitive UV-flashes enabled me to cover a wider range of Ca^{2+} concentrations to construct a membrane current/Ca^{2+} concentration relationship for TRPM4 as depicted in Figure 3.1.2 D, the resulting apparent $K_{D,Ca}$ for the membrane current was 0.89 μM. Notably, naïve, non-transfected HEK293 cells only displayed a small, very slowly inactivating Ca^{2+}-activated membrane current with a substantially lower apparent $K_{D,Ca}$ (0.33 μM) as depicted in Figure 3.1.2 E.

I also noticed that the UV-flash only transiently increased the Ca^{2+} concentration, but for extracting the apparent $K_{D,Ca}$ of the current/Ca^{2+} relationship it was unimportant where exactly between two consecutive UV-flashes this relationship was derived from (e.g. the first 10%, last 10% or the entire period). As depicted in Figure 3.1.3, no significant difference of the apparent $K_{D,Ca}$ was observed among these three time periods.

Thus, these two experimental protocols facilitated the characterization of Ca^{2+} activated TRPM4 currents with respect to their current density, $K_{D,Ca}$, activation and deactivation kinetics.
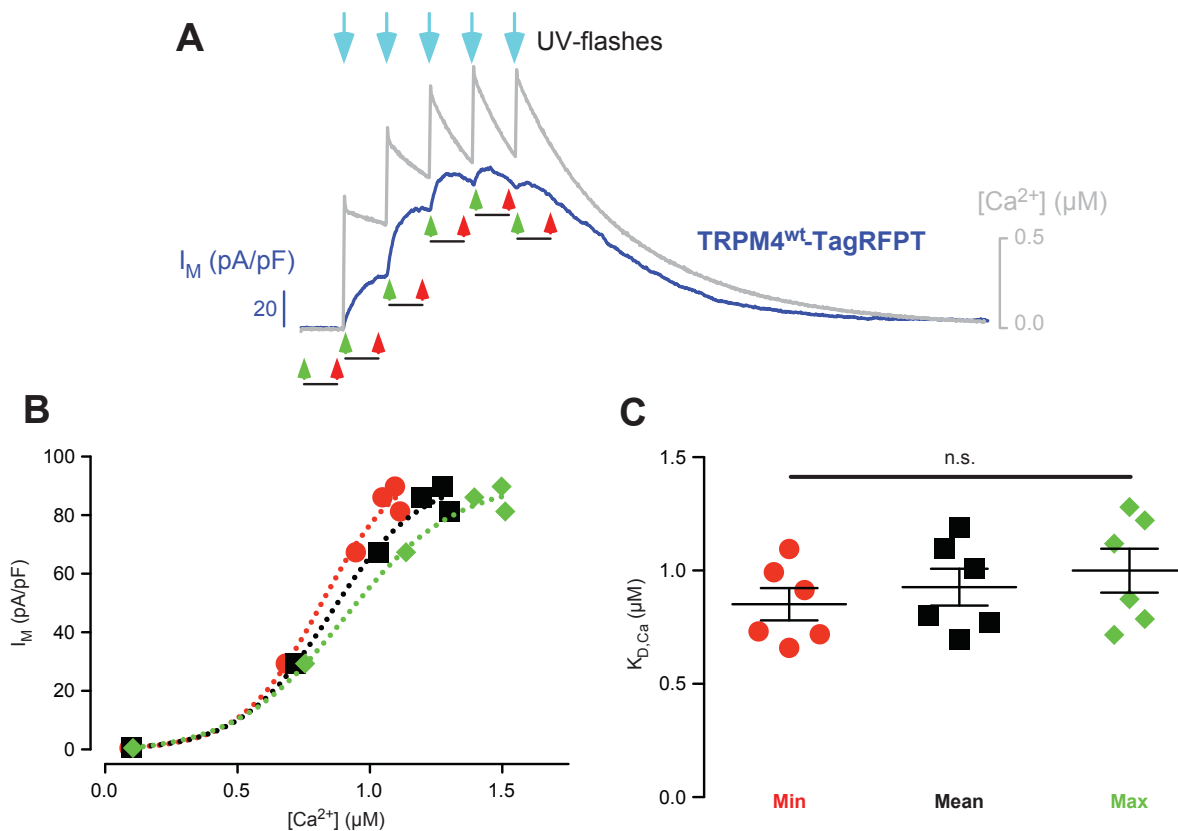
Figure 3.1.3 Derivation the apparent $K_{D,Ca}$ of TRPM4[wt] channel.
(A) Series of UV-flashes caused multiple Ca^{2+} transients (grey trace) and induced TRPM4[wt] membrane current (blue trace). (B) Membrane current vs. Ca^{2+} concentration relationships were constructed using the first 10% (green), last 10% (red) or the entire time period (black) following/between UV-flashes. Colours correspond to the colours used in (A&C). (C) Statically analysis of an experimental series with 6 cells from 2 different preparations. The resulting $K_{D,Ca}$ values were statistically not different. Taken from [206].

3.1.2.2 UV-flash assay recapitulates the gain-of-function property of the TRPM4^{E7K} mutant

In transiently transfected HEK293 cells, Kruse and coworkers reported that the E7K mutation was associated with an increased TRPM4 current density. They also provided a putative underlying mechanism and suggested that the substitution of glutamic acid at position 7 to lysine attenuated the deSUMOylation of the TRPM4 protein. This impaired the endocytosis progress of TRPM4 channel and caused accumulation of the protein on the plasma membrane[59]. I employed this well-characterized gain-of-function mutation to further scrutinize my experimental UV-flash approach for the characterization of TRPM4 currents.

Through targeted site-specific mutation, I constructed a plasmid encoding the PFHBI-associated mutant TRPM4^{E7K}. Both TRPM4^{wt} and TRPM4^{E7K} plasmids were transiently expressed in HEK293 cells and TRPM4 currents were recorded at a holding potential of +80 mV as shown in Figure 3.1.4. As expected, Ca^{2+} jumps produced substantially more currents for the E7K mutant than for the wt (Figure 3.1.4 A and B). The TRPM4^{E7K} current density (normalized with the Ca^{2+} concentration) was 123.3±20.04 pA/pF/µM, which was approximately 2-fold of that of the TRPM4^{wt} (63.83±8.542 pA/pF/µM; Figure 3.1.4 C). The apparent $K_{D,Ca}$ for both proteins were found to be indistinguishable (1.102±0.0955 µM vs. 0.9932±0.1262 µM for TRPM4^{wt} and TRPM4^{E7K}, respectively; Figure 3.1.4 D). Single UV-flash experiments enabled the investigation of the channel´s activation and deactivation kinetics and I found both properties to be unaltered (Figure 3.1.4 E and F).

Next, I investigated the expression of TRPM4^{wt} and TRPM4^{E7K} at the global and the plasma membrane level. As described before[45], I also found the characteristic highly- and core-glycosylated proteins in whole cell lysates (Figure 3.1.5 A left, marked by the closed and open arrowheads, respectively). While the analysis of the Western blot revealed similar expression on the global level (Figure 3.1.5 A right), plasma membrane expression was dissimilar as depicted in Figure 3.1.5 B. The Western blot analysis of the surface expression revealed an approximately 40% increased immunoreactivity for the E7K mutant when compared to wt (see Figure 3.1.5 B right).
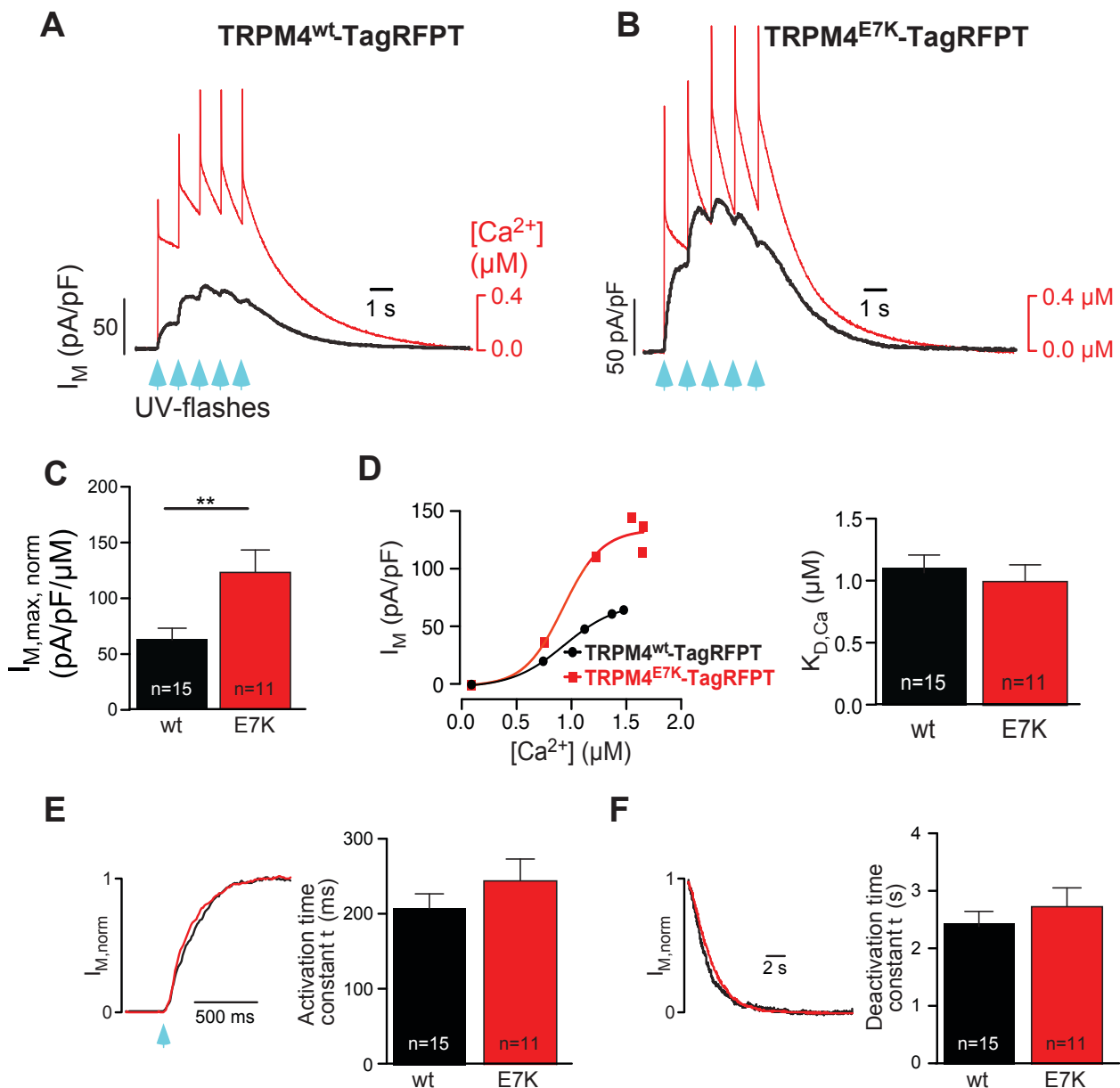
Figure 3.1.4 TRPM4^{E7K} is a gain-of-function mutation.

(A) and (B) display TRPM4^{wt} and TRPM4^{E7K} currents activated by trains of UV-flashes in HEK293 cells transiently expressing TRPM4^{wt} and TRPM4^{E7K}. (C) Statistical synopsis of peak membrane currents. (D) Ca^{2+} dependences of TRPM4^{wt} and TRPM4^{E7K} were obtained by plotting membrane current vs. Ca^{2+} concentration shown in (left), bar graphs of K$_{D,Ca}$ calculated from data are displayed in the right panel. (E and F) Summarizes the channel's activation and deactivation kinetics. Modified from [206].

These data not only showed that I could readily recapitulate properties of the E7K mutant described earlier[59], but also depicted that neither glycosylation nor the kinetic properties of the channel protein appeared to be altered by this amino acid exchange.

A Global expression

180 kDa
130 kDa
55 kDa
43 kDa

WT E7K NT

Anti-TagRFPT

Anti-Actin

Normalized total expression (a.u.)

B Surface expression

180 kDa
130 kDa
130 kDa
95 kDa
55 kDa
43 kDa

WT E7K

Anti-TagRFPT

Anti-a$_1$ Na/K ATPase

Anti-Actin

Normalized surface expression (a.u.)
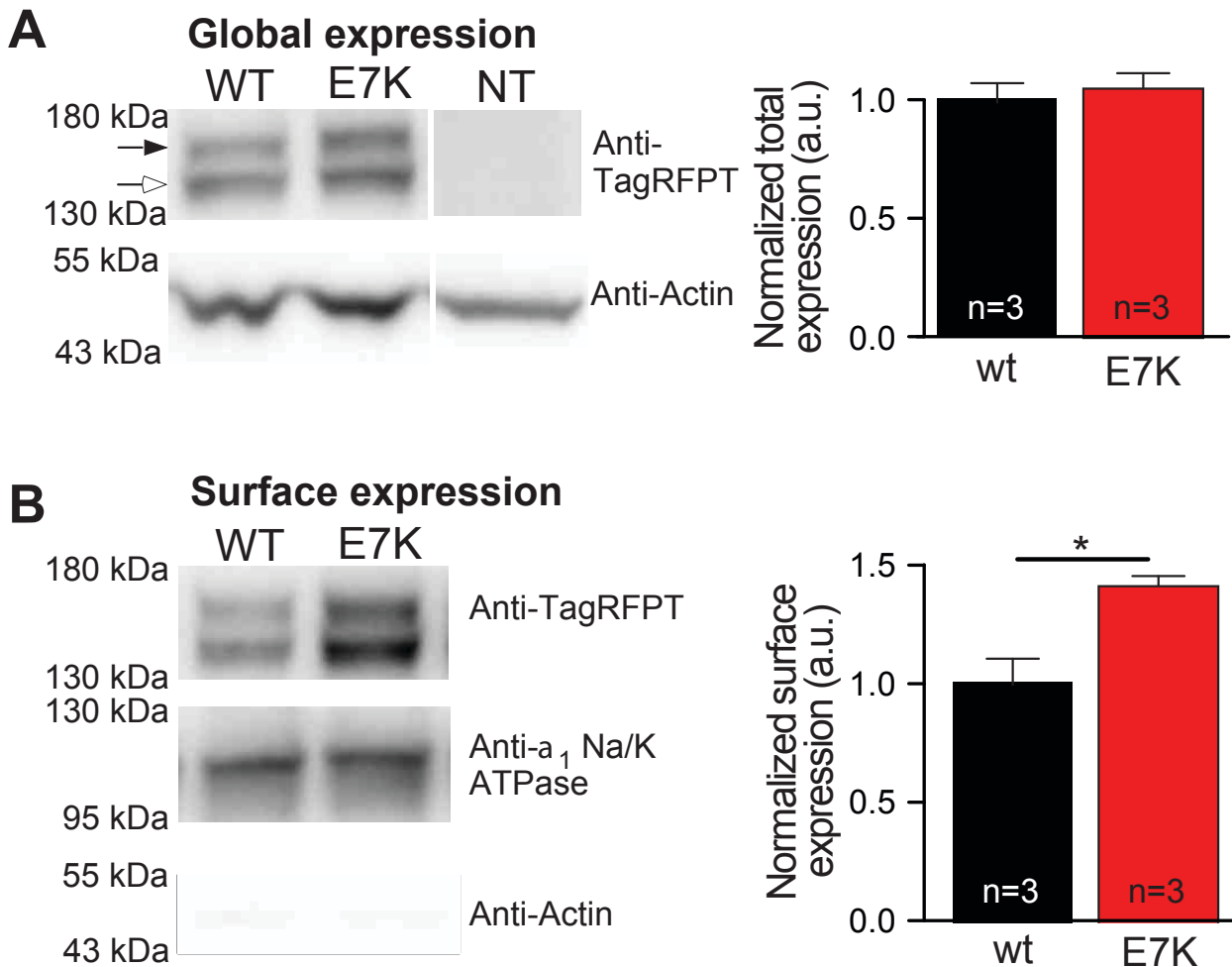
Figure 3.1.5 Expression of TRPM4^{wt} and TRPM4^{E7K}.

Cellular expression of TRPM4^{wt} and TRPM4^{E7K} shown in (A) and plasma membrane expression shown in (B). With the white and black arrowheads representing highly-glycosylated and core-glycosylated forms of TRPM4, respectively. TRPM4 protein was stained with anti-TagRFPT antibodies. Staining with anti-Actin and anti-Na$^+$/K$^+$ ATPase alpha1 antibody served as loading control for the total and surface level, respectively. Modified from [206]

3.1.3 A432 is a crucial amino acid to modulate TRPM4's properties

3.1.3.1 Gain-of-function in TRPM4^{A432T} is associated with aberrant deactivation kinetics.

TRPM4^{A432T} has been associate with human cardiac conduction diseases, such as the isolated cardiac conduction disease[61] and childhood atrioventricular block[93], but the mechanisms leading to such diseases are largely unclear and discussed controversially. Taking the advantage of the UV-flash assay, I employed fast photolytic uncaging of caged Ca^{2+} to study TRPM4's properties.
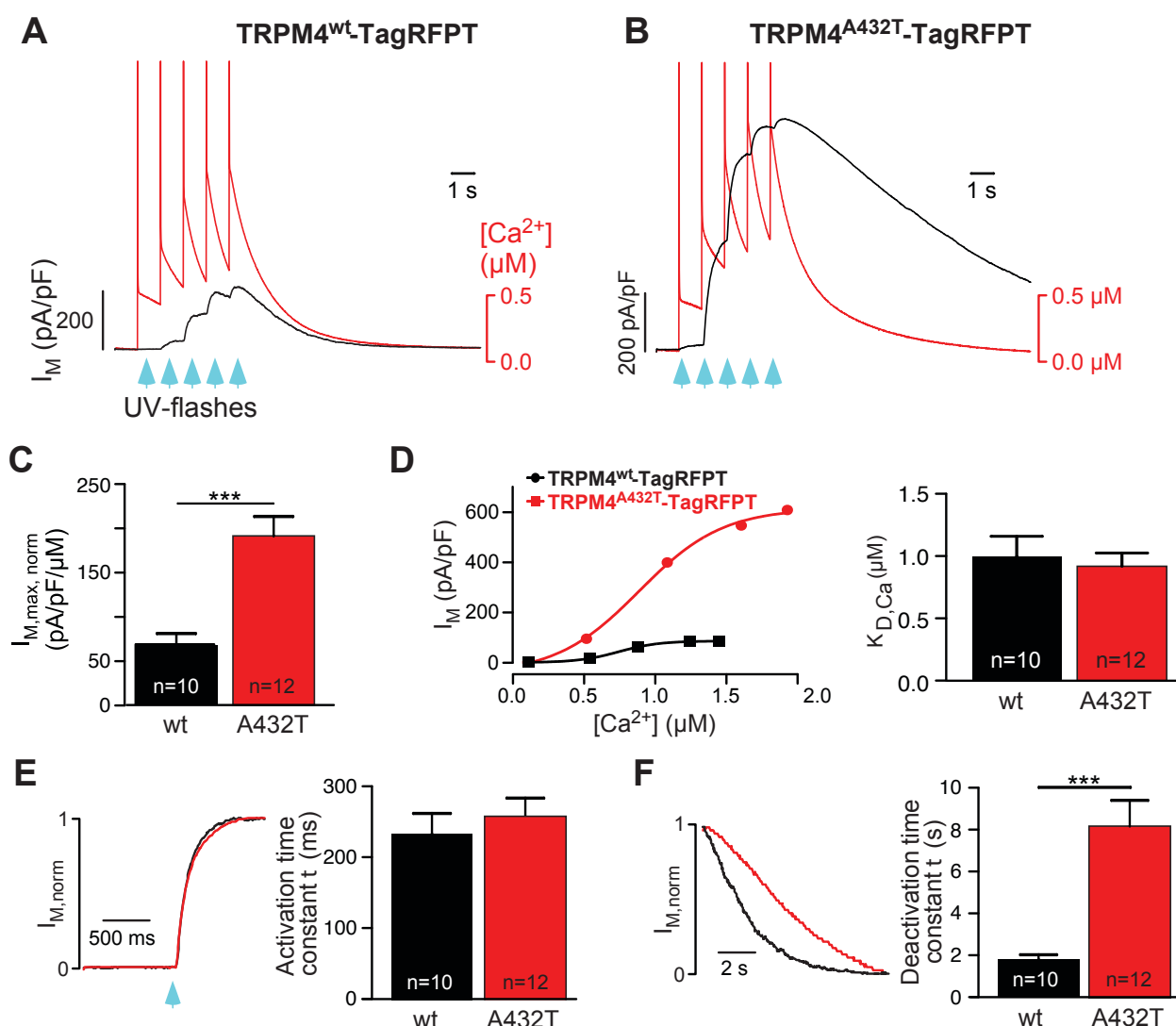
Figure 3.1.6 TRPM4[A432T] mutation displays altered kinetic properties in dynamic Ca^{2+} assay.
TRPM4 currents were activated by UV-flashes in HEK293 cells transiently expressed TRPM4[wt] (A) and TRPM4[A432T] (B) in the whole-cell patch clamp configuration at a holding potential of +80 mV. Currents are indicated in black, the Ca^{2+} concentrations are in red. Statistical analysis of the membrane current density is depicted in (C). (D) Exemplified current/Ca^{2+} relationships for TRPM4[wt] (black) and TRPM4[A432T] (red) (left panel) and statistical summary (right panel). Ca^{2+} dependent activation (E) and deactivation (F) of TRPM4 variants. Modified from [206].

As described above, I constructed the mutation TRPM4[A432T] and transiently expressed it in HEK293 cells. The holding potential was +80 mV during trains of UV-flashes to activate TRPM4 currents (Figure 3.1.6 A and B). Current recordings during trains of UV-flashes indicated a substantial increase in the normalized membrane current (Figure 3.1.6 A, B and C, 190.7±21.82 pA/pF/µM vs. 68.03±12.70 pA/pF/µM for TRPM4[A432T] and TRPM4[wt], respectively). The Ca^{2+} sensitivity of both TRPM4 variants was not changed, the apparent $K_{D,Ca}$ in both TRPM4[wt] (0.9814±0.1638 µmol, n=10) and

TRPM4^{A432T} (0.9085±0.1051 µmol, n=12) depicted no significant difference. Noteworthy, my kinetic analysis revealed aberrant deactivation kinetics that were slowed down by a factor of four from 1.939±0.2213 s (n=10) in wt to 8.167±1.049 s (n=7) in A432T variant (Figure 3.1.6 F).
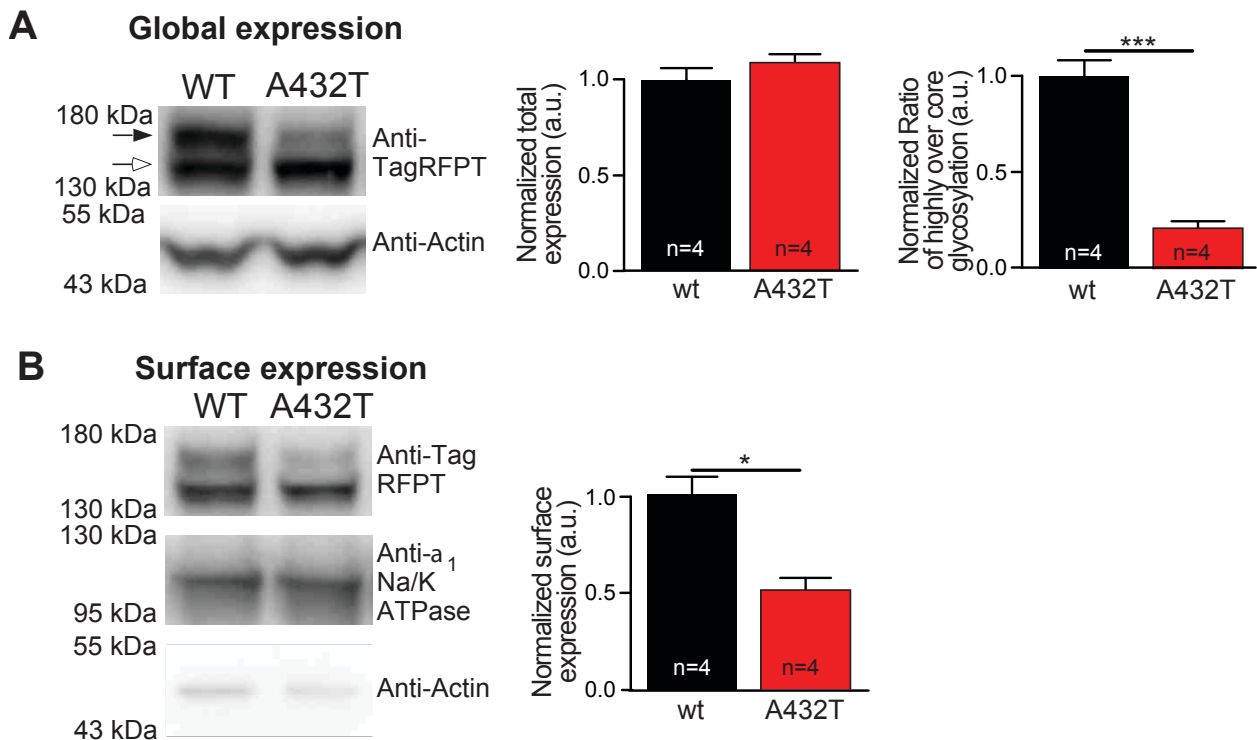
Figure 3.1.7 Decreased plasma membrane protein for TRPM4^{A432T}.
Exemplified western blots of whole cell lysates (A, left) and the statistical analysis of global expression (A, middle) and normalized ratios of highly-glycosylated and core-glycosylated TRPM4 proteins (A, right). Surface expression exemplified in (B, left) and statistical summary in (B, right) Modified from [206].

Further investigations of the protein expression revealed the characteristic highly- and core-glycosylated proteins in whole cell lysates (Figure 3.1.7 A, marked by the closed and open arrowheads, respectively)[45]. Additionally, the global protein expressions were indistinguishable (Figure 3.1.7 A). I found a substantial reduction in the presence of the highly-glycosylated protein. In the TRPM4^{A432T} mutant the occurrence of the highly-glycosylation was only 20% of that of the wt protein (Figure 3.1.7 A, right). The ratios of highly-glycosylation and core-glycosylation were 0.9175±0.07612 (n=6) and 0.1958±0.03220 (n=3) in TRPM4^{wt} and TRPM4^{A432T}, respectively. Unexpectedly, Western blot analysis of the surface expression (Figure 3.1.7 B) indicated a substantially reduced membrane expression in TRPM4^{A432T} (around 50% lower; Figure 3.1.7 B, right).

The investigations in HEK293 cells have shortcomings when compared to the cardiac myocytes. One of the most prominent is the obvious absence of other contributing current components, such as the Na^+/Ca^{2+} exchanger or the plethora of potassium currents that shape the cardiac action potentials. I further scrutinized my results on human induced pluripotent stem cell-derived cardiac myocytes (hiPS-CMs), which have been infected with TRPM4^{wt} and TRPM4^{A432T} adenovirus.
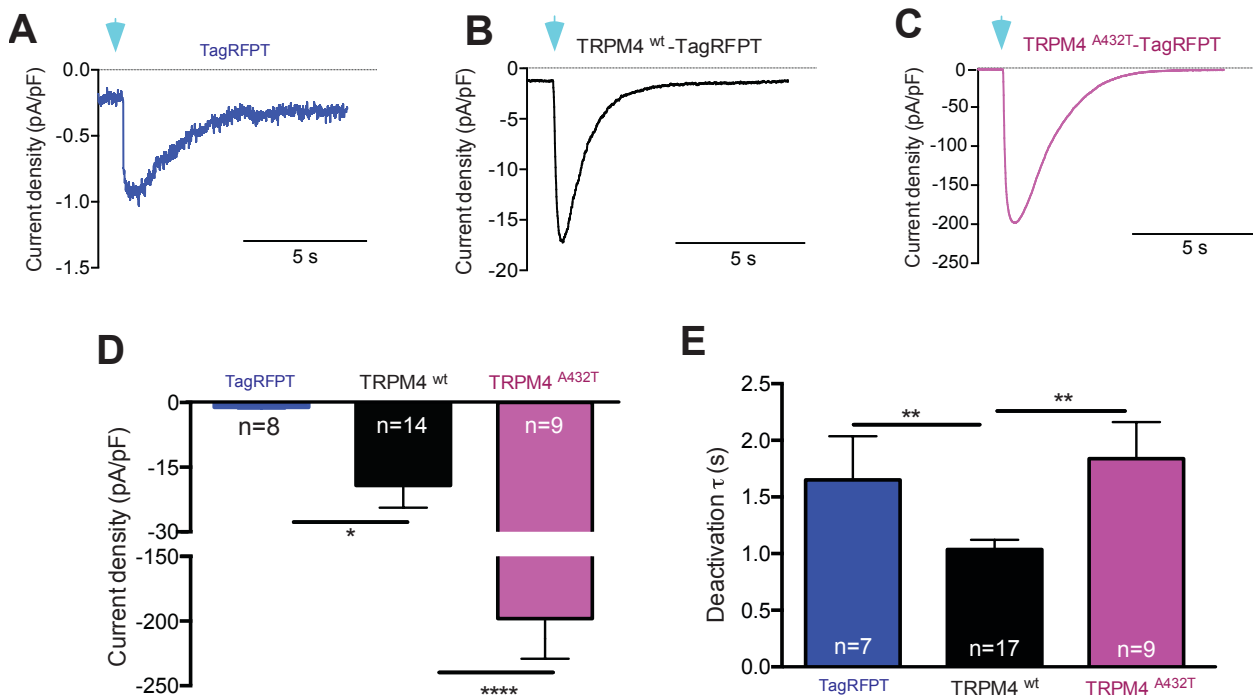
Figure 3.1.8 TRPM4^{A432T} exhibits aberrant deactivation kinetics in hiPS-CMs.

Current recorded in hiPS-CMs infected with TagRFPT (A), TRPM4^{wt} (B) and TRPM4^{A432T} (C) virus, respectively. (D) summarizes the current density and (E) depicts the deactivation time constant. Note the different scales for the membrane currents for A-C.

As shown in Figure 3.1.8, when hold at -80 mV, in hiPS-CMs transfected with Tag-RFPT virus, the naïve Ca^{2+} activated-currents was on average 1.2±0.29 pA/pF, while the current density increased to 198.1±31.1 pA/pF (n=9) following TRPM4^{A432T} expression, which was almost 10 times of the current density in TRPM4^{wt} (19.2±5.15 pA/pF, n=14) as shown in Figure 3.1.8 D. When I compared the deactivation kinetics of the TRPM4 channels, the naïve Ca^{2+} activated-currents displayed a slower deactivation kinetic (1.650±0.3867 s, n=7) than that of TRPM4^{wt} (1.036±0.08574 s, n=9). The deactivation kinetic of TRPM4^{A432T} (1.839±0.3217 s, n=17) was nearly one-fold slower than that of TRPM4^{wt} as summarized in Figure 3.1.8 E.

3.1.3.2 TRPM4^{A432T} generates excessive membrane current during human cardiac action potentials.
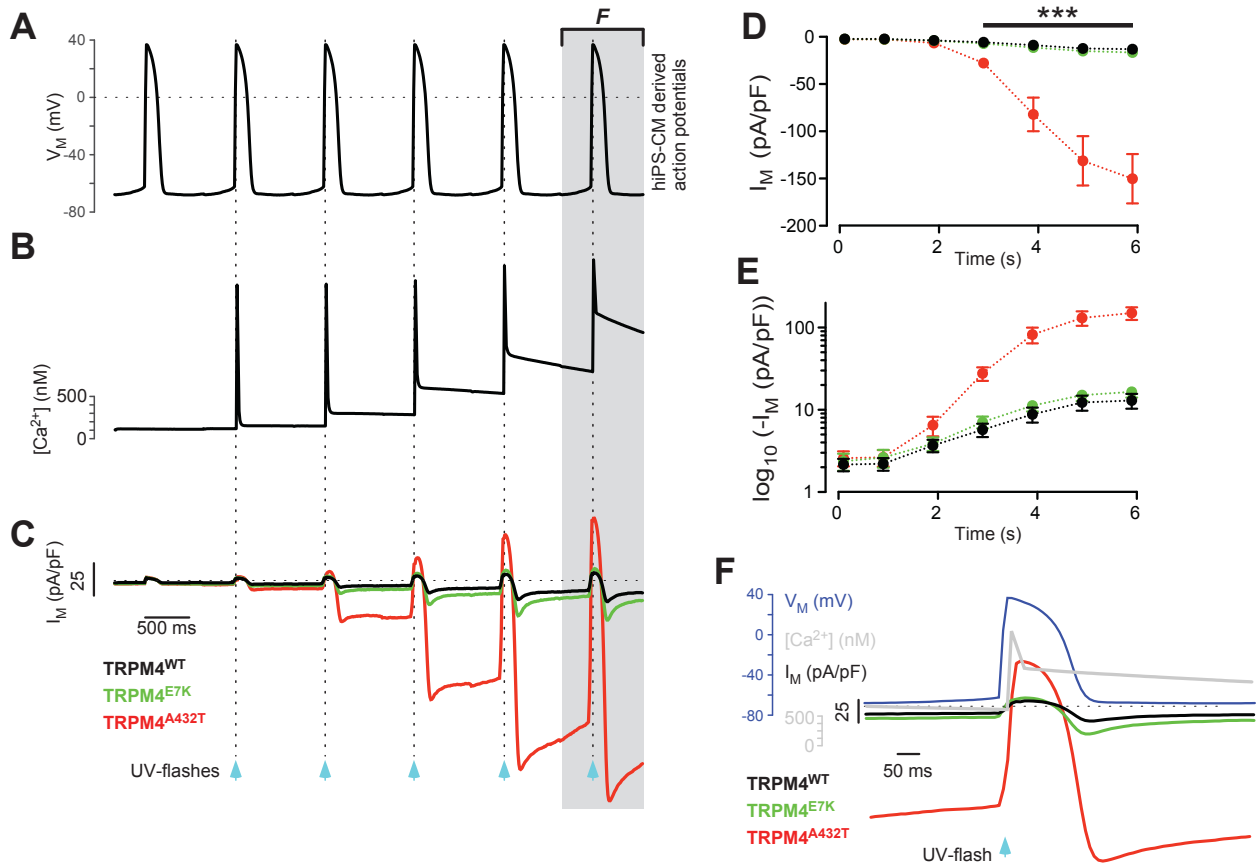
Figure 3.1.9 Membrane currents of TRPM4 variants during human ventricular action potentials. Ventricular action potentials were recorded in human induced pluripotent stem cells-derived cardiac myocytes (hiPS-CMs) from a control patient and used as a potential template for play-back in voltage-clamped HEK293 cells expressing TRPM4 variants. Vertical dashed lines indicate time points for the UV flashes applied to the NP-EGTA loaded cells. (A) Action potentials from a typical ventricular hiPS-CM. (B) Resulting representative trace for the intracellular Ca^{2+} concentration. (C) Typical membrane currents resulting from the command voltage profile shown in (A). HEK293 cells expressed TRPM4wt (black), TRPM4^{E7K} (cyan) and TRPM4^{A432T} (red) proteins. (D-E) Statistical analysis of a population of HEK293 cells. Membrane currents were probed at the time points indicated by the numbers (1-6) in (C) and plotted against the time point. Color-coding corresponds to the colors used in (C). Note the linear scale in (D). For (E) we replotted the values on a semi-logarithmic scale to allow appreciation of the lower current components. Taken from [206].

To obtain additional insights into the putative disease contribution of the A432T mutation in modifying the cardiac myocyte´s electrophysiology, especially also in comparison to the well characterized E7K mutation, I recorded action potentials in identified ventricular-like hiPS-CMs as described recently[207]. I used such action potentials as templates for voltage-clamp experiments in HEK293 cells expressing different variants of TRPM4 (Figure 3.1.9 A). Additionally, I triggered Ca^{2+} release (Figure 3.1.9 B) immediately after the onset of the action potentials (vertical dashed lines in Figure 3.1.9) to mimic increases in Ca^{2+} that accompany cardiac action potentials. The wt and the TRPM4^{E7K} displayed small membrane currents and showed no significant difference (black and cyan trace and symbols in Figures 3.1.9 C, D and E). These findings and the ones described in Kruse and co-workers[59] were in line with the observation that this mutation increased the membrane current density leaving the other properties unchanged. In contrast to that, the TRPM4^{A432T} variant, owing to its substantially altered deactivation kinetics, depicted majorly deformed and progressively increasing membrane currents (red trace and symbols in Figure 3.1.9 C, D and E) following Ca^{2+} activation. Thus, even though both TRPM4^{E7K} and TRPM4^{A432T} are gain-of-function mutations, they made very different contributions to membrane currents during cardiac action potentials based on their distinct underlying mechanisms. These data strongly suggest that indeed alterations in the kinetic properties of TRPM4 contribute to human cardiac arrhythmia.

3.1.3.3 TRPM4^{A432T}'s abnormal deactivation kinetics are not controlled by glycosylation, cPKC-dependent phosphorylation or Ca^{2+} dependent changes in the plasma membrane PIP$_2$ levels.

In the following, I performed additional studies to gain further insight into the mechanisms underlying the aberrant deactivation kinetics of the TRPM4^{A432T} mutant.

Glycosylation is the principal form of post-translational modification of the TRPM4 protein[46]. I wondered whether the reduced protein glycosylation in A432T (Figure 3.1.7 A) might be causally related to the channel´s altered deactivation and thus envisaged an experimental intervention to modulate TRPM4´s glycosylation in the wt protein. Tunicamycin is an antibiotic known for its property to potently decrease protein glycosylation[46]. As shown in Figure 3.1.10 A, Tunicamycin treatment (10 µg/ml for 24 hours) indeed reduced the highly-glycosylated band and accumulated the core-

glycosylated band. The ratio of highly-glycosylation and core-glycosylation was significantly reduced more than 50% by the treatment when compared to that of control (DMSO), but interestingly the deactivation of TRPM4 channel did not change as shown in Figure 3.1.10 B. These results indicated changes of glycosylation by Tumicamycin or in the A432T mutant were not the reason for the slower deactivation of the TRPM4[A432T] channel.
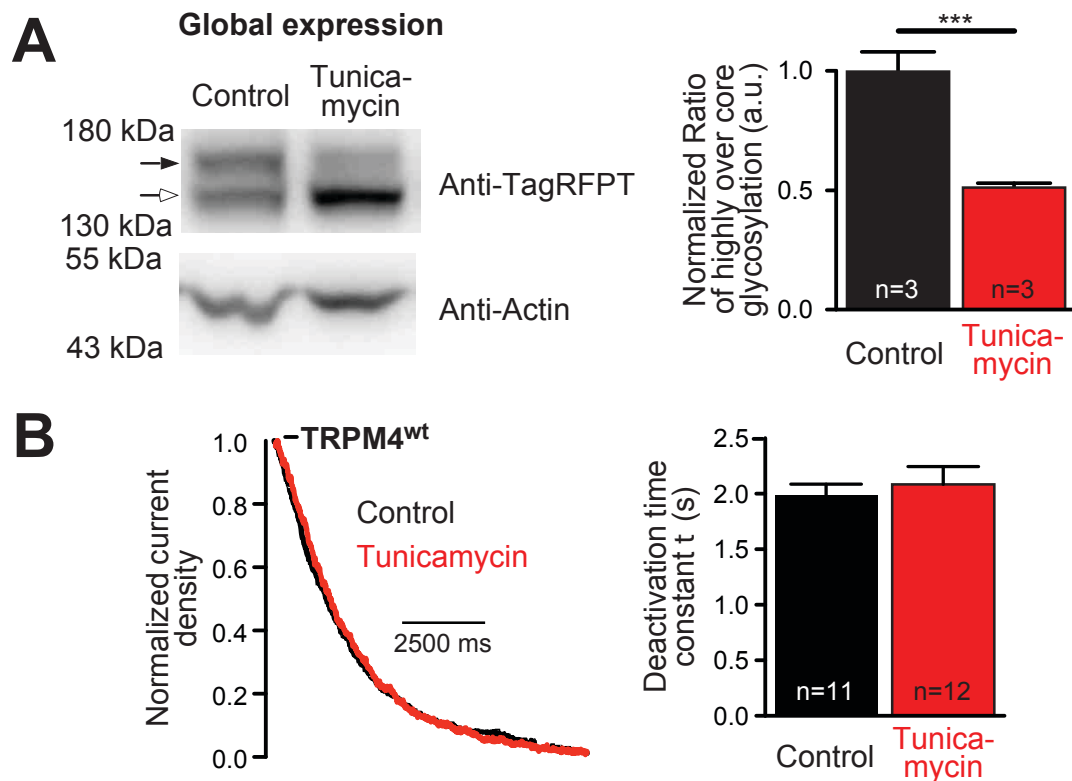
Figure 3.1.10 Tunicamycin fails to alter the deactivation of TRPM4.

(A) HEK293 cells transiently expressed TRPM4[wt] were pre-treated with Tunicamycin (10 µg/ml; 24 hours) and the resulting effects are summarized. The total expressions of TRPM4 protein with or without Tunicamycin treatment are depicted in the left pane. The right panel indicates changes of glycosylation of TRPM4 described as the ratio of highly- over core-glycosylated protein. (B) typical deactivation currents of TRPM4 with or without Tunicamycin pre-treatment are normalized by the maximal current amplitude (left). Deactivation time constants are statistically analysed (right). Modified from [206].

While the TRPM4[wt] protein contains multiple putative PKC phosphorylation sites[40], the A432T mutation adds yet another Threonine available for phosphorylation and I investigated whether Ca^{2+}-dependent cPKC-mediated TRPM4 phosphorylation might be affecting deactivation kinetics. GÖ6983, an PKC inhibitor for several PKC isozymes (PKCα, PCKβ, PKCγ, PKCξ)[208], was applied in patch clamp recordings. Cells

transiently expressing TRPM4^{wt} and TRPM^{A432T} were both incubated with 1 μM GÖ6983 for 10 minutes at room temperature. None of the variants, TRPM4^{wt} nor TRPM^{A432T}, showed changes in the deactivation time constants before and after GÖ6983 treatment as shown in Figure 3.1.11. These results depicted that the cPKC induced phosphorylation was unable to alter the deactivation kinetics in either TRPM4 variants.
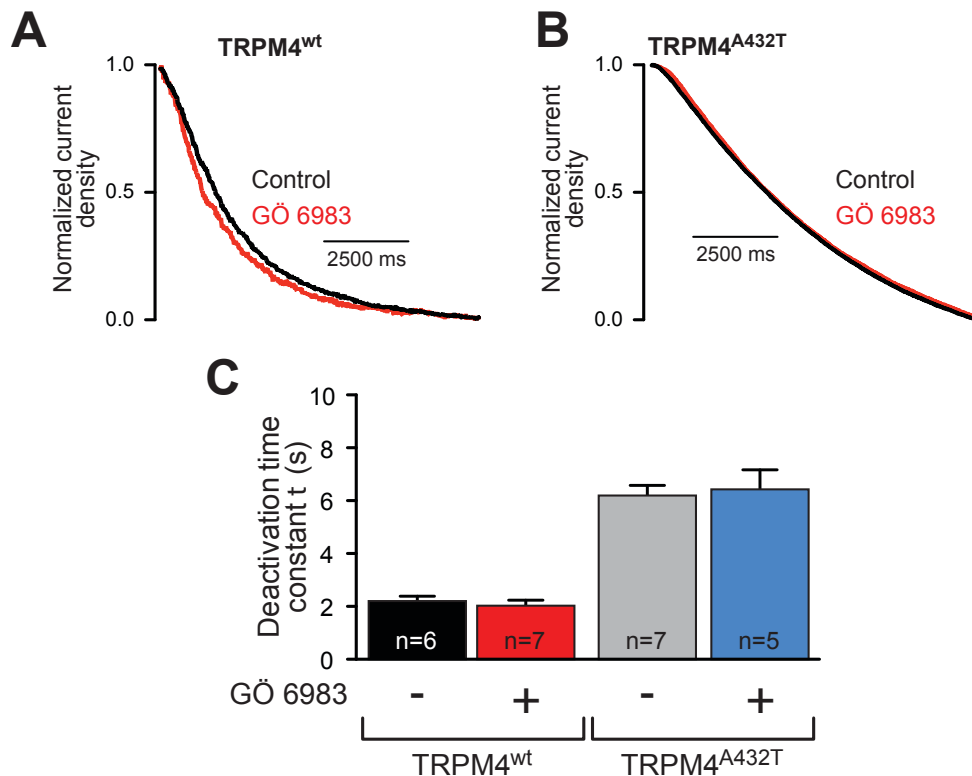
Figure 3.1.11 cPKC inhibitor GÖ6983 (1 μ M) fails to altered the deactivation of TRPM4 variants. (A) and (B) illustrate the normalized inactivation current recorded in TRPM4^{wt} and TRPM4^{A432T} with or without GÖ 6983 treatment, respectively. The Statistic analysis is summarized in (C). Modified from [206].

Phosphatidylinositol 4,5-biphosphate (PIP$_2$) was reported to regulate the function of the TRPM4 channel and its administration counterbalanced TRPM4's desensitization to Ca^{2+} in inside-out patches and overcame the rundown of TRPM4 currents in whole-cell patch-clamp recordings[41]. PIP$_2$ was regarded as a regulator for the gating of TRPM4 channels and could rescue them from desensitization[51]. Thus I investigated whether changes in the plasma membrane PIP$_2$ content following UV-flash mediated Ca^{2+} increases and Ca^{2+} dependent activation of e.g. PLCδ might contribute to the altered deactivation behavior of the TRPM4 protein. U73122 (10 μM) is a potent inhibitor of PLCs[208], but its application did not alter the deactivation of TRPM4^{wt} (Figure 3.1.12

A). Despite the reported increased TRPM4^{wt} current density[209], the activation was also unchanged (see Figure 3.1.12 B).
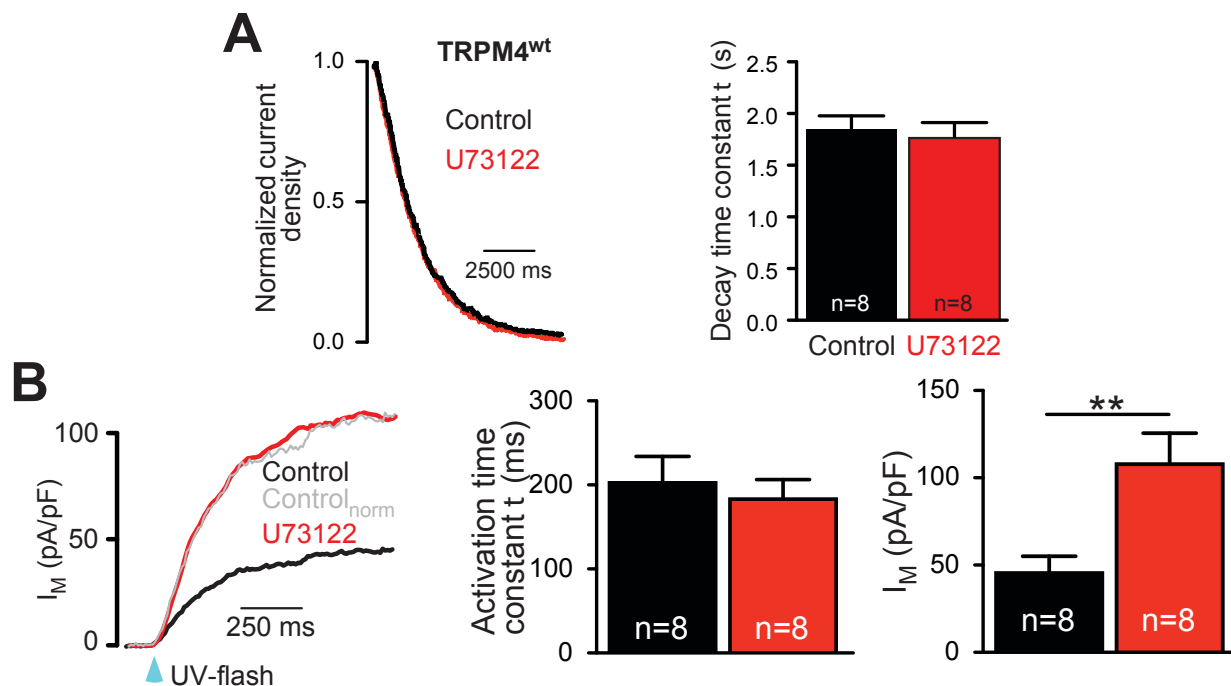
Figure 3.1.12 Effects of PLCs inhibitor U73122 on of TRPM4 channel.

(A) illustrates the normalized inactivation kinetics in TRPM4^{wt} expressing cells with or without U73122 treatment. (B) U73122 increases membrane currents (right panel) without altering its activation kinetics (left and middle panel). Grey trace in the left panel represents a scaled version of the control trace to indicate similar activation kinetics. Modified from [206].

These data clearly indicated that neither an altered glycosylation nor cPKC-induced phosphorylation or accumulation of PIP$_2$ on plasma membrane contributed to the altered TRPM4^{A432T} deactivation.

3.1.3.4 The bulkiness of the amino acid at position 432 modulates the properties of TRPM4 channels

The A432T mutation was associated with a plethora of changes in the channel´s behavior, notably, 4-times slowed down deactivation, almost 3-fold increased current density despite a reduced surface expression and a decreased presence of the highly-glycosylated protein. All of these findings suggested that the A432 position in the TRPM4 protein might represent a key site determining many of the TRPM4's channel properties. The new Threonine at this position might be causally linked to the altered properties. I therefore conducted a more systematic mutation analysis of this amino acid at position 432.
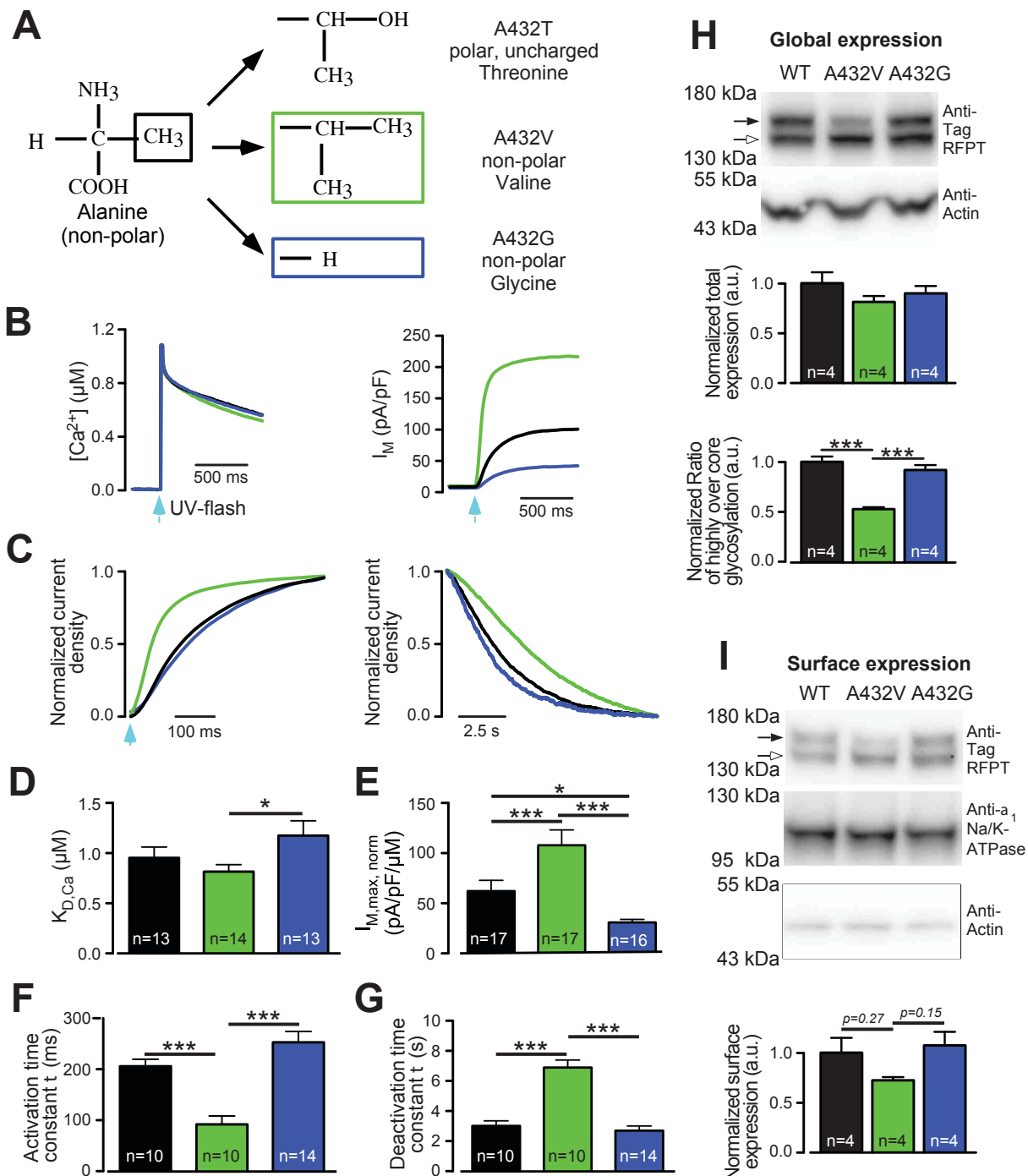
Figure 3.1.13 Bulkiness of the amino acid at position 432 is critical for TRPM4´s properties.

(A) Structure and polarity of TRPM4 variants. Colour coding for this figure indicated by the colour of the rectangles. (B, left panel) illustrates the UV-flash photolysis-induced Ca^{2+} jumps and the resulting activation time course of the induced membrane current (B, right panel). (C) depicts the normalized activation (left) and deactivation (right) membrane currents. (D-G) Summarized the statistical evaluation of the given parameters. (H-I) Depicts the expression analysis of three TRPM4 variants on the global level (H) and the plasma membrane level (I). The analysis of the ratio of highly-glycosylated and core-glycosylated TRPM4 proteins are summarized in the bottom panel of (H). Modified from [206].

In TRPM4^{wt}, Alanine432 possesses a non-polar, small side chain. In the following set of experiments, I modulated the bulkiness of residues' side chain at site 432 by substituting Alanine either by the smallest possible non-polar amino acid, Glycine, or by a slightly bulkier amino acid, Valine (Figure 3.1.13 A). As shown in Figure 3.1.13, even such small changes at position 432 caused substantial alterations of the channel´s properties. Increasing the size of residue's side chain (TRPM4^{A432V}) enhanced the membrane current densities and resulted in a substantial gain-of-function (Figure 3.1.13 B, right and E). As indicated in Figure 3.1.13 C (right panel) and G, TRPM4^{A432V} displayed a slower deactivation. The deactivation time constant (7.262±0.5224 s, n=10) was 2-fold more than that of the wt protein (3.187±0.3498 s, n=10). Interestingly, this was associated with a faster activation (Figures 3.1.13 C, left and F). Nevertheless, I didn't find any significant differences on membrane protein expressions between TRPM4^{A432V} and TRPM4^{wt} (Figure 3.1.13 I), while the presence of the highly-glycosylated protein was significantly reduced in TRPM4^{A432V} in comparison to TRPM4^{wt} (Figure 3.1.13 H top and bottom panels). In contrast, reducing the bulkiness of the residue's side chain (substitution by Glycine), I found opposite effects for almost all the parameters tested when compared to the Valine substitution. The Glycine substitution (TRPM4^{A432G}) can best be described as a loss-of-function mutation with less membrane current density in comparison to the wt channel (Figure 3.1.13 B and E). With a slightly increased apparent $K_{D,Ca}$ (Figure 3.1.13 D), TRPM4^{A432G} displayed unchanged activation and deactivation properties when compared to TRPM4^{wt} (Figure 3.1.13 F and G). Besides, protein expression and protein glycosylation were also unchanged by this TRPM4^{A432G} mutation (Figure 3.1.13 H and I). These data supported the notion that the bulkiness of the amino acid at position 432 regulated the gating properties of TRPM4 channel.

Besides, I constructed another two mutations, TRPM4^{A432D} (negative charge) and TRPM4^{A432K} (positive charge) to further investigate the effects of substituting the Alanine^{432} by charged residues (Figure 3.1.14). Surprisingly, both of these mutations (TRPM4^{A432D} and TRPM4^{A432K}) lacked substantial Ca^{2+} activated currents (Figure 3.1.14 B and C). Despite similar global protein expression and the reduced plasma membrane expression solely shown in TRPM4^{A432D} but not in TRPM4^{A432K} (Figure 3.1.14 E and F). Notably, expression of the highly-glycosylated protein was greatly reduced for both modifications (Figure 13.1.14 E).
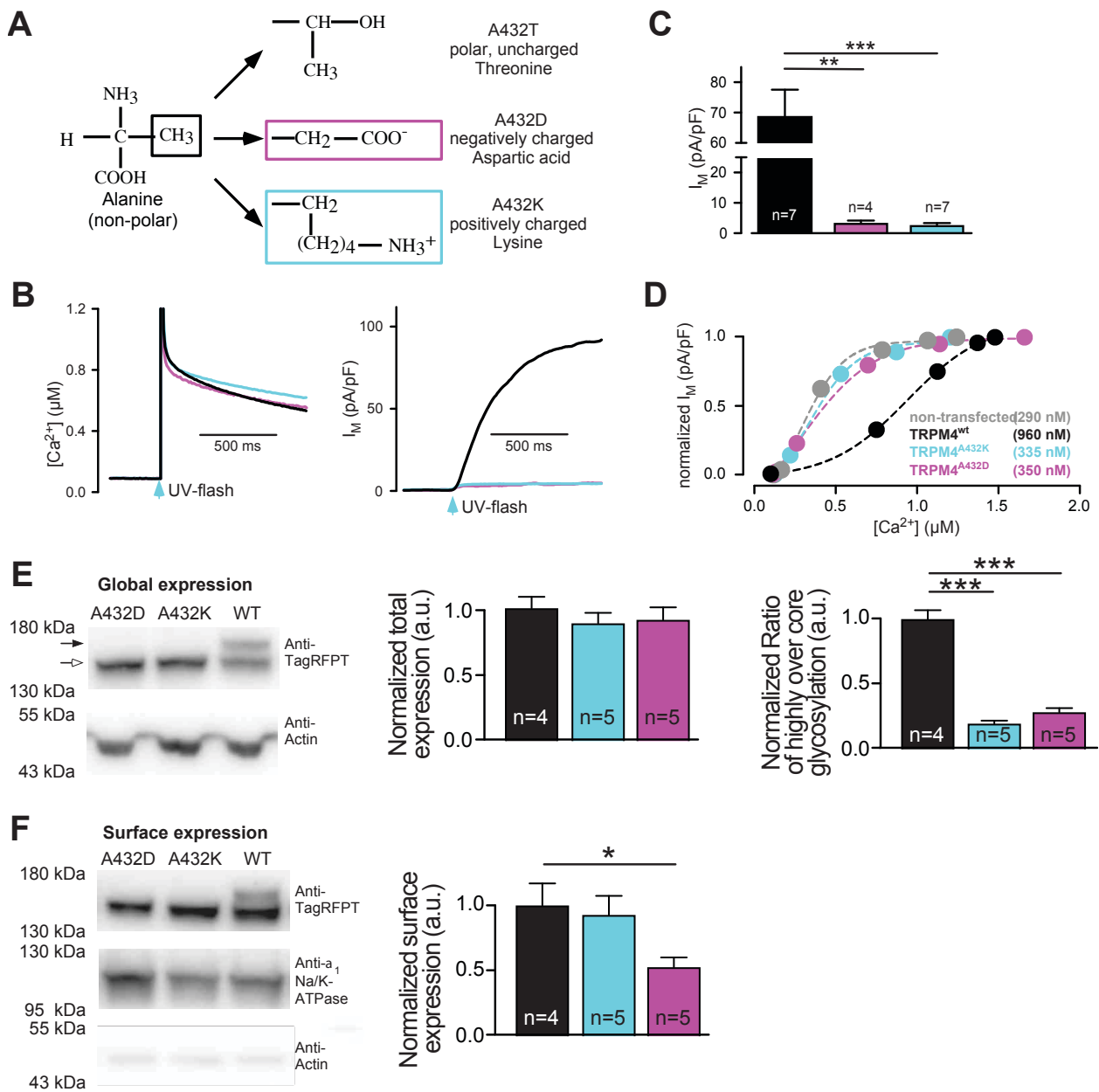
Figure 3.1.14 Charged residue substitutions at site 432 render TRPM4 channel non-functional.

(A) Structure and charges of TRPM4 variants. Colour coding for this figure indicated by the colour of the rectangles. (B, left panel) illustrates the Ca^{2+} jumps induced by UV-flash photolysis and the resulting membrane currents are shown in (B, right panel). (C) summarizes the maximal current densities activated by Ca^{2+} in a train of UV-flashes. (D) displays typical membrane current/Ca^{2+} relationship for the TRPM4 variants depicted and non-transfected HEK293 cells (grey). Expression analysis of the three TRPM4 variants is shown in (E) for global level and (F) for plasma membrane level. The arrows in (E) highlight the highly- and core-glycosylated (closed and open arrowhead, respectively) TRPM4 variant. The ratio of highly glycosylated and core glycosylated TRPM4 proteins are analysed and summarized in the right panel of (E). Modified from [206]

When I compared the resulting current/Ca^{2+} relationships I found that the Ca^{2+} activated membrane currents in HEK293 cells expressing TRPM4^{A432D} and TRPM4^{A432K} resembled the properties of currents recorded in non-transfected cells rather than those currents from TRPM4 expressing cells (Figure 3.1.14 D). Based on these results I concluded that both mutations (TRPM4^{A432D} and TRPM4^{A432K}) did not generate Ca^{2+}-activated membrane currents.

3.1.3.5 Mutations at position 432 change the compactness of TRPM4´s MHR3 domain

The MHRs are identified as homology regions within the TRPM family. Based on recent publications on the 3D structure of the TRPM4 protein position 432 locate in the MHR3 domain, which bridges the MHR1/2 and MHR4 domain[210,211]. The reported structures of TRPM4 provide a suitable template for structural modeling. With the help of Dr. Hongmei Wang from Prof. Flockerzi's lab, we proposed a scheme that might assist in appreciating the underlying molecular mechanism (Figure 3.1.15).

we performed simulations and refinements of TRPM4's structure and compared the changes within the MHR3 domain between wt and mutant proteins. The Alanine432 could form hydrophobic interactions with its surrounding residues V401, P438 and F440 and maintain a stable structure for normal function of TRPM4 channel (Figure 3.1.15 A). Substitution of Alanine by Threonine in the TRPM4^{A432T} mutant results in increased interactions between the amino acid at position 432 and its surrounding residues (V401, R437, P438, F440, V441 and L444), and such a molecular mechanism might eventually result in a more compact structure of MHR3 domain (Figure 3.1.15 B). We identified a similar mechanism for the TRPM4^{A432V} mutant (Figure 3.1.15 D). In the TRPM4^{A432G} mutant structure, lack of side chain, the Glycine lost the interactions with its surrounding residues and form a random coil in the MHR3 domain (Figure 3.1.15 D). Due to the bulkiness of Aspartate and Lysine, TRPM4^{A432D} and TRPM4^{A432K} mutants could interact with its surrounding residues L397, V401, F414 R437, P438, F440, V441 and L444 to form strong repulsion forces which affect the movement of surrounding helix, consequently destabilizing the MHR3 domain (Figure 3.1.15 E&F).

Based on the structure modeling, I proposed that the mutations at the position 432 altered the behavior of TRPM4 channels because of the modification of the

compactness of the MHR3 domain, which might further affect other domains in the TRPM4 protein.
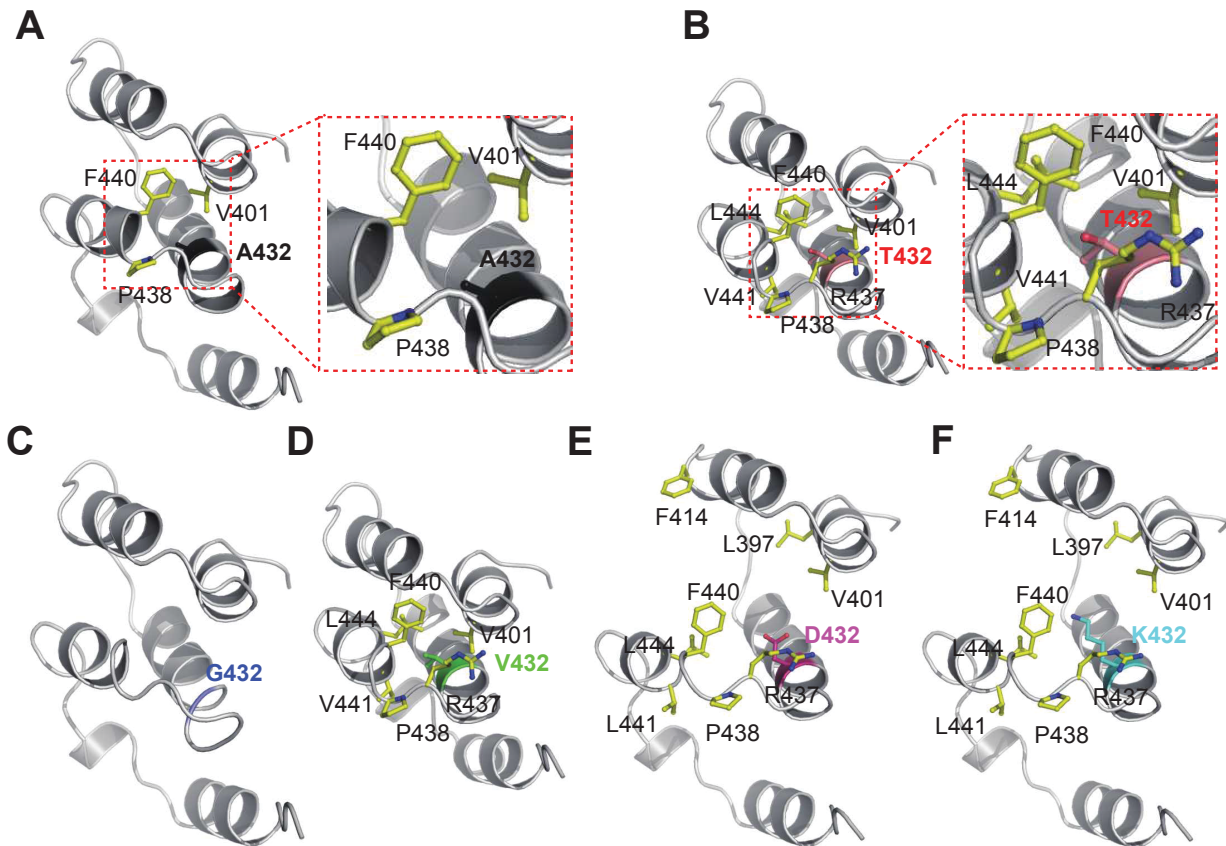
Figure 3.1.15 Structure of TRPM4´s MHR3 domain.

(A) The alanine432 forms hydrophobic interactions with adjacent residues V401, P438 and F440 (A, insert) in the TRPM homology region (MHR) 3 domain. (B) In the A432T variant, the threonine interacts with additional residues (V401, R437, P438, F440, V441 and L444; B, insert) forming a more compacted MHR3 domain. (C) The glycine of A432G loses the interactions with its surrounding residues and form a random coil. (D) The valine residue of A432V, like the A432T variant, favors more interactions with its surrounding residues yielding a more compact MHR3 domain in comparison to the wild-type. Substitution of A432 by negatively charged residue (E) or positively charged residue (F) may promote interactions with residues L397, V401, F414, R437, P438, F440, V441 and L444, which affect the surrounding helix movement and destabilize the MHR3 domain. The structure is based on the coordinates of human TRPM4[210] (PDB code 5WP6). Taken from [206]

3.1.3.6 The artificial mutation R1062Q speeds up TRPM4´s deactivation kinetics and counterbalances the aberrant function of TRPM4^{A342T}

TRPC, TRPM, and TRPV channels contain a so-called TRP domain, which refers to a homologous block of residues following the S6 segment at the C-terminus of the

protein[212]. The most conserved sequence in the TRP domain is the TRP box motif comprising six amino acids (EWKFAR) in the TRPC subfamily or five amino acids (WKFQR) in the TRPM subfamily[36,213]. The TRP box plays an important role in regulating the function of TRP channels. In the TRPV4 channel, the TRP box was reported to stabilize the closed state of the channel by interacting with the S4-S5 linker[214]. Another study revealed that a mutation of the positively charged amino acid of the TRP box reduced the PIP_2 sensitivity of the TRPM8 channel[215]. Nillius *et al*. reported that the TRP box is not the main domain for PIP_2 interaction in the TRPM4 channel. Interestingly, the mutant TRPM4[R1062Q] within the TRP box indeed changed the kinetics of TRPM4 showing a faster deactivation and a decreased peak current[41].

In the following experiment, I investigated a putative functional rescue of the altered deactivation kinetics of TRPM4[A432T] mutant by combining the artificial mutation R1062Q with A432T. I wondered whether such a faster deactivation (with R1062Q in the TRP box motif) would functionally rescue the slow deactivation caused by the TRPM4[A432T] mutation.

I thus compared the properties of TRPM4 proteins carrying A432T and R1062Q single or double mutations and the wt protein with particular emphasize on activation and deactivation kinetics (Figure 3.1.16 A and B). With an assay employing a single UV-flash, the TRPM4[R1062Q] (blue traces and bars in Figure 3.1.16 A and B) current was characterized by a significantly faster activation (133.0±9.512 ms) and deactivation kinetics (1.976±0.15 s) compared to the wt protein (211.7±21.69 ms and 2.92±0.26 s, respectively, black traces and bars in Figure 3.1.16 A and B). Notably the double mutant TRPM4[A432T, R1062Q] showed a faster activation (123.5±16.07 ms) with a 'compensatory action' on the deactivation, which was substantially reduced from 9.49±0.74 s (A432T, res traces and bars in Figure 3.1.16 A and B) to 4.41±0.45 s (double mutant, magenta traces and bars in Figure 3.1.16 A and B). It is noteworthy to mention that deactivation in the double mutant was still slightly slower than that in the wt protein. Despite the lack of differences in their Ca^{2+} sensitivity (Figure 3.1.16 C), a similar 'compensatory effect' was also found for the membrane current density. The TRPM4[A432T] mutant displayed an increased current density, while the double mutants´ current density was reduced more than 50% from 153.8±15.36 pA/pF/µM (n=13) (TRPM4[A432T]) to 72.38±11.41 pA/pF/µM (n=13). This value was significantly larger than that of TRPM4[R1062Q] (32.35±6.01

pA/pF/µM, n=14) but indistinguishable from the wt protein (47.89±8.91 pA/pF/µM, n=14) (Figure 3.1.16 D).
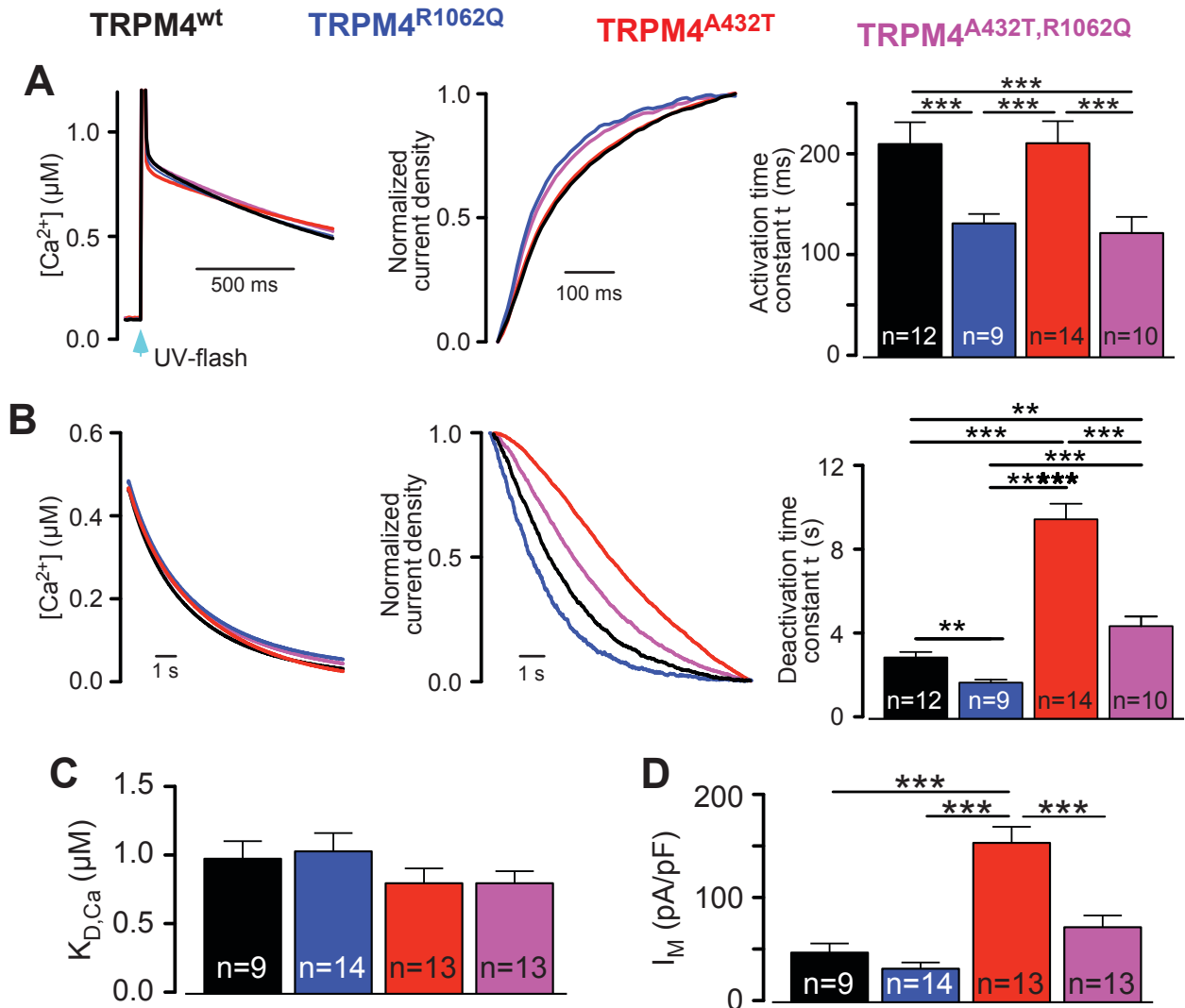
Figure 3.1.16 Artificial mutation R1062Q counterbalanced the aberrant electrophysiological properties observed in the A432T mutant.

(A, middle) depicts membrane current activated by Ca^{2+} jumps shown in (A, left) under the UV-flash pulse stimulation. Normalized membrane currents are summarized in (A, right). (B, left and middle) displayed the Ca^{2+} decay and current deactivation of TRPM4 variants, respectively. Deactivation time constants are collected in (B, right). The $K_{D,Ca}$ and membrane currents are shown in (C) and (D), respectively.

A Western-blot analysis of the cellular (Figure 3.1.17 A) and plasma membrane (Figure 3.1.17 B) expression depicted similar expression levels for TRPM4[wt], TRPM4[R1062Q] and TRPM4[A432T/R1062Q], but an almost total loss of the highly-glycosylated proteins for the double mutant TRPM4[A432T/R1062Q] (Figure 3.1.17 C).

These results clearly indicated that the R1062Q mutant within the TRP box was able to modulate the gating of the TRPM4 channel and displayed the ability to partially rescue the aberrant behavior of TRPM4^{A432T} mutation.
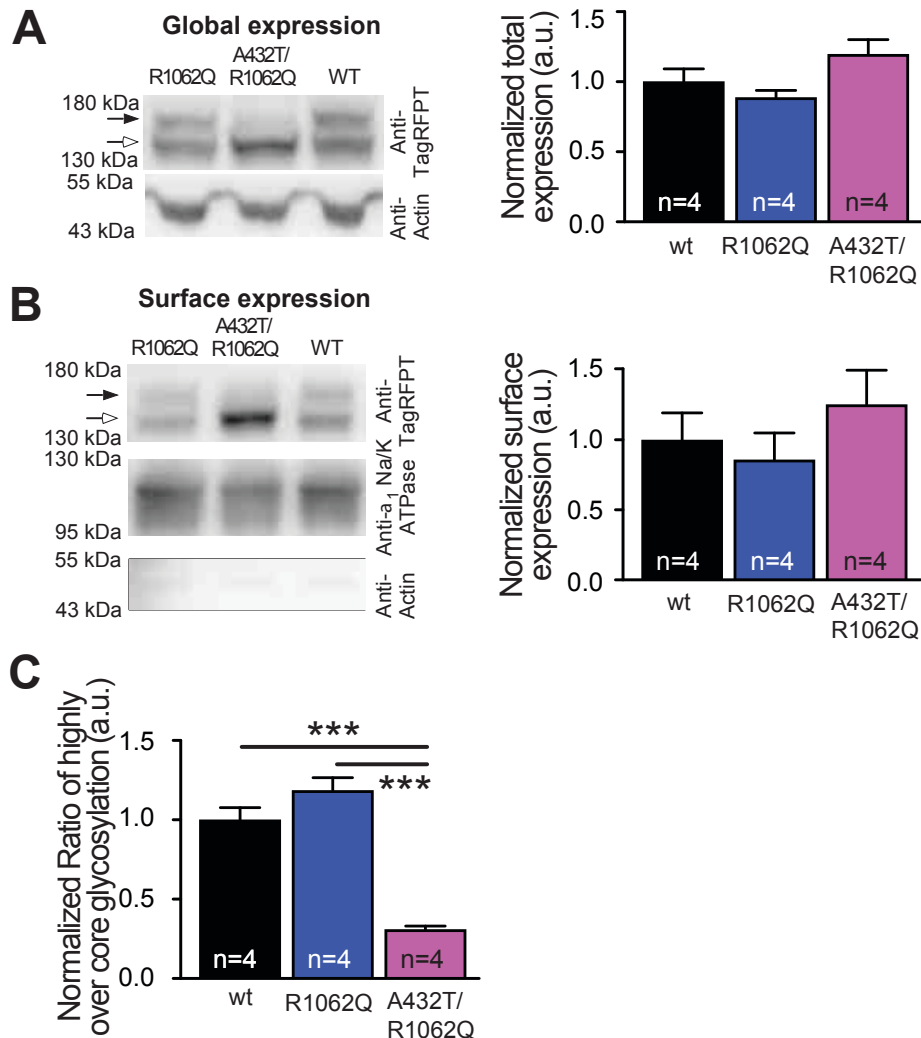
Figure 3.1.17 Expression of TRPM4^{wt}, TRPM4^{R1062Q} and TRPM4$^{A432T+R1062Q}$.

Exemplified western blots of whole cell lysates (A, left) and the statistical analysis (A, right). Surface expression exemplified in (B, left) and statistical summary (B, right). White and black arrowheads represented highly-glycosylated and core-glycosylated forms of TRPM4, respectively. The normalized ratios of highly-glycosylated and core-glycosylated TRPM4 proteins are depicted in (C).

3.1.4 Effect of additional human mutations on the electrophysiological properties of the TRPM4 channel.

Recently, additional mutations in the *TRPM4* gene have been identified in inherited cardiac conduction diseases[93,99,192], but not all of them have been well studied. By

using my UV-flash approach, I systematically studied nine of these mutations (Table 3.1) and their influences on TRPM4's properties.

Table 3.1 Summary of investigated TRPM4 mutations

Mutations	Location	Phenotype
Q131H[94]	N-terminal, cytoplasmic	RBBB, LAHB
D561A[92,94]	N-terminal, cytoplasmic	BrS, AVB
T677I[93]	N-terminal, cytoplasmic	AVB
G737R[93,99]	N-terminal, cytoplasmic	BrS, AVB
Y790H[94]	S1	AVB
G844D[94]	S2-S3 linker	RBBB, LAHB
R892C[92]	S4	AVB
K914R[94]	S4-S5 linker	AVB
P970S[94]	Pore region	RBBB

RBBB: right-bundle branch block; LAHB: left anterior hemiblock; AVB: atrioventricular block; BrS: Brugada syndrome.

The Q131H missense mutation was identified in a 49 years old man with incomplete right-bundle branch block (RBBB) and left anterior hemiblock (LAHB)[94]. Although Q131 is located in a putative CaM-binding site[94], the effect of this substitution on the TRPM4 protein is still unknown. I investigated the function of TRPM4^{Q131H} by the UV-flash assay. As depicted in Figure 3.1.18, surprisingly, TRPM4^{Q131H} showed no significant difference in Ca^{2+} sensitivity, current density and channel kinetics when compared to TRPM4^{wt}.

D561A was identified in patients with BrS and showing AVB phenotype[92,94]. This mutation located at the N-terminus of TRPM4 channel, while no experimental results on the properties of the mutant are available[94]. In my experiment, TRPM4^{D561A} and TRPM4^{wt} were transiently transfected into HEK293 cells and the membrane currents were investigated with the established UV-flash assay. My results indicated that TRPM4^{D561A} possessed similar electrophysiological properties just like TRPM4^{wt} (Figure 3.1.19).
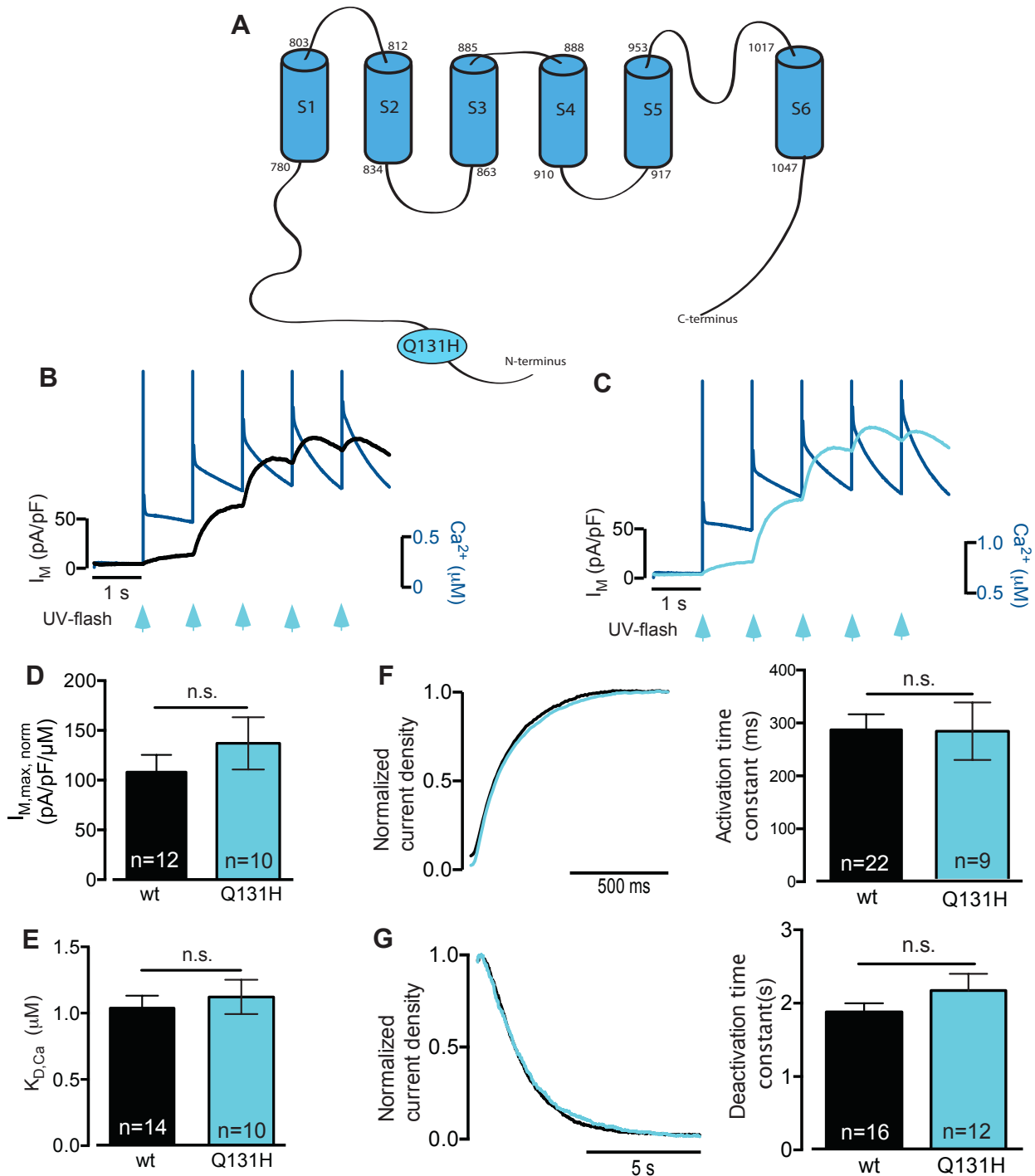
Figure 3.1.18 Q131H mutant does not alter TRPM4's properties.

(A) Schematic drawing of TRPM4 indicates the location of Q131H mutation. Typical currents activated by UV flashes are shown in (B) for wt and (C) for Q131H mutant, the dark blue color indicates Ca^{2+} changes. The current density and apparent $K_{D,Ca}$, activation are summarized in (D) and (E). (F) displays the normalized activation currents (left) and the statistical analysis of the activation time constants (right). The normalized deactivation currents are shown in (G, left) and the statistical analysis of deactivation time constants is in (G, right)
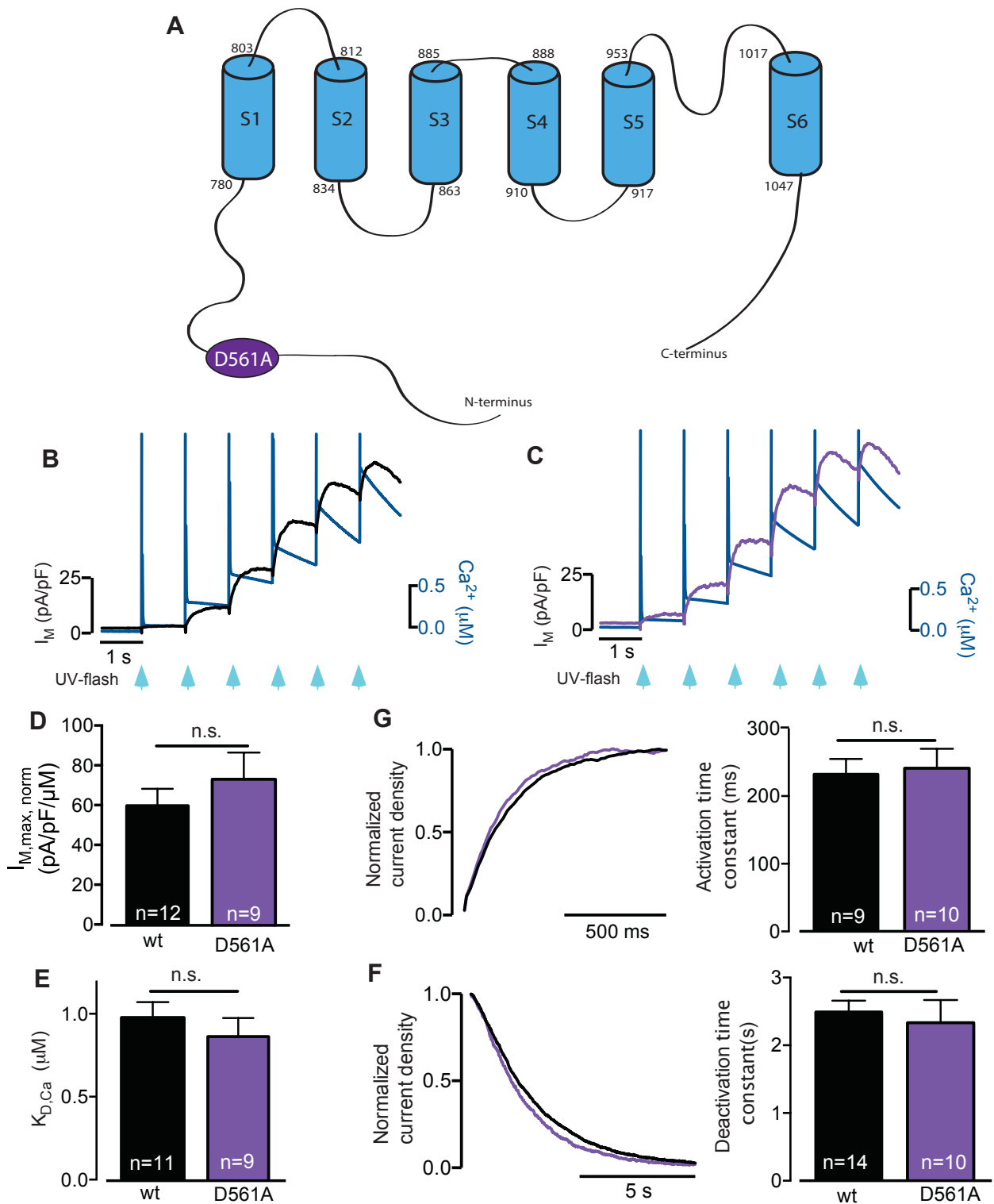
Figure 3.1.19 D561A mutant does not alter TRPM4's properties.

(A) Schematic drawing of TRPM4 indicates the location D561A mutation. Typical currents activated by UV flashes are shown in (B) for wt and (C) for D561A mutant, the dark blue color indicates Ca^{2+} changes. The current density and apparent $K_{D,Ca}$, activation are summarized in (D) and (E). (F) displays the normalized activation currents (left) and the statistical analysis of the activation time constants (right). The normalized deactivation currents are shown in (G, left) and the statistical analysis of deactivation time constants is in (G, right)
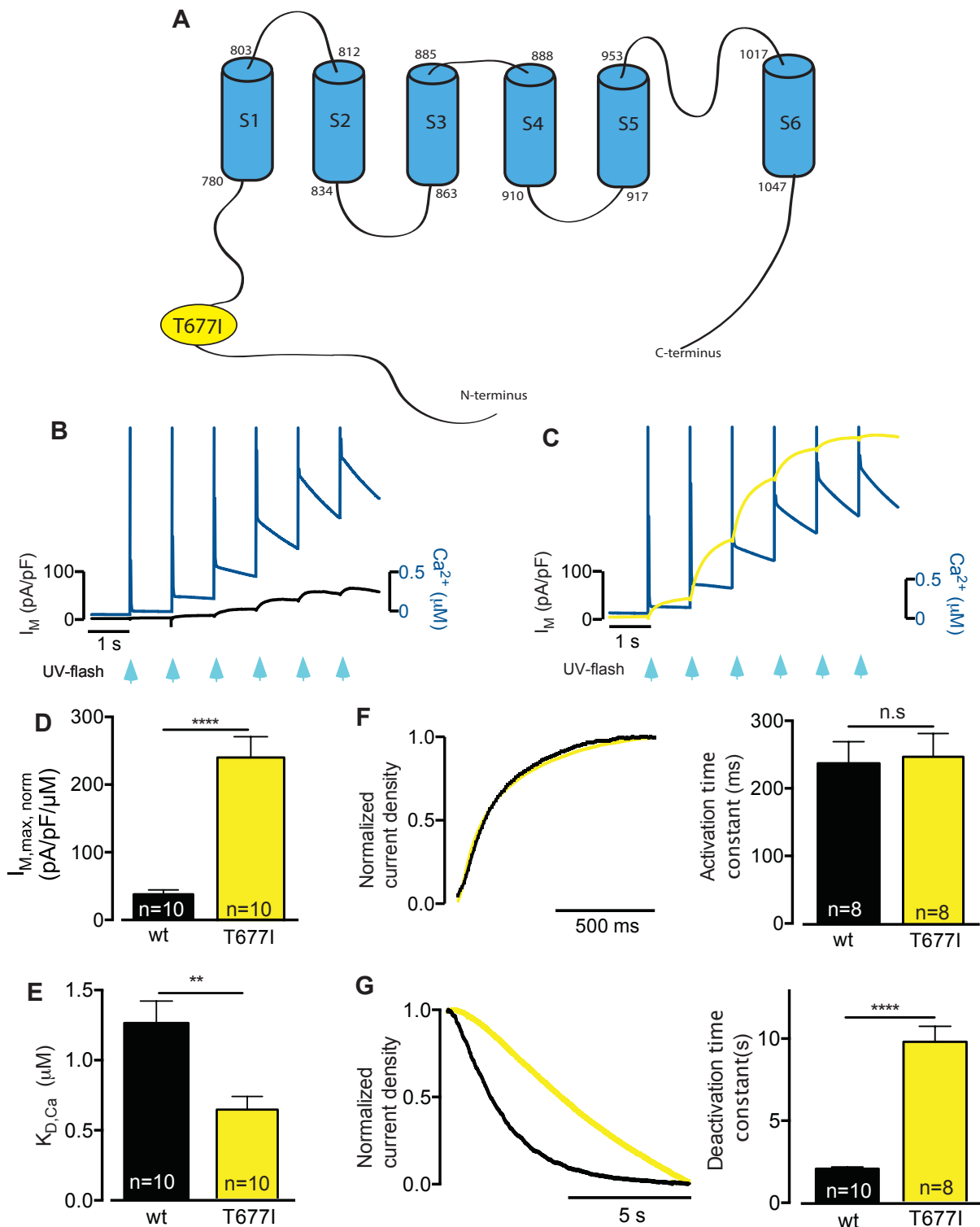
Figure 3.1.20 T677I mutant alters TRPM4's current density, apparent $K_{D,Ca}$ and deactivation kinetics. (A) Schematic drawing of TRPM4 indicates the location of the T677I mutation. Typical currents activated by UV flashes are shown in (B) for wt and (C) for T677I mutant, the dark blue color indicates Ca^{2+} changes. The current density and apparent $K_{D,Ca}$, activation are summarized in (D) and (E). (F) displays the normalized activation currents (left) and the statistical analysis of the activation time constants (right). The normalized deactivation currents are shown in (G, left) and the statistical analysis of deactivation time constants is in (G, right)
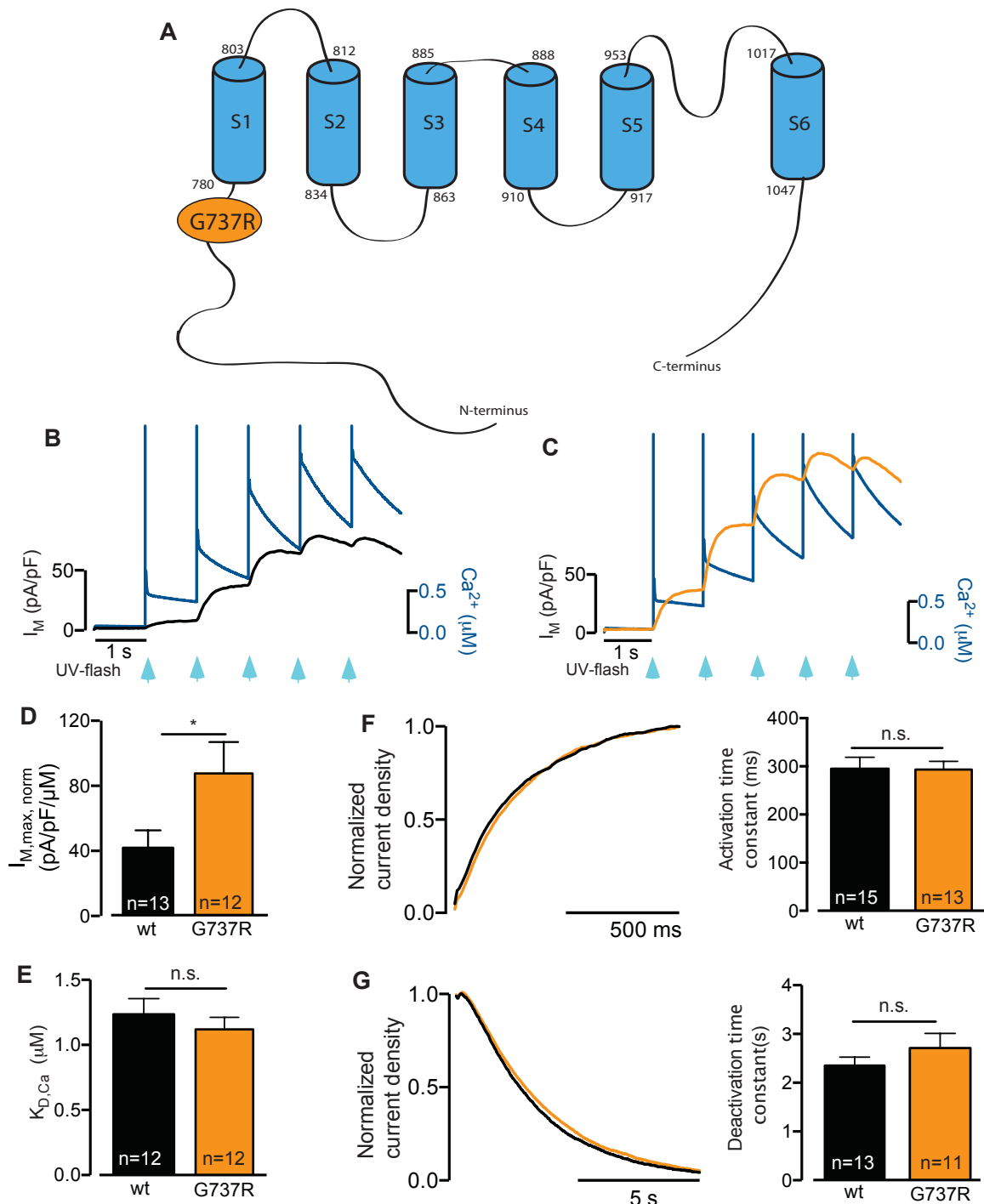
Figure 3.1.21 G737R mutant increases TRPM4's current density with otherwise unchanged properties.

(A) Schematic drawing of TRPM4 indicates the location of the G737R mutation. Typical currents activated by UV flashes are show in (B) for wt and (C) for G737R mutant, the dark blue color indicates Ca^{2+} changes. The current density and apparent $K_{D,Ca}$, activation are summarized in (D) and (E). (F) displays the normalized activation currents (left) and the statistical analysis of the activation time constants (right). The normalized deactivation currents are shown in (G, left) and the statistical analysis of deactivation time constants are in (G, right)

T677I is a recently identified mutation of TRPM4 in patients with complete AVB[93]. It locates in the N-terminus within the MHR4 domain[210]. Syam and coworkers reported that TRPM4^{T677I} did not show any significant changes in current density when compared to the wt protein[93]. By using the UV-flash assay, I further explored whether the T677I altered the other properties of the TRPM4 channel. Unexpectedly, in my experiments, TRPM4^{T677I} exhibited a substantially higher Ca^{2+} sensitivity, the apparent $K_{D,Ca}$ was reduced from 1.266±0.1562 μM (n=10) in TRPM4^{wt} to 0.635±0.09328 μM (n=10), and the current was increased to more than six-fold (37.77±6.493 pA/pF/μM, n=10 in TRPM4^{wt} vs. 242.2±30.63 pA/pF/μM, n=10 in TRPM4^{T677I}) with a slower deactivation and unchanged activation kinetics (Figure 3.1.20).

The G737R mutation was first reported in BrS[99] and the results from Syam *et al.* confirmed that this mutation also occurs in childhood AVB with an allele frequency≥0.1%[93]. I further explored the effect of the G737R variants on TRPM4's behavior and my results indicated that besides the increased current density (41.90±10.78 pA/pF/μM, n=13 in TRPM4^{wt} vs. 87.19±19.25 pA/pF/μM, n=12 in TRPM4^{G737R}), the other properties (apparent $K_{D,Ca}$, activation and deactivation kinetics) were unchanged (Figure 3.1.21).

In four members of a French family, the heterozygous missense mutation Y790H was identified[94]. The four mutation carriers exhibited congenital AVB with variable degrees. The Y790H mutation is not in the cytoplasmic parts of protein, instead it locates within S1 (Figure 3.1.22 A)[210,216]. In my experiments, I investigated the effect of this mutation on TRPM4's properties and found that like the T677I mutant, TRPM4^{Y790H} displayed an increased current density (270.4±26.37 pA/pF/μM, n=13 TRPM4^{Y790H} vs.108.1±17.23 pA/pF/μM, n=12 in TRPM4^{wt}) with a lower apparent $K_{D,Ca}$ (0.3613±0.0410 μM, n=13 in TRPM4^{Y790H} vs. 1.038±0.0944 μM, n=14 in TRPM4^{wt}). The activation became slightly but insignificantly faster and no significant difference when compared to TRPM4^{wt}, while the deactivation was substantially slowed down from 2.131±0.1342 s (n=16) in wt to 8.556±0.9366 s (n=16) in TRPM4^{Y790H} mutation.
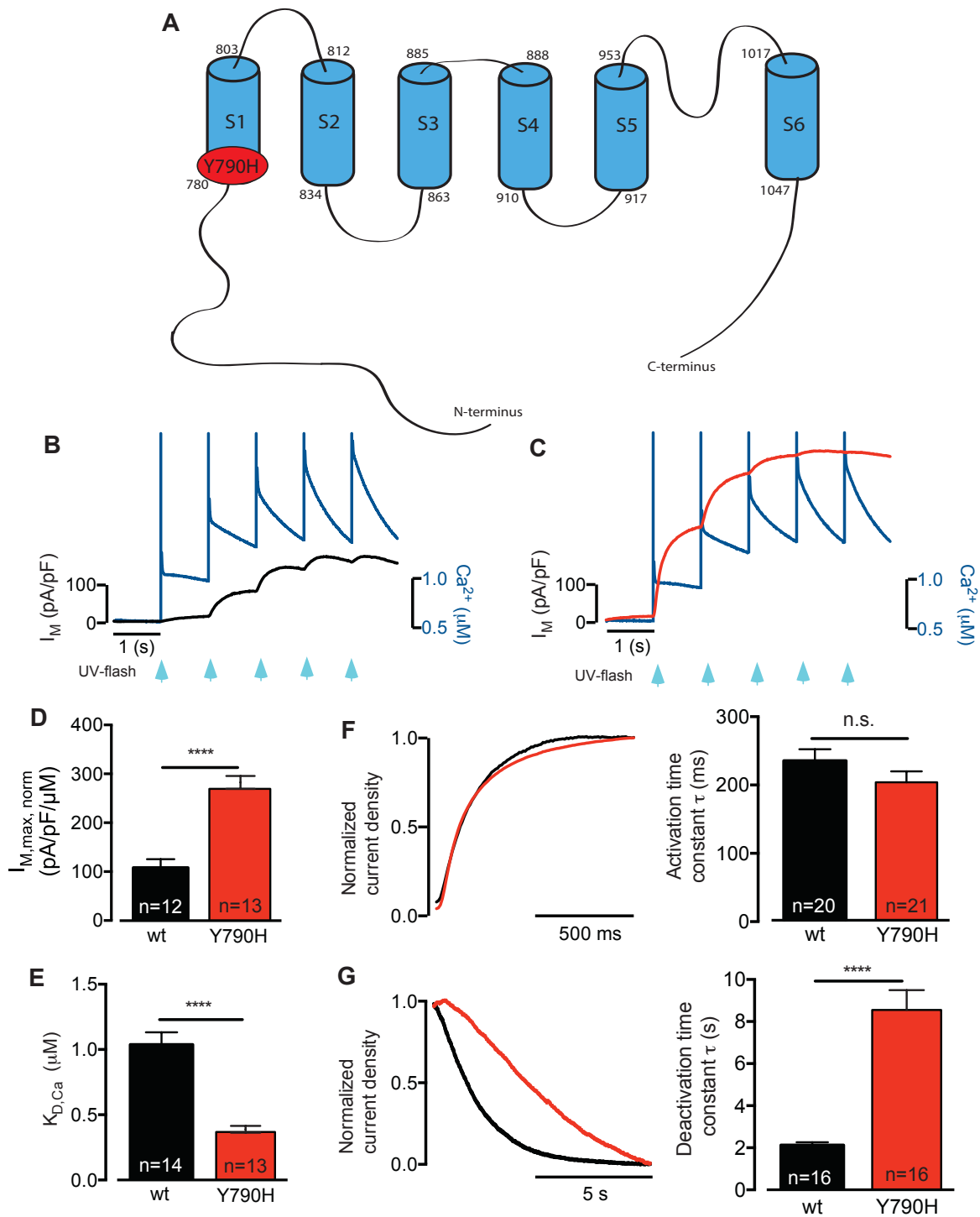
Figure 3.1.22 Y790H mutant alters TRPM4's current density, apparent $K_{D,Ca}$ and deactivation kinetics.

(A) Schematic drawing of TRPM4 indicates the location of the Y790H mutation. Typical currents activated by UV flashes are show in (B) for wt and (C) for Y790H mutant, the dark blue color indicates Ca^{2+} changes. The current density and apparent $K_{D,Ca}$, activation are summarized in (D) and (E). (F) displays the normalized activation currents (left) and the statistical analysis of the activation time constants (right). The normalized deactivation currents are shown in (G, left) and the statistical analysis of deactivation time constants is in (G, right)
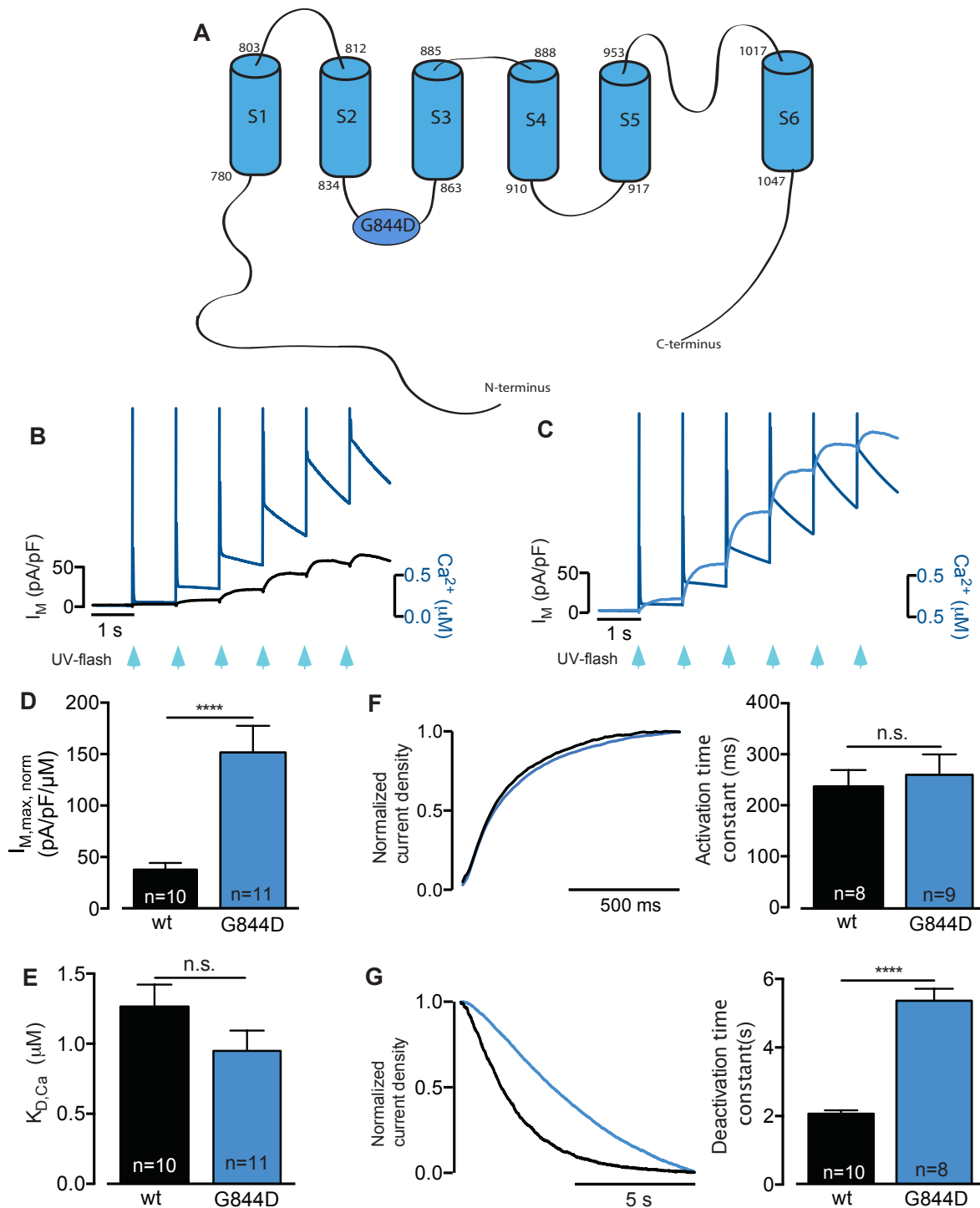
Figure 3.1.23 G844D mutant increases TRPM4's current density with a slow deactivation.

(A) Schematic drawing of TRPM4 indicates the location of the G844D mutation. Typical currents activated by UV flashes are show in (B) for wt and (C) for G844D mutant, the dark blue color indicates Ca^{2+} changes. The current density and apparent $K_{D,Ca}$, activation are summarized in (D) and (E). (F) displays the normalized activation currents (left) and the statistical analysis of the activation time constants (right). The normalized deactivation currents are shown in (G, left) and the statistical analysis of deactivation time constants is in (G, right)

In patients with the autosomal dominant isolated cardiac conduction disease, the G844D mutation was identified and locates in the cytoplasmic linker between the S2 and S3 of the TRPM4 protein[94,210]. As reported by Liu and coworkers, I also found that TRPM4^{G844D} dramatically elevated the current density (Figure 3.1.23 B), without altering the Ca^{2+} sensitivity (Figure 3.1.23 C). Employing my UV-flash approach, I further demonstrated that TRPM4^{G844D} mutation exhibited a slower deactivation with an unchanged activation when compared to wt protein (Figure 3.1.23 D and E).

At site 892 of the TRPM4 protein, two mutations have been identified in patients with progressive familial block type I: R892H and R892C[92]. The carrier with the R892H variant presented a complete AVB, but in this patient a missense mutation in the *SCN5A* gene was also identified, indicating that R892H alone may not be the sole reason for the observed cardiac conduction disorders[92]. Thus, I only focused on the mutation R892C, which was identified in another patient. I found that the R892C mutation had no apparent effect on the invested properties of the TRPM4 channel as shown in Figure 3.1.24.

The amino acid substitution K914R in the S4-S5 linker of TRPM4[210] was found in a Turkish family with a member presenting severe AVB 3° before the age 2[94]. K914R is located within a predicted SUMOylation site[94]. However, whether the behavior of TRPM4 was affected by this mutation was still unknown. My experiments showed that the TRPM4^{K914R} mutant was characterized by an increased current density (335.6±30.93 pA/pF/μM, n=10 vs.108.1±11.23 pA/pF/μM, n=12 in TRPM4^{wt}) and a slower activation and deactivation kinetics (585.8±99.29 ms, n=13 and 6.710±0.5610 s, n=14 in TRPM4^{K914R}, vs. 291.8±37.26 ms, n=17 and 1.881±0.1164 s, n=16 in TRPM4^{wt}). No effect on the Ca^{2+} sensitivity was detected (Figure 3.1.25).

A P970S mutation in the pore-forming region of the TRPM4 protein[210] was found in a German family, both the 44-year-old father and his 15-year-old daughter carried this amino acid substitution, and presented a mild electrocardiographic phenotype characteristic for an incomplete RBBB[94]. I found that the TRPM4^{P970S} mutation did not alter the investigated properties of TRPM4 channel, as known in Figure 3.1.26.
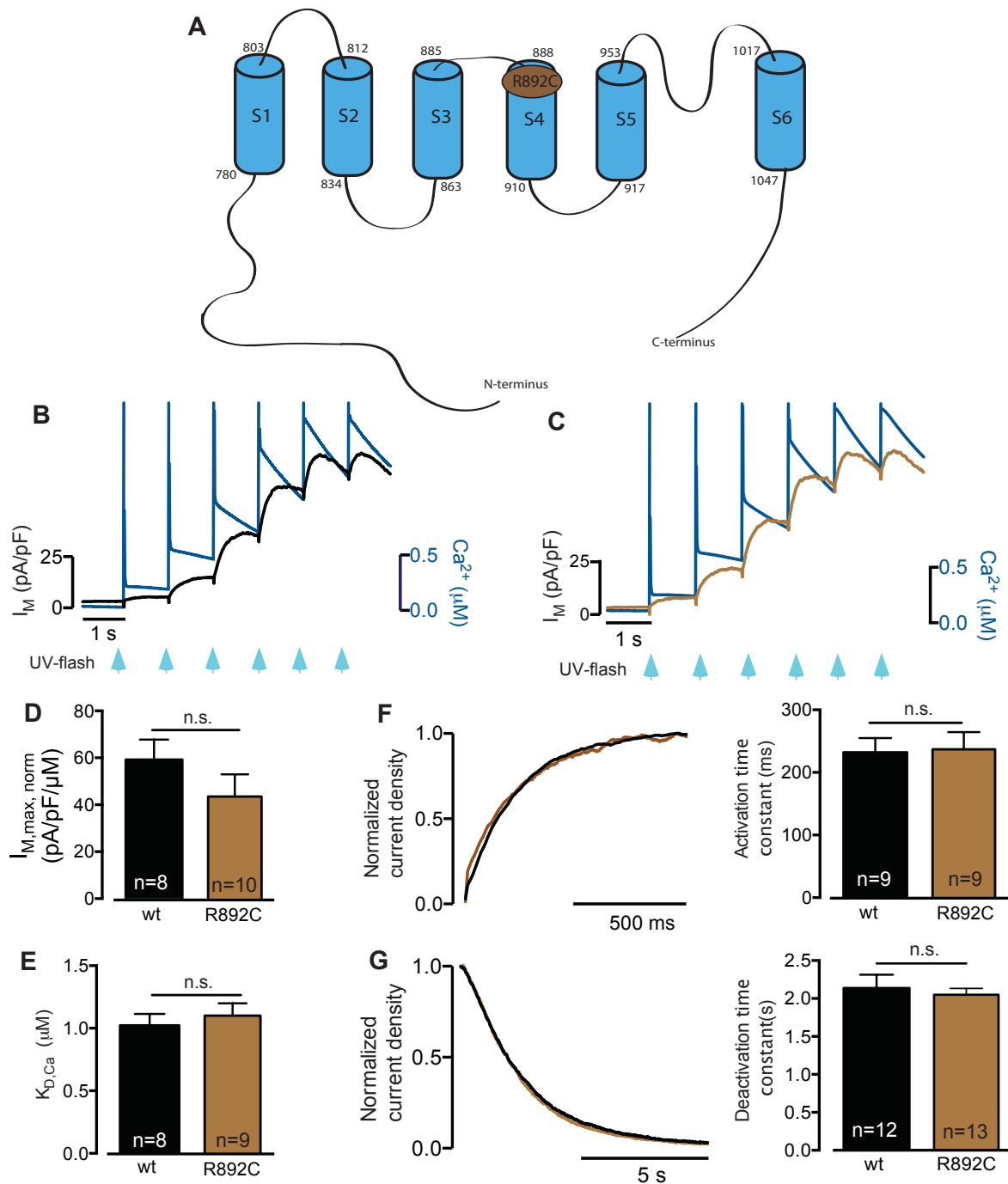
Figure 3.1.24 R892C mutant doesn't alter TRPM4's properties.

(A) Schematic drawing of TRPM4 indicated the location of the R892C mutation. Typical currents activated by UV flashes are show in (B) for wt and (C) for R892C mutant, the dark blue color indicates Ca^{2+} changes. The current density and apparent $K_{D,Ca}$, activation are summarized in (D) and (E). (F) displays the normalized activation currents (left) and the statistical analysis of the activation time constants (right). The normalized deactivation currents are shown in (G, left) and the statistical analysis of deactivation time constants is in (G, right).
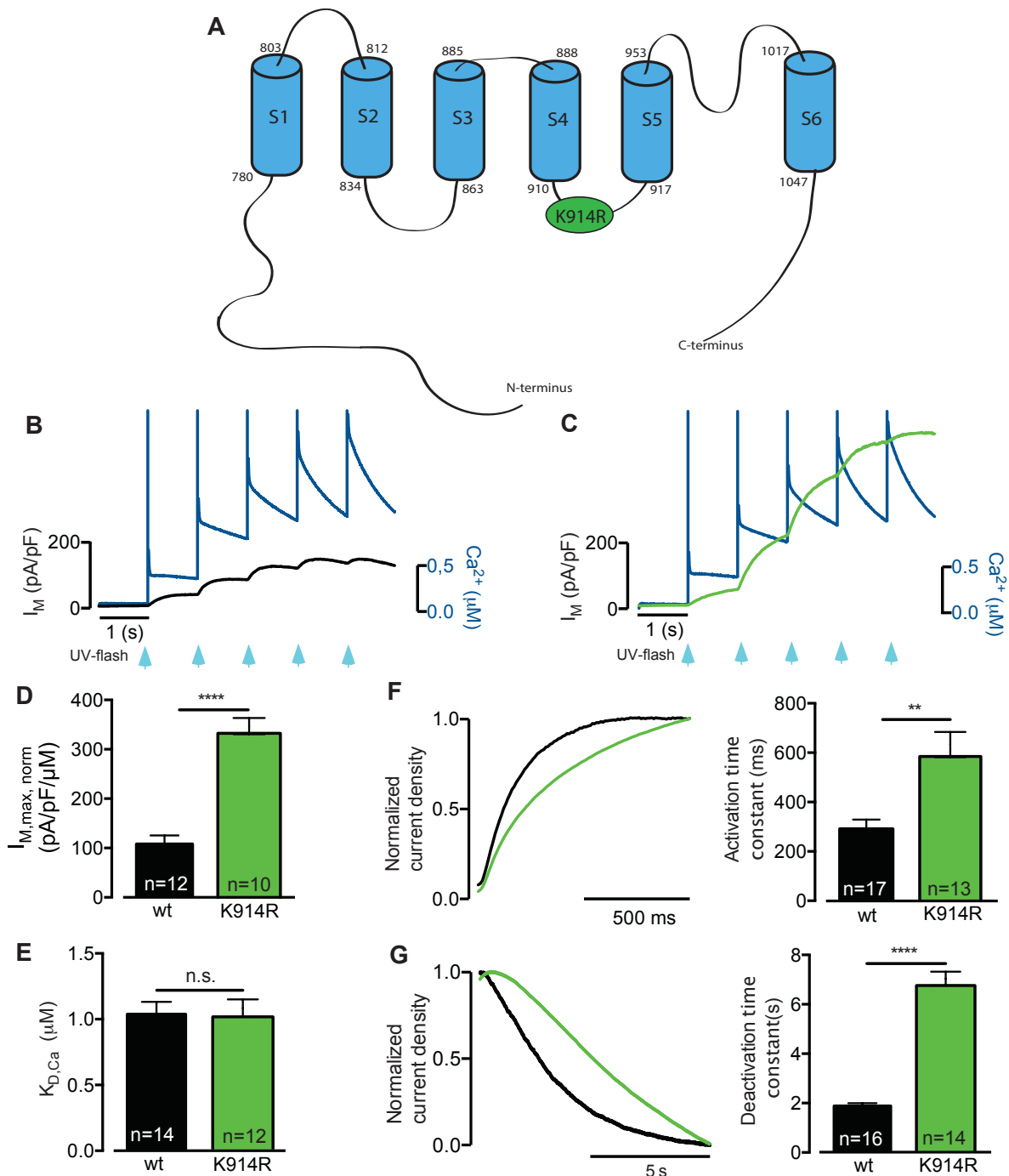
Figure 3.1.25 K914R mutant depicts an increased membrane current with altered gating kinetics.

(A) Schematic drawing of TRPM4 indicates the location of K914R. Typical currents activated by UV flashes are show in (B) for wt and (C) for K914R mutant, the dark blue color indicates Ca^{2+} changes. The current density and apparent $K_{D,Ca}$, activation are summarized in (D) and (E). (F) displays the normalized activation currents (left) and the statistical analysis of the activation time constants (right). The normalized deactivation currents are shown in (G, left) and the statistical analysis of deactivation time constants is in (G, right)
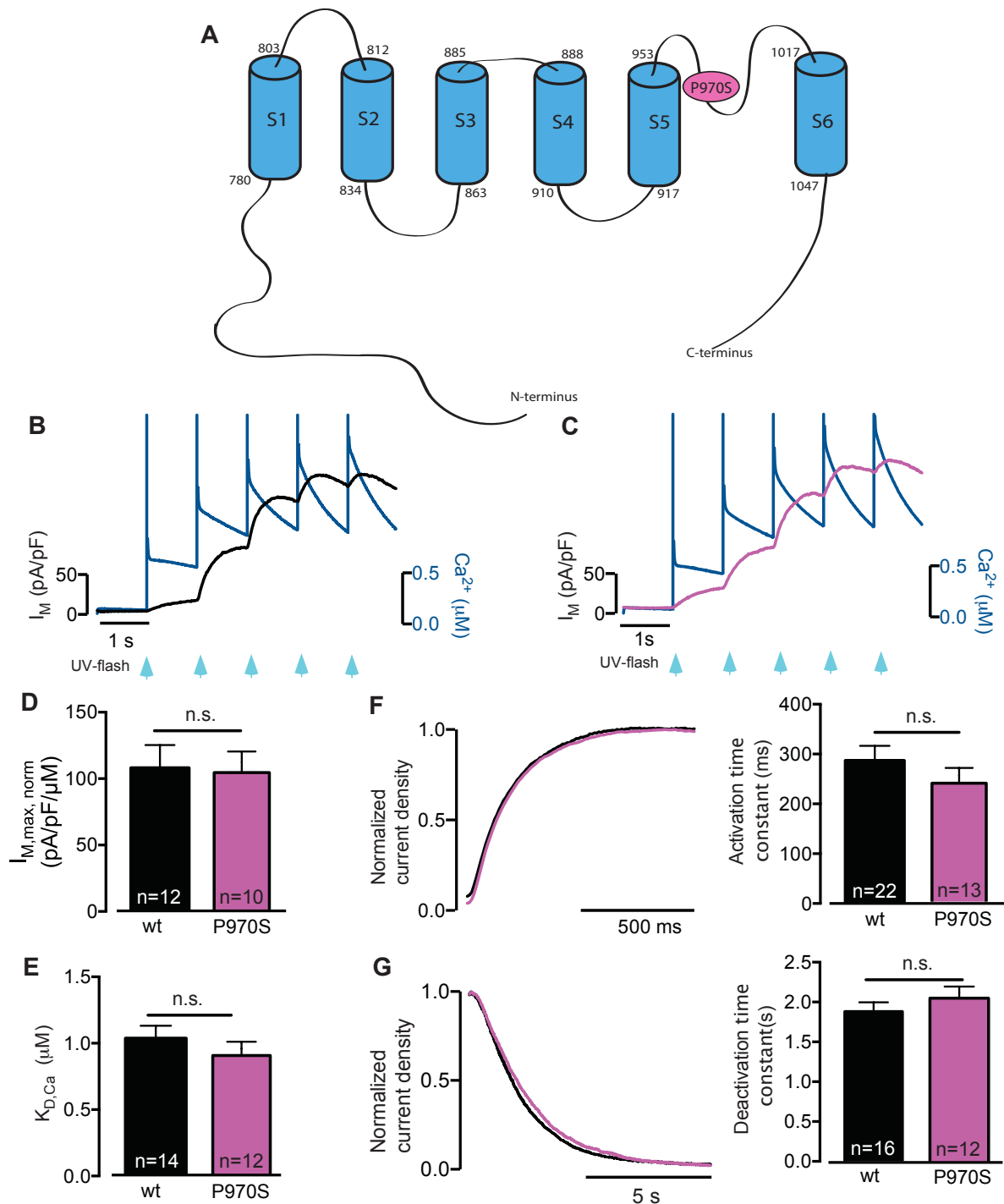
Figure 3.1.26 P970S mutant doesn't alter TRPM4's properties.

(A) Schematic drawing of TRPM4 indicated the location of the P970S mutation. The typical currents activated by UV flashes are show in (B) for wt and (C) for P970S mutant, the dark blue color indicates Ca^{2+} changes. The current density and apparent $K_{D,Ca}$, activation are summarized in (D) and (E). (F) displays the normalized activation currents (left) and the statistical analysis of the activation time constants (right). The normalized deactivation currents are shown in (G, left) and the statistical analysis of deactivation time constants is in (G, right)

3.2 The interaction between TRPC1 and TRPC4

3.2.1 TRPC1 failes to form receptor activated homomeric channels.

TRPC1 is widely expressed in various native cell types, organ systems and organisms and plays important roles in physiological and pathological processes [20,131,134,217,218]. To investigate whether expression of TRPC1 alone could form a functional channel in my experiments, TRPC1 was heterologously expressed in HEK293 cells stably expressing the $G_{i/o}$-coupled M_2 receptor[156] (M_2R HEK293). Carbachol (Carb, 25µM) was used to activate the M_2 receptor and investigated whether muscarinic receptor stimulation could activate TRPC1 channels.
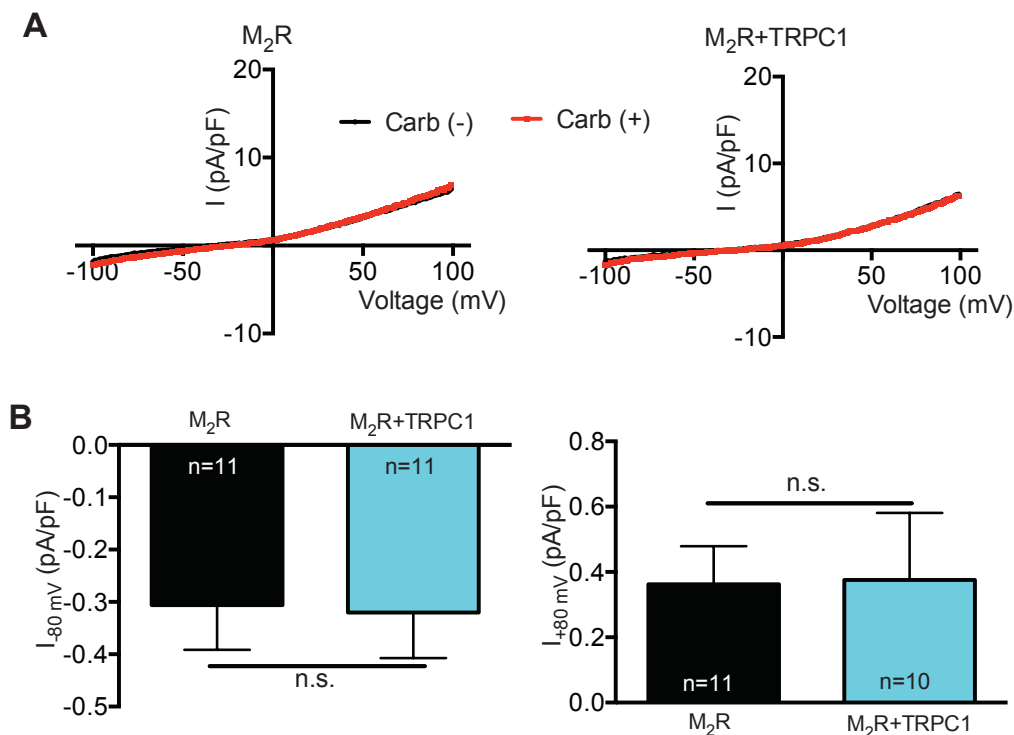
Figure 3.2.1 Homomeric recombinant TRPC1 fails to form functional receptor-activated channel.
(A) The I-V relationships from M_2R HEK293 cell (right) and TRPC1 M_2R HEK293 cells (left) before and after Carbachol treatment (black and red, respectively). Current densities at -80 mV and +80 mV are summarized in (B, right) and (B, left), respectively.

As shown in Figure 3.2.1 A, in both, M_2R HEK293 and TRPC1 M_2R HEK293 cells, Carbachol application failed to elicit any membrane current displaying superimposable current-voltage relationships (I-V) before and after Carbachol treatment (3.2.1 A black and red traces, respectively). The current densities at both -80 mV and +80 mV showed no significant difference between TRPC1 expressing and non-expressing cells,

indicating that no detectable current through TRPC1 channels was induced by the Carbachol application.

Since most Ca^{2+} entry pathways also conduct Mn^{2+}[20], I utilized Mn^{2+} induced Fura-2 fluorescence quenching as a direct and very sensitive method to detect and quantify Ca^{2+} entry and further clarify TRPC1's Ca^{2+} permeability. The quench rates of the Fura-2 fluorescence showed no difference before (Figure 3.2.2 A) and after (Figure 3.2.2 B) Carbachol application in TRPC1 M_2R HEK293 cells compared with the non-transfected cells.
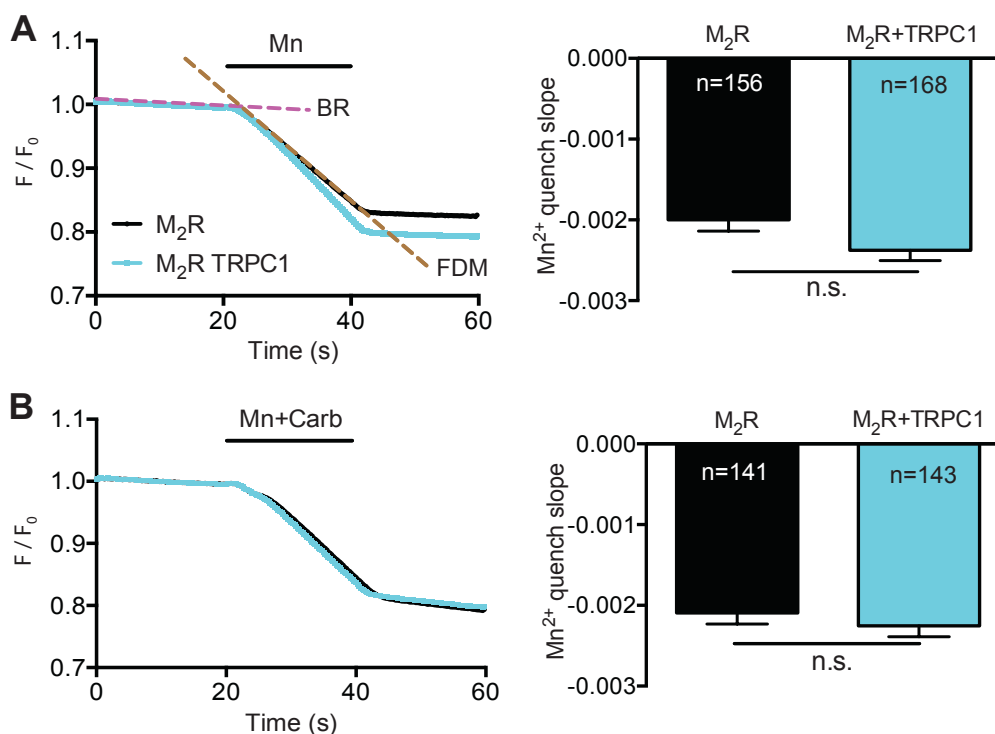
Figure 3.2.2 Mn^{2+} quench experiment to quantify TRPC1's Ca^{2+} permeability when expressed alone. 1 mmol/L $MnCl_2$ or 1 mmol/L $MnCl_2$ plus 25 µmol/L Carbachol are applied at 20-40 s. Purple dashed line: bleaching rate (BR), Grey dashed line: fluorescence decrease during Mn^{2+} application (FDM). Mn^{2+} quench slope is calculated as the difference: FDM-BR. (A) and (B) depicts the typical quench curves and statistical analysis when cells were treated with Mn^{2+} and Mn^{2+} plus Carbachol, respectively.

Taken together, my results indicated that homomeric TRPC1 channels were unable to form functional receptor-operated channel. This could be due to mislocalization of the channel protein. Exogenously expressed, TRPC1 might exhibit an intracellular location, probably in the ER membrane and may fail to reach the plasma membrane to form functional receptor-activated channels[219].

3.2.2 TRPC1 contributes to heteromeric TRPC4/TRPC1 channel complex and reduced its Ca^{2+} permeability.

The heterotetrameric TRPC4/TRPC1 has been widely reported[124,175,180,191]. It displays unique biophysical properties when compared to the homotetrameric TRPC4[124,180]. In the following experiment, TRPC1 was transiently expressed in HEK293 cells stably expressing the M_2 receptor and TRPC4 (M_2R TRPC4 HEK293) to elucidate its behavior when co-expressed with TRPC4 channels.
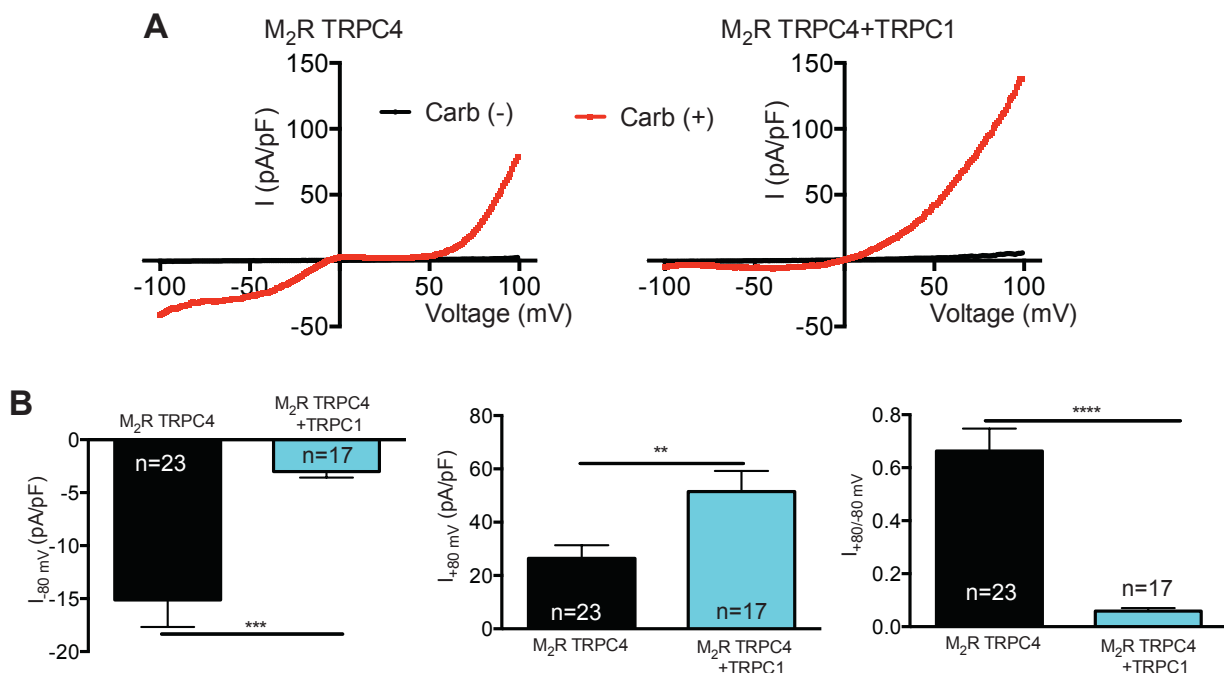
Figure 3.2.3 TRPC1 forms heteromeric channel complexes with TRPC4.
(A) Typical I-V relationships from M_2R TRPC4 HEK293 cells (right) and TRPC1 M_2R TRPC4 HEK293 cells (left) before (black) and after (red) Carbachol treatment. Current densities at both +80 mV and -80 mV are summarized in (B, right) and (B, middle), respectively. Rectification factors calculated from the current density between -80 mV and +80 mV are summarized in (B, left).

As shown in Figure 3.2.3, Carbachol treatment of M_2R TRPC4 HEK293 cells elicited membrane currents with an I-V relationship displaying double rectification (Figure 3.2.3 A, left), which was very different when compared to that of the TRPC4/TRPC1 heteromeric channels recorded in M_2R TRPC4 HEK293 cells transiently expressing TRPC1. Here I found an outward rectifying I-V relationship (Figure 3.2.3 A, right). The current density at -80 mV reduced from 15.12±2.556 pA/pF (n=23) in TRPC4 to 3.014±0.5586 pA/pF (n=17) in TRPC4/TRPC1 expressing cells, whereas at +80 mV the outward current recorded in TRPC4/TRPC1 expressing cells increased to 51.48±7.749

pA/pF (n=17) when compared to that of TRPC4 expressing cells (26.42±4.916 pA/pF, n=23). The current density ratio of -80 mV and +80 mV was used as a rectification factor to indicate the difference in I-V relationship signature, which was dramatically reduced in TRPC4/TRPC1 channel complex (Figure 3.2.3 A, left). In the Mn^{2+} quench experiments, under resting conditions I found a significant acceleration of Mn^{2+} entry in TRPC1 M_2R TRPC4 HEK293 cells when compared to the M_2R TRPC4 HEK293 cells (-0.001191±0.00005, n=147 vs. -0.000808±0.00003, n=149) as shown in Figure 3.2.4 A. The Mn^{2+} quench rates obtained from M_2R TRPC4 HEK293 cells were substantially larger following Carbachol application (-0.01390±0.0007, n=153) when compared to those from TRPC1 M_2R TRPC4 HEK293 cells (-0.00289±0.0002, n=140).
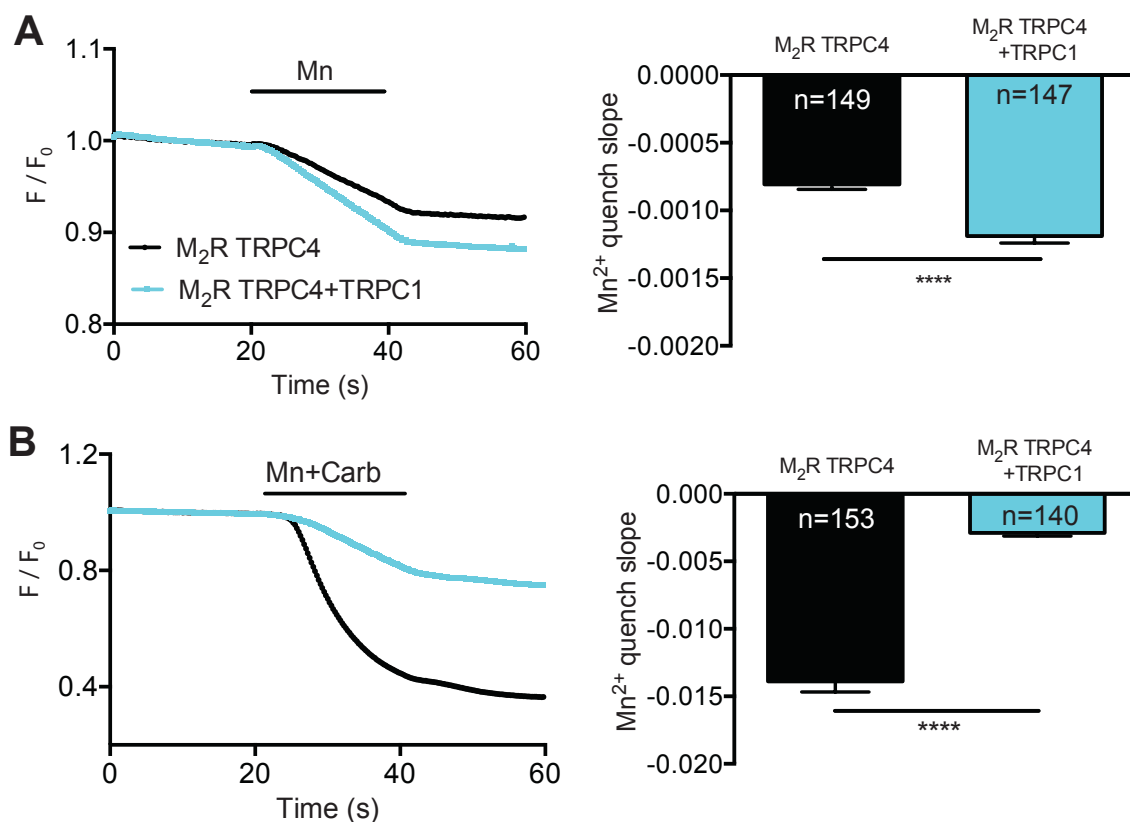
Figure 3.2.4 TRPC1 influences the Ca^{2+} permeability of TRPC4.
(A) and (B) displays the Mn^{2+} quench rate of TRPC4 and TRPC4/TRPC1 with and without Carbocachol applications, respectively.

These results show that TRPC1 was able to form functional heteromeric channel complexes with TRPC4, which showed channel properties distinct from those of the homomeric TRPC4 channel as reported previously[124,180]. Interestingly, significant acceleration of Ca^{2+} entry was found in TRPC4/TRPC1 complexes when compared to the homomeric TRPC4 channels under resting conditions. Surprisingly, following

stimulation with Carbachol, the TRPC4 homomers conducted more Ca^{2+} than the TRPC4/TRPC1 heteromer.

3.2.3 The chimera TRPC1C4$_{Pore}$'s effect on TRPC4/TRPC1 channel complex

The molecular determinants responsible for the distinct characteristics of the heteromeric TRPC4/TRPC1 channel complexes remain elusive. To address this issue, I collaborated with Prof. Flockerzi's lab and they constructed a chimera TRPC1C4$_{Pore}$, by substituting the pore region of TRPC1 with the TRPC4 pore motif to identify the putative role of TRPC1 pore region in TRPC4/TRPC1 channel complexes.

TRPC1C4$_{Pore}$ was transiently expressed in M$_2$R HEK293 cells, but no membrane currents could be recorded in these cells in the conditions described (Figure 3.2.5). Ca^{2+} influx was again quantified by Mn^{2+} quench but no difference of the Mn^{2+} quench rate was observed between TRPC1 and TRPC1C4$_{Pore}$ with or without Carbachol treatment, confirming the patch clamp recordings.

After that, TRPC1C4$_{Pore}$ was transiently expressed in M$_2$R TRPC4 HEK293 cells. Following Carbachol application, membrane currents with a double rectifying I-V relationship were obtained in TRPC4/TRPC1C4$_{Pore}$ expressing cells, which was different from that of TRPC4/TRPC1 channel complexes that showed an outwardly rectifying current (Figure 3.2.6 A). The inward current was increased from 3.014±0.5586 pA/pF (n=17) in TRPC4/TRPC1 to 8±1.837 pA/pF (n=19) in TRPC4/TRPC1C4$_{Pore}$ while the outward membrane current changed to the opposite direction, reduced from 51.48±7.749 pA/pF (n=17) to 22.66±3.007 pA/pF (n=19). The ratio of current density at -80 mV and +80 mV, the aforementioned rectifying factor, increased to 0.61±0.09 (n=19) in TRPC4/TRPC1C4$_{Pore}$, which was almost 9-fold higher than that of TRPC4/TRPC1 (0.07±0.02, n=19).

In the Mn^{2+} quench experiments, no differences were detected between TRPC4/TRPC1 and TRPC4/TRPC1C4$_{Pore}$ channel complexes under resting conditions (Figure 3.2.7 A), while TRPC4/TRPC1C4$_{Pore}$ exhibited an increased Ca^{2+} entry after Carbachol application when compared to TRPC4/TRPC1 (Figure 3.2.7 B).
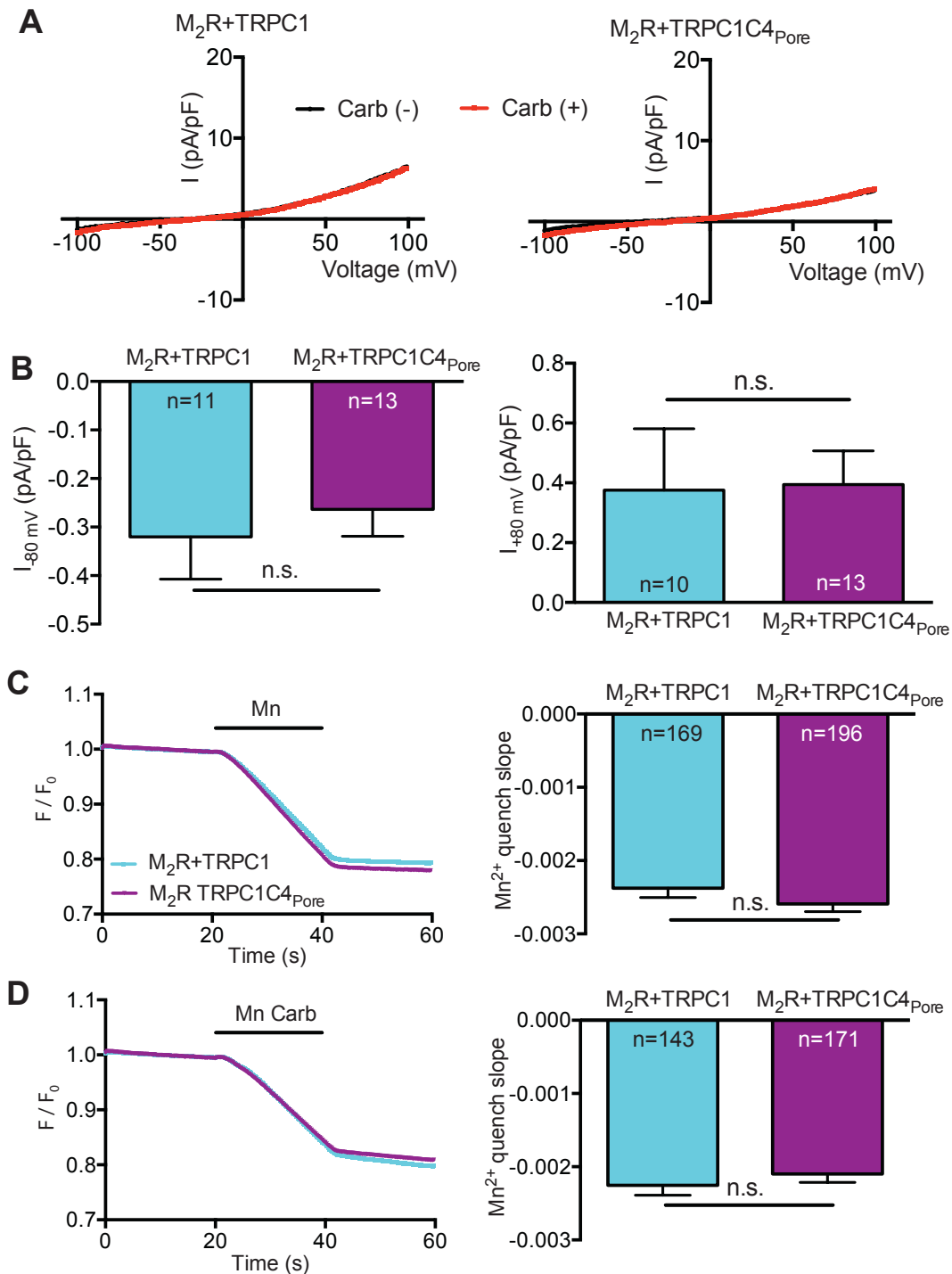
Figure 3.2.5 Homomeric recombinant TRPC1C4$_{Pore}$ fails to form functional receptor-operated channels.

(A) The I-V relationships of M$_2$R HEK293 cell (right) and TRPC1C4$_{Pore}$ M$_2$R HEK293 cells (left) before and after Carbachol treatment. Current densities at both +80 mV and -80 mV are summarized in (B, right) and (B, left), respectively. (C) and (D) depicts the Mn^{2+} quench rates of TRPC1C4$_{Pore}$ expressing and non-transfected cells before and after Carbachol applications, respectively.
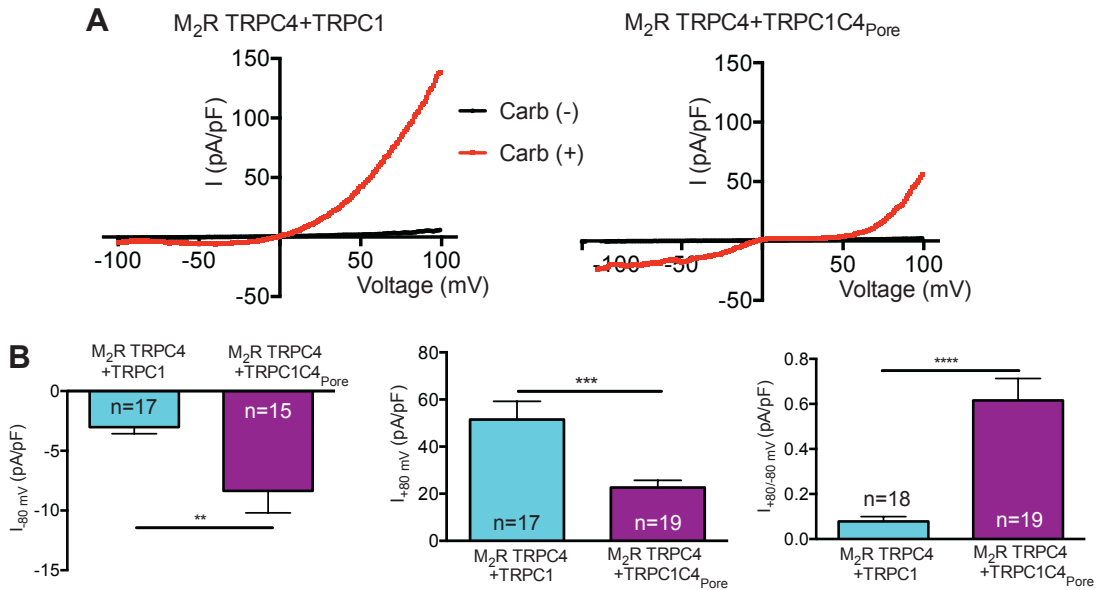
Figure 3.2.6 TRPC1C4$_{Pore}$ displays different electrophysiological property when compared to TRPC1.

(A) The I-V relationships of TRPC1 M$_2$R TRPC4 HEK293 cells (right) and TRPC1C4$_{Pore}$ M$_2$R TRPC4 HEK293 cells (left) before and after Carbachol application. Current densities at both +80 mV and -80 mV are summarized in (B, right) and (B, middle), respectively. Rectification factors calculated from the current density between +80 mV and -80 mV are summarized in (B, left).
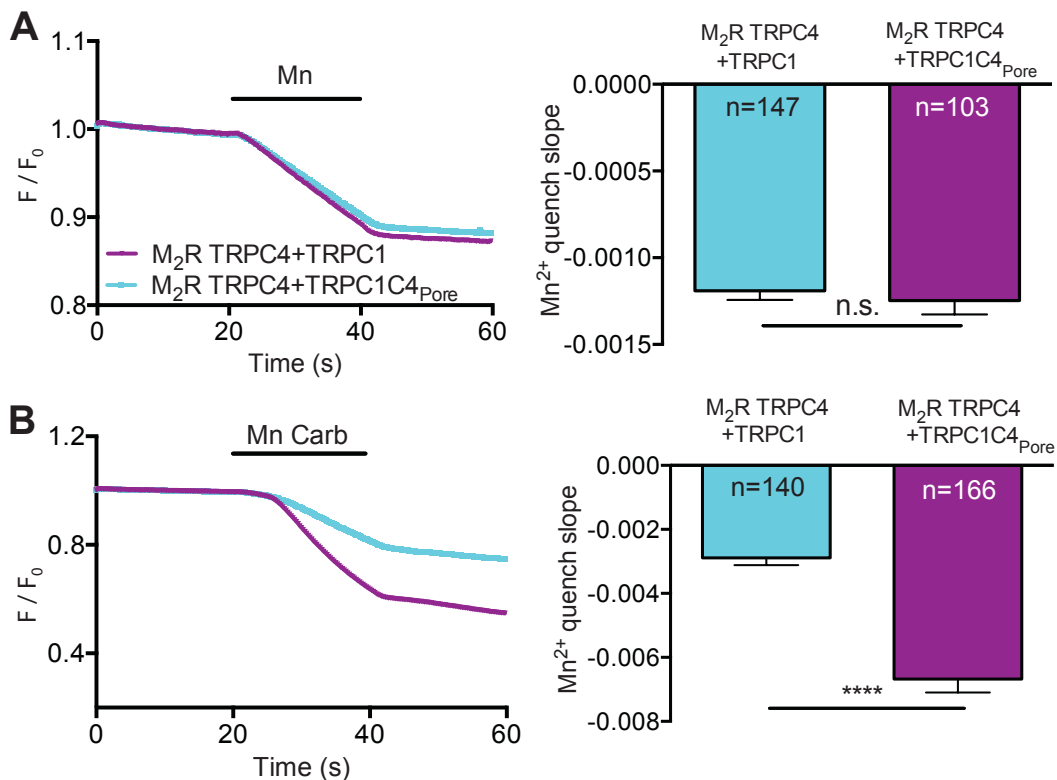
Figure 3.2.7 TRPC1C4$_{Pore}$ increases the Ca^{2+} permeability of the TRPC4/TRPC1 channel complex.

(A) and (B) depict the Mn^{2+} quench rates of TRPC1C4$_{Pore}$ expressed and non-transfected M$_2$R TRPC4 HEK293 cells before and after Carbachol applications, respectively.

These results indicated that when the pore region of TRPC1 was replaced by the pore region of TRPC4 and co-expressed with the TRPC4 protein, it retained similar properties as the TRPC4 homomers such as the double rectifying I-V relationship and the increased Ca^{2+} influx following Carbachol stimulation.

3.2.4 The chimera $TRPC4C1_{Pore}$ partially mimics the Ca^{2+} influx of TRPC1 channel

Based on these results, it seems that the pore region of TRPC1 might play a key role in regulating the Ca^{2+} influx of the TRPC4/TRPC1 heteromers. Therefore, the chimera $TRPC4C1_{Pore}$, substituting the pore region of TRPC4 by the TRPC1 pore segment, was constructed to further clarify the role of the TRPC1 pore region.

$TRPC4C1_{Pore}$ was transiently expressed in M_2R HEK293 cells. In these cells Carbachol failed to elicit any membrane currents and there was no difference between $TRPC4C1_{Pore}$ transfected and non-transfected M_2R HEK293 cells. This indicated that the pore region replacement impaired TRPC4's ability to be activated by Carbachol stimulation (Figure 3.2.8 A and B). An increased Mn^{2+} quench rate indicating a significant but small increase in Ca^{2+} entry was independent of the Carbachol treatment (Figure 3.2.8 C and D).

Then I transfected $TRPC4C1_{Pore}$ into M_2R TRPC4 HEK293 cells (in Figure 3.2.9). The chimeric channels showed a similar current when compared to TRPC4 following induction by Carbachol treatment. However, the $TRPC4C1_{Pore}$ transfected cells displayed membrane currents with similar rectifying properties to the TRPC4 homomer with a double rectifying I-V relationship rather than an outward rectification seen for the TRPC4/TRPC1 complexes (Figure 3.2.3 A, right).

The Mn^{2+} quench approach was again employed to evaluate $TRPC4C1_{Pore}$'s influences on Ca^{2+} entry. As shown in Figure 3.2.10 A, under resting conditions, the Mn^{2+} quench rate of $TRPC4C1_{Pore}$ M_2R TRPC4 HEK293 cells increased to -0.001909±0.00009 (n=103), which was 2-fold of that in M_2R TRPC4 HEK293 cells (-0.000808±0.00003, n=149). Following Carbachol treatment, a substantial Mn^{2+} quench was observed in M_2R TRPC4 HEK293 cells (-0.01373±0.00075, n=152), which was almost 2-fold of that

in TRPC4C1$_{Pore}$ M$_2$R TRPC4 HEK293 cells (-0.007614±0.00061, n=130) (Figure 3.2.10 B).
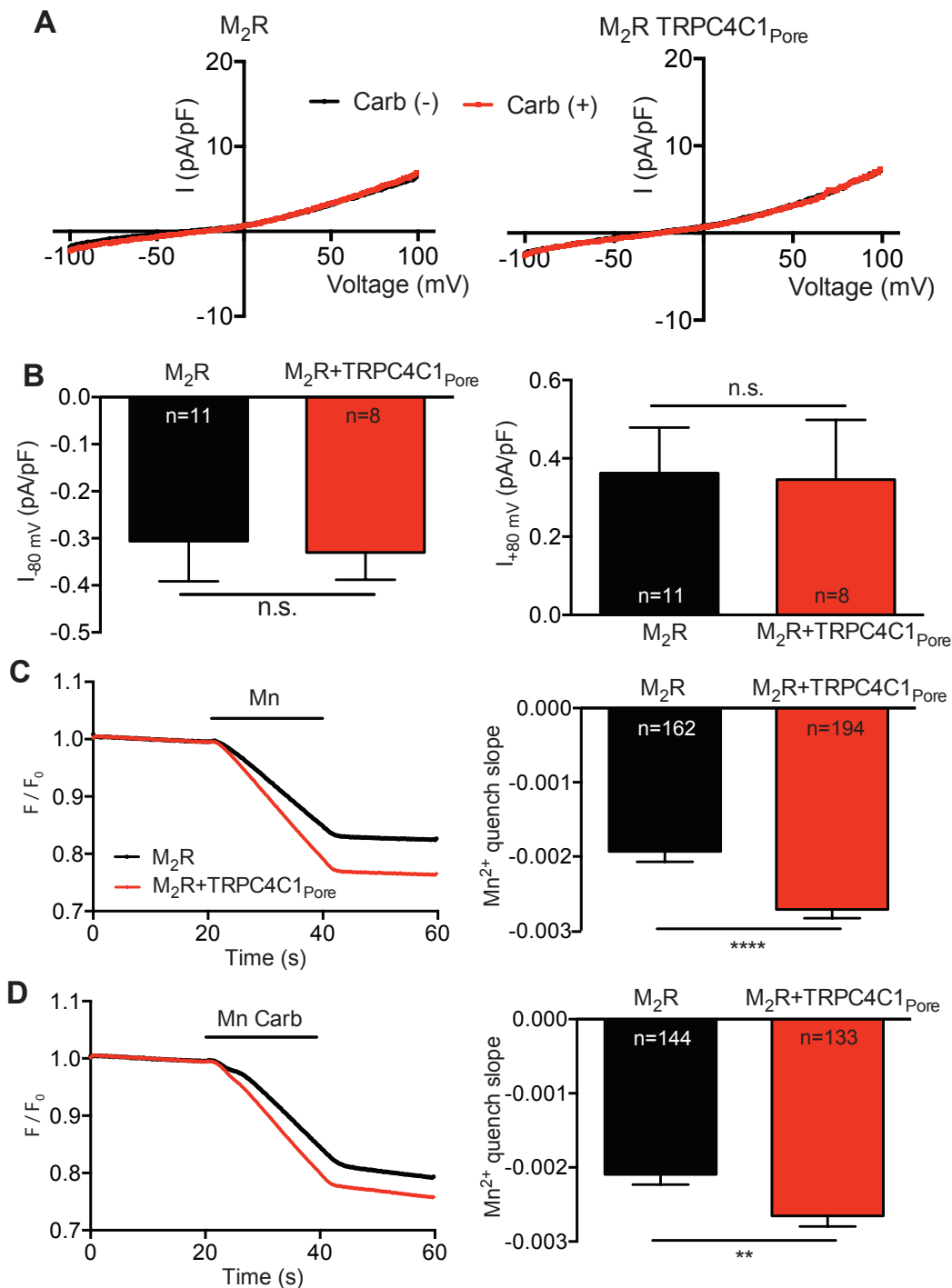
Figure 3.2.8 Homomeric recombinant TRPC4C1$_{Pore}$ displays a marginal Ca^{2+} permeability.

(A) The I-V relationships of HEK293 M$_2$R cell (right) and TRPC4C1$_{Pore}$ transiently expressed in HEK293 M$_2$R cells (left) before and after Carbachol treatment. Current densities at both +80 mV and -80 mV are summarized in (B, right) and (B, left), respectively. (C) and (D) depict the Mn^{2+} quench rates of TRPC4C1$_{Pore}$ expressed and non-transfected cells with and without Carbachol applications, respectively.
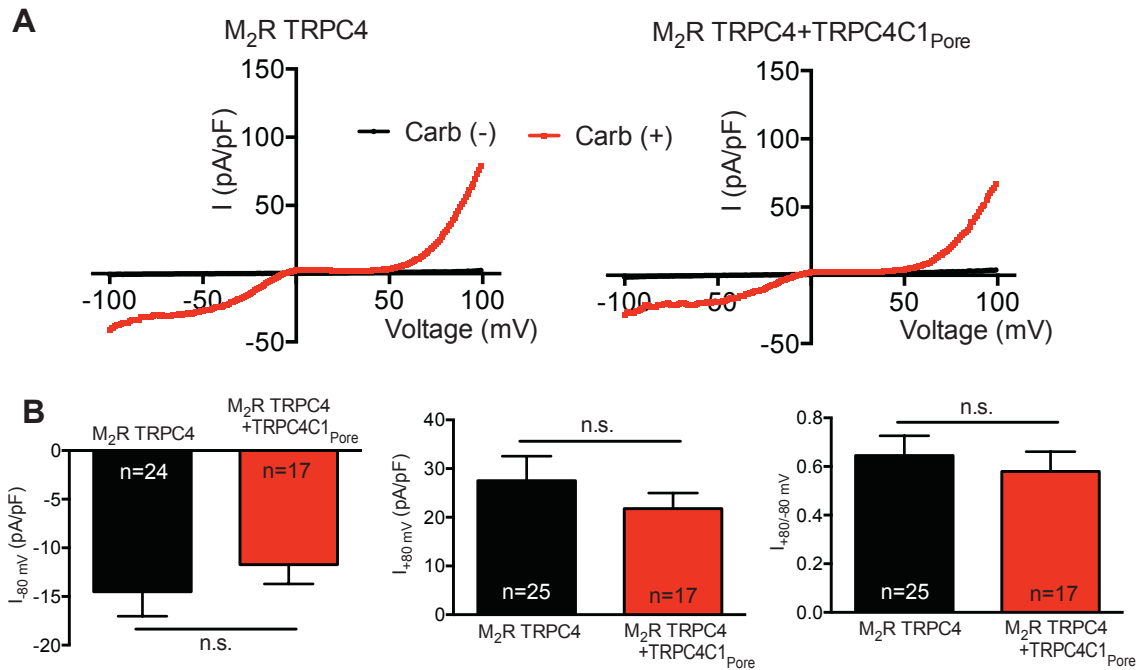
Figure 3.2.9 TRPC4C1$_{Pore}$ displays similar electrophysiological property to TRPC4.

(A) The I-V relationships of M$_2$R TRPC4 cells (right) and TRPC4C1$_{Pore}$ transiently expressed M$_2$R TRPC4 cells (left) before and after Carbachol treatment. Current densities at both +80 mV and -80 mV are summarized in (B, right) and (B, middle), respectively. Rectification factors calculated from the current density between +80 mV and -80 mV are summarized in (B, left).
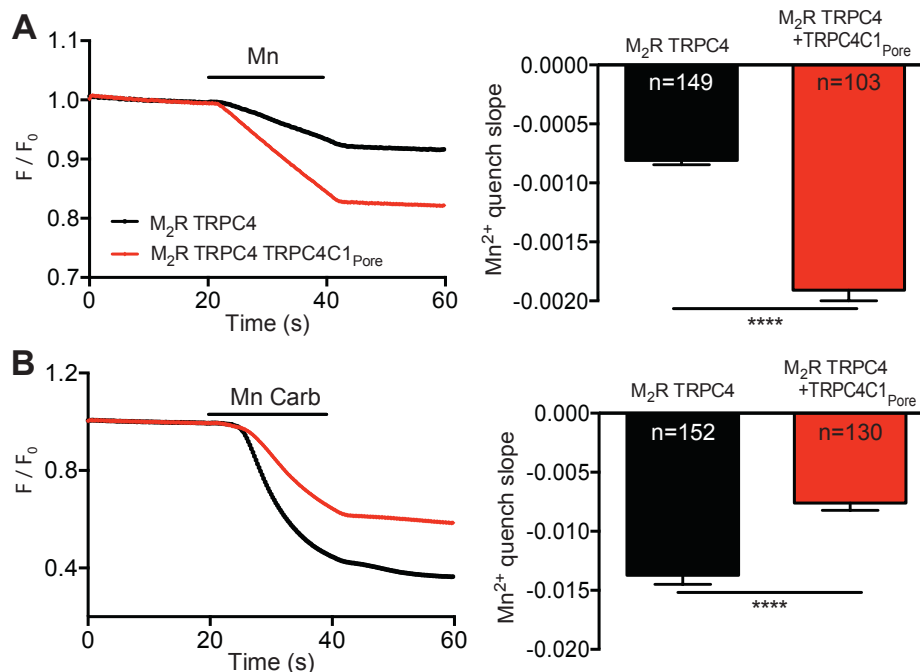
Figure 3.2.10 TRPC4C1$_{Pore}$ reduces the Ca^{2+} permeability of TRPC4 channel complex induced by Carbachol.

1 mmol/L MnCl$_2$ or 1 mmol/L MnCl$_2$ plus 25 µmol/L Carbachol were applied in Mn^{2+} quench experiment, (A) and (B) depict the Mn^{2+} quench rates of TRPC4C1$_{Pore}$ expressed and non-transfected cells with and without Carbocachol applications, respectively.

Patch clamp recordings indicated that, even though the pore region of the TRPC4 protein was replaced by the pore region of TRPC1, the TRPC4C1$_{Pore}$ still resembled the electrophysiological property of the TRPC4 channel. However, in Mn^{2+} quench experiments, I observed that the TRPC4C1$_{Pore}$ indeed influenced the Ca^{2+} entry in both M$_2$R HEK293 cells and M$_2$R TRPC4 HEK293 cells, showing the characteristics of the TRPC1 channel. These results further suggested that the pore region of TRPC1 may be the key motif to regulate the Ca^{2+} influx of TRPC4/TRPC1 channel complexes.

3.2.5 TRPC1$_{G-S}$ channel increases the Ca^{2+} entry of TRPC1/TRPC4 heteromeric channel complexes

The substitution of a conserved glycine by a serine located in the cytosolic S4-S5 linker forced the TRPC4 and TRPC5 channel into a fully open state[8]. Because of the high homology of TRPC1 with TRPC4 and TRPC5, I wondered whether a similar position is present in TRPC1. By alignment of the TRPC1 sequence with those of TRPC4 and TRPC5, the conserved glycine residue was identified at position 623 in TRPC1 protein, consequently, a site directed mutation was carried out to replace the glycine with a serine residue, which corresponds to the G-S mutation in TRPC4 or TRPC5.

The TRPC1$_{G-S}$ was expressed in M$_2$R HEK293 cells, as illustrated in Figure 3.2.11. Carbachol failed to elicit currents and there was no difference in the current density between the transfected and non-transfected cells at both +80 mV and -80 mV. Moreover, no difference in the Mn^{2+} quench rate was observed between transfected and non-transfected cells in the presence or absence of Carbachol.

Next, TRPC1$_{G-S}$ was expressed in M$_2$R TRPC4 HEK293 cells to clarify whether this G-S mutation would alter the properties of TRPC4/TRPC1 heteromeric channel complexes. As shown in Figure 3.2.12 A, the I-V relationship of TRPC4/TRPC1$_{G-S}$ channel complex showed outward rectification. The inward currents and the ratio between -80 mV and +80 increased in TRPC4/TRPC1$_{G-S}$ without altering the outward currents when compared to TRPC4/TRPC1.

In the following Mn^{2+} experiments, no differences were detected for TRPC4/TRPC1 and TRPC4/TRPC1$_{G-S}$ under resting conditions (Figure 3.2.13 A), but TRPC1$_{G-S}$ displayed an increased Mn^{2+} entry following stimulation with Carbachol (Figure 3.2.13 B).
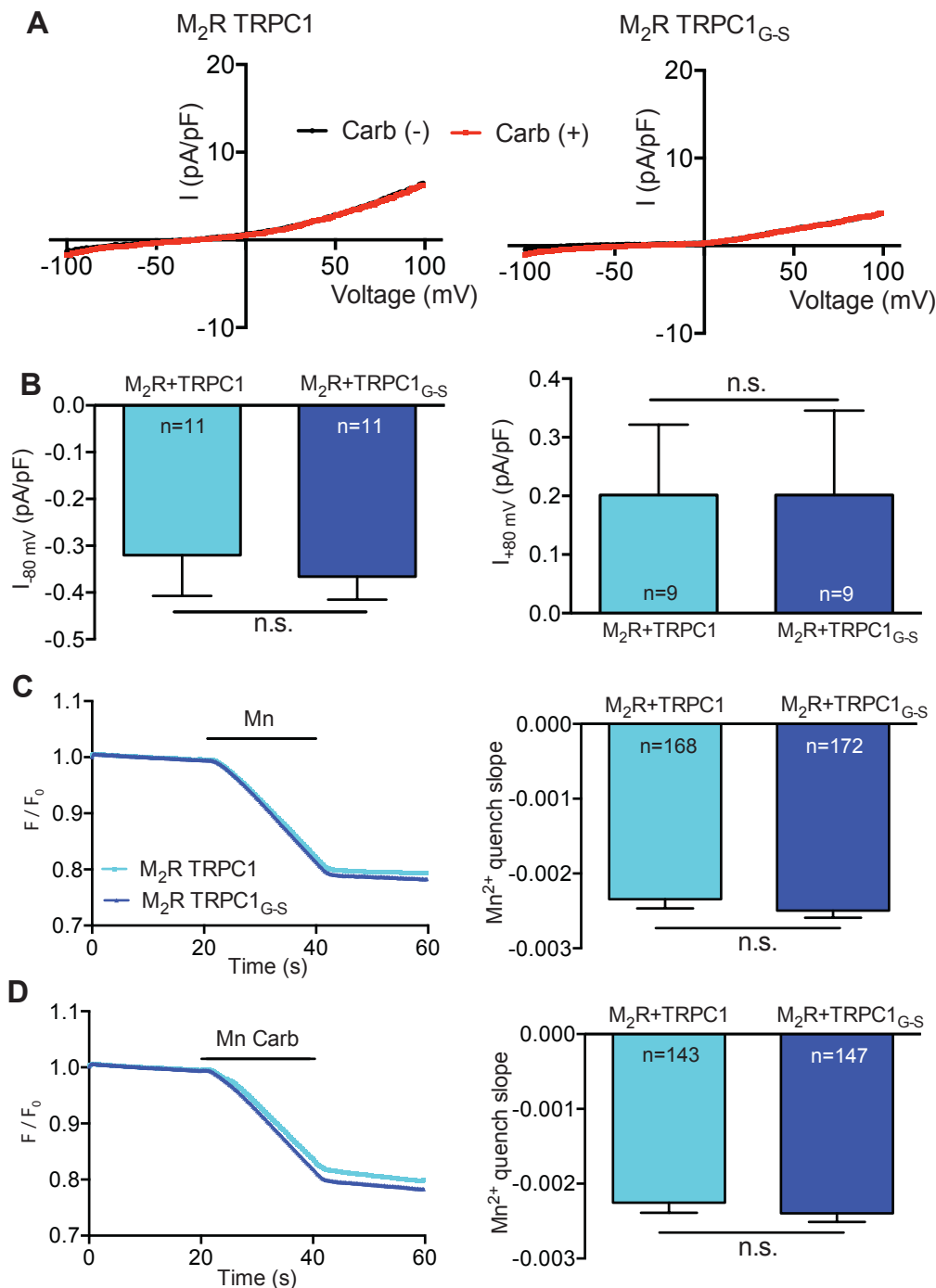
Figure 3.2.11 Homomeric recombinant TRPC1$_{G-S}$ is unable to form a functional receptor-operated channel when expressed in M$_2$R HEK293 cells.

(A) The I-V relationships from M$_2$R HEK293 cell (right) and TRPC1$_{G-S}$ M$_2$R HEK293 cells (left) before and after Carbachol treatment. Current densities at both +80 mV and -80 mV are summarized in (B, right) and (B, left), respectively. (C) and (D) depict the Mn^{2+} quench rates of TRPC4C1$_{Pore}$ expressed and non-transfected cells with and without Carbocachol treatment, respectively.
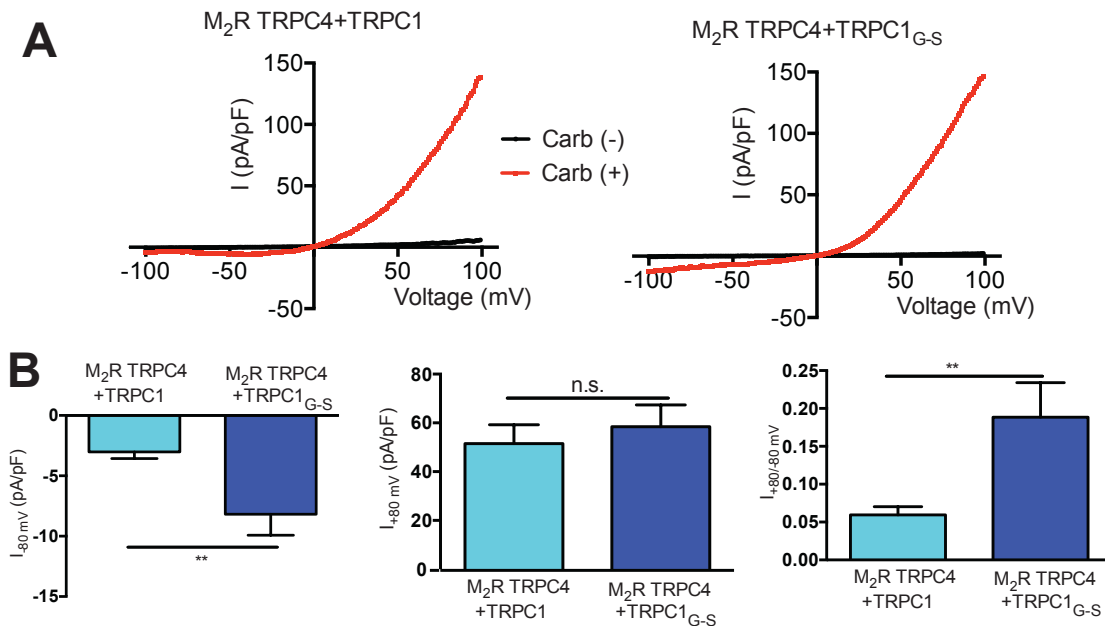
Figure 3.2.12 TRPC1$_{G-S}$ increases the inward current of TRPC4/TRPC1 channels.

(A) The I-V relationships of TRPC1 M$_2$R TRPC4 cells (right) and TRPC1$_{G-S}$ M$_2$R TRPC4 cells (left) before and after Carbachol treatment. Current densities at both -80 mV and +80 mV are summarized in (B, right) and (B, middle), respectively. Rectification factors calculated from the current density between -80 mV and +80 mV are summarized in (B, left).
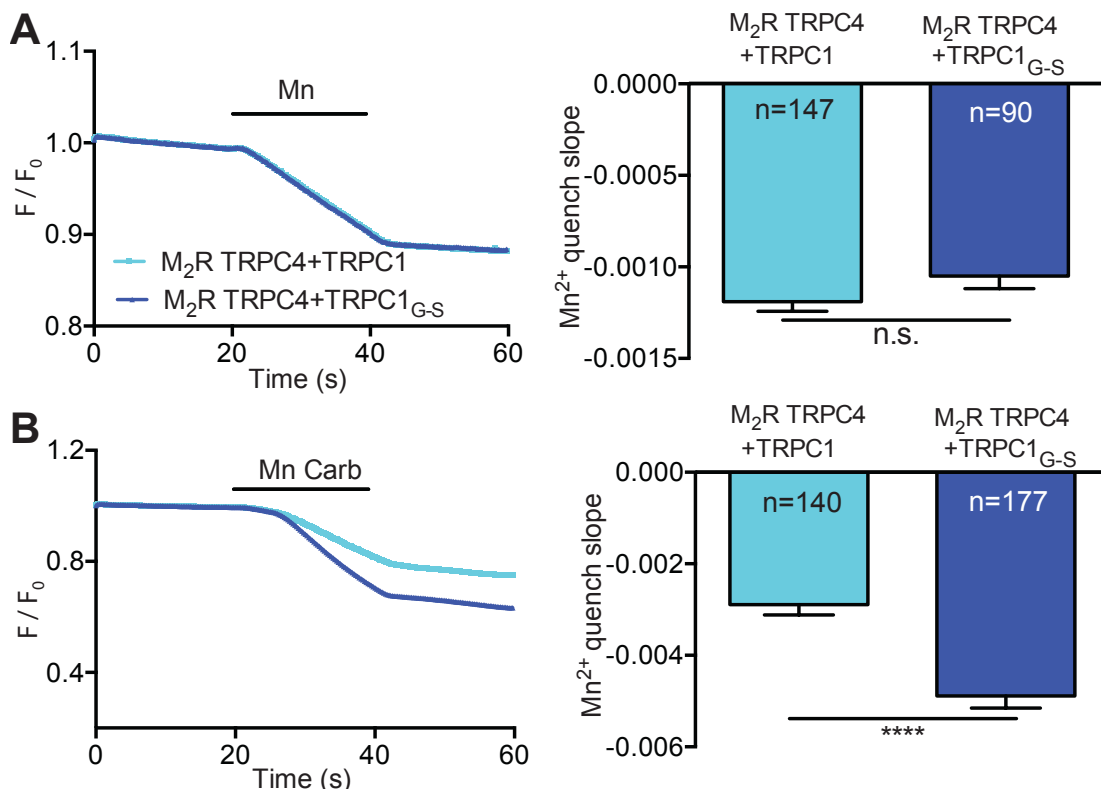
Figure 3.2.13 TRPC1$_{G-S}$ increases the Ca^{2+} permeability in TRPC4/TRPC1 channel complex.

(A) and (B) depict the Mn^{2+} quench rates of TRPC1$_{G-S}$ expressed and non-transfected cells with and without Carbocachol treatment, respectively.

4. Discussion

4.1 TRPM4

4.1.1 UV-Flash assay

The established approach to study a Ca^{2+} activated nonselective cation channel such as the TRPM4 channel, is to control intercellular Ca^{2+} concentration through the pipette solution and measure the resulting membrane currents[59,61]. Nevertheless, this approach bears quite a few shortcomings such as how to change the intracellular Ca^{2+} concentration, a procedure that appears rather challenging in whole cell recording[195]. Furthermore, as shown in a study on human TRPM5 it is the rate of rise in intracellular Ca^{2+} that affected the channel's activation, demonstrating the importance of the temporal dynamics of intracellular Ca^{2+} concentration on channel's gating kinetics[196]. The introduction of Ca^{2+} uncaging techniques, by using photolabile Ca^{2+} chelators such as 2-nitro-4, 5-dimethoxyphenyl-EDTA (DM-nitrophen)[197] and o-nitrophenyl-EGTA (NP-EGTA)[198] paved a way to control the changes of intracellular Ca^{2+} concentration and thus study the function of TRPM4 channel in a more physiological condition. Caged Ca^{2+} chelators are loaded into cells through the patch pipette and Ca^{2+} liberation is triggered by UV-flashes in a controlled and spatially uniform manner[202] and, simultaneously, intracellular Ca^{2+} dynamics can be recorded with appropriate Ca^{2+} sensors[220,221].

NP-EGTA with its broad absorption spectra in the UV (220 nm-400 nm)[198] was chosen as the Ca^{2+} caged compound in my experiments because of its primary advantage of high selectivity for binding Ca^{2+} over Mg^{2+} in comparison to DM-nitrophen[222]. There are two kinds of Ca^{2+} sensitive fluorescent indicators: ratiometric (dual-wavelength) and non ratiometric (single wavelength) indicators. Ratiometric measurements offer several advantages including the ability for quantitative Ca^{2+} measurements and taking into account the effects of photo bleaching, indicator leakage and uneven loading of individual cells to provide more reproducible and reliable results. Both, Indo-1 (dual emission ratiometric) and Fura-2 (dual excitation ratiometric) are the two most commonly used ratiometric Ca^{2+} indicators[223]. However, the overlap

between NP-EGTA's absorption spectra and Indo-1's or Fura-2's excitation wavelength prohibited the employment of these two ratiometric Ca^{2+} indicators.
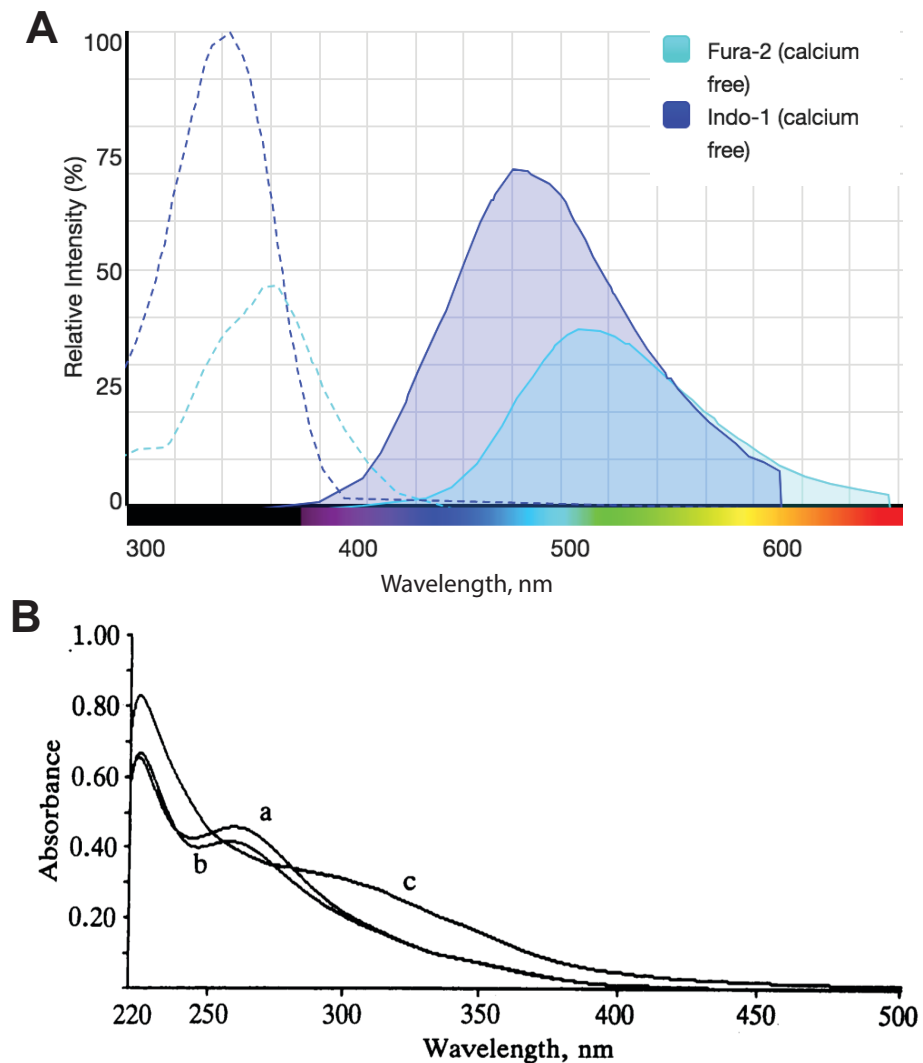
Figure 4.1.1 Absorption spectra of Fura-2, Indo-1 and NP-EGTA.

(A) The excitation and emission spectrum of two ratio metric Ca^{2+} indicator Fura-2 and Indo-1 (from ThermoFisher Fluorescence SpeactraViewer). (B) The absorption spectrum of NP-EGTA (66.5 μM) in buffer solution (40 mM HEPES, 100 Mm KCl, pH7.2) is shown in a. The spectrum changes in saturating Ca^{2+} conditions (0.2 mM) (b). Spectrum of this same sample after photolysis for 300s (c)[198].

Based on my preliminary results, I indeed observed a strong fluorescent signal change during the continuous illumination at 340 nm without UV-flash application with both, NP-EGTA and Indo-1 present in the pipette solution, indicating that the photolabile dependent Ca^{2+} release of NP-EGTA could be induced by the excitation wavelength of Indo-1 (Figure 4.1.2).
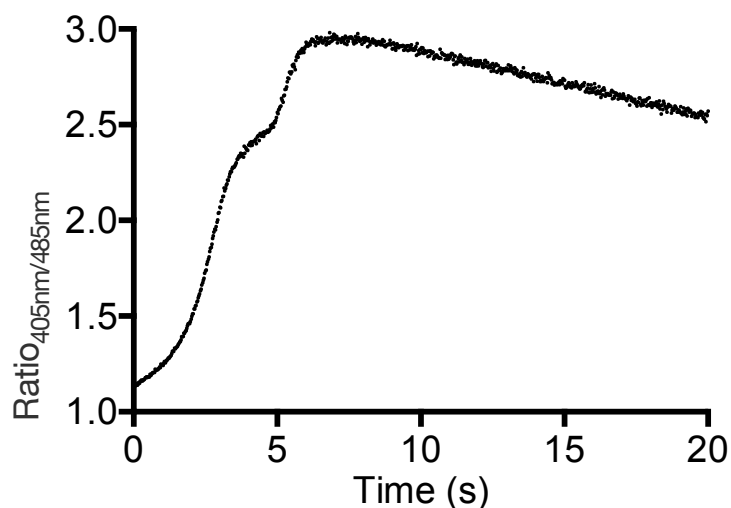
Figure 4.1.2 Ca^{2+} changes induced by the excitation wavelength (340 nm) of Indo-1. Recorded from HEK293 cells loaded with Ca^{2+} caged compound NPEGTA and Ca^{2+} dye Indo-1 without UV-flash stimulation.

Although single-wavelength Ca^{2+} indicators are not ideal for quantitative measurements, a practical approach towards quantification is to express the fluorescence signal relatively to its starting signal (denoting as F/F_0 or $\Delta F/F_0$) to correct for uneven indicator concentrations and provide comparable data between experiments[223]. Initially, I picked Fluo-4 as the Ca^{2+} indicator and added it to a NP-EGTA based pipette solution and loaded it into cells through patch pipettes. Following the application of a series of UV-flashes, induced TRPM4 currents could be recorded by patch-clamp, but no synchronized change of the Ca^{2+} signal was observed, indicating that Fluo-4 might not be the right indicator, probably because of its low kD value. Another option was to utilize an indicator with lower Ca^{2+}-binding affinity, which usually are also fast Ca^{2+} sensors. Fluo-4FF is an analogue of Fluo-4 with a Ca^{2+}-binding affinity of 10 µM, which would be used to detect intracellular Ca^{2+} concentration changes when Fluo-3 and Fluo-4 are already saturated. In my following experiments, I found that Fluo-4FF was suitable to detect the dynamic changes of the Ca^{2+} concentration following UV-flashes. For this I generated pipette solutions with pre-defined resting, basal Ca^{2+} concentration. With the knowledge of the resting Ca^{2+} concentration (at F_0) I was then able to determine the intracellular Ca^{2+} concentration quantitatively (see Methods section). Single Ca^{2+} transients elicited by an individual UV-flash permitted the analysis of the activation and deactivation kinetics of TRPM4 membrane currents. A train of Ca^{2+} jumps resulted in a wider range of Ca^{2+} concentrations from which I was able to generate quantitative

membrane current/Ca^{2+} concentration relationships. For TRPM4^{wt}, my data compared well with data published earlier[195] supporting the validity of my experimental approach. The apparent $K_{D,Ca}$ value found here (around 0.9-1 µM, Figure 3.1.2) also compares well with the range of values reported in cellular experiments that range from 0.5 to 20 µM[38]. Although my UV-flash method did not produce stable Ca^{2+} plateaus following the uncaging event, this was uncritical for the determination of the apparent $K_{D,Ca}$ (Figure 3.1.3).

Employing these strategies, I carefully scrutinized my approach with a well characterized TRPM4 mutation associated with human progressive familiar heart block type I (PFHBI)-E7K[45,59]. These reports and my results (Figure 3.1.4 and Figure 3.1.5) both support the notion that the E7K mutation´s effect worked through a rather straightforward mechanism by increasing plasma membrane expression through slowed down endocytosis resulting in a gain-of-function[45,59].

By using the UV-flash approach to release Ca^{2+} from NP-EGTA for activating TRPM4 currents, which avoided to expose cells into high intracellular Ca^{2+} concentrations for an extended time period and better reflected the "physiological" activation of the TRPM4 channel[195]. With this method, my results in TRPM4^{E7K} not only showed increased current amplitudes, which is line with the published data[59], but also provided additional information about the activation and deactivation kinetics of TRPM4 channels. They appeared to be unchanged (see Figure 3.1.4)

4.1.2 Aberrant deactivation induced gain-of-function in the A432T mutant might contribute to the occurrence of cardiac arrhythmia

The A432T mutant in the TRPM4 protein that has been associated with childhood and adult cardiac conduction block[61,93]. Interestingly, this amino acid exchange has been described as both, loss-of-function[93] and gain-of-function mutation[61]. My experimental approach for the first time revealed a multitude of changes in the behavior of this mutant channel protein when compared to the wt protein (Figure 3.1.6). While the apparent $K_{D,Ca}$ and the activation time constant were unchanged, all other parameters investigated were altered substantially: a nearly 2-fold increase in membrane current density, 50% reduction in plasma membrane expression, almost 4-fold slower deactivation and less than 20% of the glycosylation ratio (Figure 3.1.6 and Figure 3.1.7).

The major difference between the studies of Syam and coworkers, Liu and coworkers and my study is that the former determined the TRPM4 membrane current density at the so-called plateau phase, that is 2 minutes after rising the intracellular Ca^{2+} concentration to around 100 µM[93]. In contrast, the latter report and my study performed the current measurements close to the maximum of the initial current peak. Considering that the second plateau might actually be attributed to secondary recruitment of TRPM4 to the plasma membrane[195,224], I might speculate that the loss-of-function described by Syam and coworkers was a result of less efficient recruitment of additional TRPM4 molecules to the plasma membrane rather than a fundamental property of the functional channel protein itself.

The most prominent and important alteration I identified with the TRPM4[A432T] mutation was its substantially slowed down deactivation, an unrecognized etiology in cardiac TRPM4-related channelopathies. To estimate the resulting membrane currents during cardiac action potentials, I recorded typical action potentials from identified ventricular-like hiPS-CMs[207] and used these as a voltage template in voltage-clamped HEK293 cells expressing different TRPM4 variants (Figure 3.1.9). Concomitant UV-flashes mediated Ca^{2+} jumps additionally mimicked the accompanying cardiac Ca^{2+} transients (Figure 3.1.9 B). Through this experimental maneuver, I am able to investigate the putative current generation of the TRPM4 variant during normal action potentials in the absence of any pharmacological intervention. I am aware that this method has drawbacks in comparison to the "real" cardiac condition. One of the most prominent ones is the lack of other current components, such as Na^{+}/Ca^{2+} exchanger current or the plethora of potassium currents that might interact with the TRPM4 current in the native cardiac myocyte. Nevertheless, I think that the use of human action potentials and the ability to experimentally manipulate the intracellular Ca^{2+} concentration warrant this experimental approach.

At low Ca^{2+} concentrations (i.e. during the first couple of action potentials), TRPM4[A432T]'s current contribution was indistinguishable from that of the wt and the E7K mutant (see Figure 3.1.9 C TimePoints 1-3). When the Ca^{2+} concentration was above around 0.5 µM, TRPM4[A432T] contributes 5-10-fold more current to the subsequent action potential. This striking finding suggests that there are two crucial and synergistic requirements to coincide for TRPM4[A432T] mutation to generate exaggerated membrane

currents: elevated Ca^{2+} concentrations and repetitive stimulations. Both result in the generation of gradually increasing membrane currents, directly consequential to the substantially slowed-down deactivation kinetics. Due to limited amounts of caged-compound in the cell, I could not to further extend the train of action potentials and Ca^{2+} jumps, but it appears feasible to assume that a lower Ca^{2+} concentration with a higher rate of action potentials might have as similar effects than higher Ca^{2+} with a lower action potential frequency. Extrapolating from these findings I might speculate that all manoeuvres which will increase diastolic Ca^{2+} and/or the frequency of the cardiac myocyte unavoidably result in vicious circle driven by exaggerated production of membrane currents depolarizing the cell membrane and thus even in diastole resulting in elevated levels of diastolic Ca^{2+} that will activate increased levels of TRPM4 current and so on. This current will substantially distort the shape of the cardiac action potential in such a way that impulse propagation, e.g. across the atrioventricular node or distribution of the action potentials in the ventricular tissue might be malfunction.

4.1.3 Modulation of TRPM4 channels by protein modifications

In the cytoplasmic N- and C-terminus, TRPM4 channel contains several binding domains, including five putative calmodulin binding sites in both N- and C-terminus, two ABC-transporter-like signature motifs, phosphorylation sites for protein kinase A (PKA) and protein kinase C (PKC), a phosphatidylinositol bisphosphate (PIP_2) binding site with similarity to a pleckstrin homology domain (PH), four Walker B motifs, as well as a coiled-coil domain in the C-terminus[38].

A glycosylation site was reported in TRPM4[45] and the complex N-glycosylation stabilizes its surface expression[46]. A growing number of studies has shown that post-translational modifications of TRPM4 may play substantial roles in regulating its function[38,46]. To determine whether the altered deactivation kinetics of TRPM4^{A432T} were mainly a consequence of the reduction of glycosylation in TRPM4 protein, TRPM4 currents were recorded in TRPM4^{wt} before and after the treatment of glycosylation inhibitor Tumicamycin. Notably, the substantially reduced glycosylation of TRPM4 protein was not a major contributor to the slowed down deactivation, because pharmacological reduction of glycosylation by Tunicamycin in TRPM4^{wt} proteins did not alter the deactivation properties of TRPM4^{wt} channel (Figure 3.1.10). The identified

glycosylation consensus sequence (Asn-Xaa-Ser/Thr, Xaa being any amino acid except Pro and Asp) in TRPM4 is located near the pore-forming loop between S5 and S6 (Asn[992]), the single N-glycosylation residue (N988Q) mutation prevents TRPM4's glycosylation[46]. However, position 432 is located at the N-terminus and thus far away from the reported glycosylation consensus sequence. How such a mutation at the N-terminus could affect glycosylation of TRPM4 protein is remains unknown.

TRPM4 contains multiple putative PKC phosphorylation sites at both, the N-terminus (Thr[88] and Thr[356]) and the C-terminus (Ser[1145] and Ser[1152]). Previous studies indicated that Phorbol ester treatment enhanced the Ca^{2+} sensitivity of TRPM4[wt] in HEK293 cells, while this effect was absent in two mutants (S1145A and S1152A), indicating that PKC-dependent phosphorylation might modulate TRPM4's Ca^{2+} sensitivity[40]. Even through the A432T mutant induced an additional possible phosphorylation site (Threonine), my results indicated that the inhibitor of cPKC (GÖ6983) didn't alter its deactivation, indicating that cPKC-mediated phosphorylation was unlikely to contribute to the altered deactivation kinetics despite the reported multiple functions of TRPM4 phosphorylation[40,48].
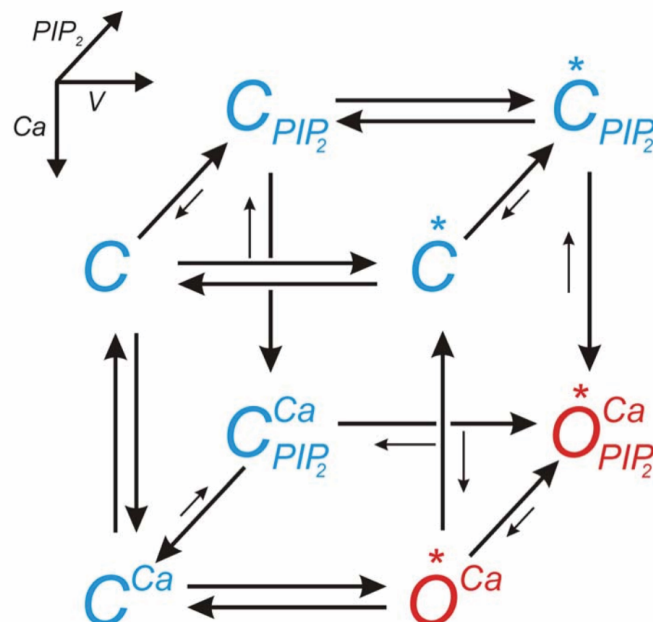
Figure 4.1.3 Schematic model to explain the combined modulation of voltage, Ca^{2+} and PIP_2 on TRPM4.

Three separate equilibria including activation/deactivation of voltage sensor, Ca^{2+}-binding /unbinding and PIP_2-binding/unbinding (represented by the three axes in the 3D scheme, respectively) are involved to govern the gating of TRPM4[41].

PIP$_2$ was reported to modulate the activity of TRPM4 by shifting the voltage dependence of TRPM4 activation towards negative potential and by increasing the Ca^{2+} sensitivity of TRPM4 about 100-fold[41]. A landmark of TRPM4 is its rapid desensitization (fast deactivation) following activation by intracellular Ca^{2+} increases, which might be explained by Ca^{2+}-dependent depletion of PIP$_2$[51]. Application of exogenous PIP$_2$ to the intracellular surface in inside-out patches recording restored the properties of TRPM4 currents[51]. A basic residues in a C-terminal pleckstrin homology (PH) domain was an important determinants for PIP$_2$'s action[41]. The binding site of PIP$_2$ was also suggested for the E733-W772 region in the N-terminus of TRPM4 by biophysical and molecular modelling methods[52]. All these data indicated that PIP$_2$ is a potent modulator of TRPM4's behaviour. In my experiments, apart from the reduced membrane current density (Figure 3.1.12), I did not observe any effect of PIP$_2$ on TRPM4's deactivation following Ca^{2+} decay, which can be explained by the observation that PIP$_2$ is unable to generate TRPM4 current when the Ca^{2+} concentration was buffered to a low level[41]. Figure 4.1.3 depicts the possible model of the combination effect of Ca^{2+}, voltage and PIP$_2$ on TRPM4 channel[41]. PIP$_2$ is not a direct activator but a modulator of TRPM4's sensitivity to Ca^{2+} and voltage[41].

4.1.4 Ala432 is a crucial amino acid to determine TRPM4's properties

The fact that this single mutation A432T, apparently far away from the pore region, the TRP box motif and other important domains of the TRPM4 protein located in the cytoplasmic C-terminal region exerted such a profound collection of alterations in the channel´s properties motivated me to perform a more rational series of mutagenesis experiments at this location. While a sole reduction in the size of the amino acid´s side chain (from a methyl-group to a single hydrogen, Alanine to Glycine) only displayed a reduced membrane current density when compared to the wt protein (Figure 3.1.13), all other parameters studied here were unchanged. In great contrast, when I increased the bulkiness of the side chain (from a methyl to a -CH(CH$_3$)$_2$ group, Alanine to Valine) without adding polarity, the properties of the channel were substantially altered. The highly-glycosylated protein was reduced (Figure 3.1.13 H), membrane current density was increased (Figure 3.1.13 E) and the activation as well as deactivation time constants were faster and slower, respectively (Figure 3.1.13 F and G). Considering all these results it appeared that an "increased bulkiness" of the side chain evoked a

plethora of channel alterations, whether the side chain was uncharged and non-polar (as for Valine) or uncharged but polar (as for Threonine). Interestingly, the partial charge carried by the hydroxyl-group in Threonine appeared to substantially influence the activation/deactivation kinetics, it caused slowing down of the deactivation while the non-polar, uncharged group increased the activation kinetics. One is almost inclined to speculate that while the bulkiness predominantly modulates the activation kinetics, the addition of a partial charge shifts the effects towards the deactivation of the membrane currents after a Ca^{2+} jump. It appears noteworthy that the reduction of the side chain to a single hydrogen decreases the Ca^{2+} sensitivity, the molecular mechanism of which remains unclear.

A final series of mutations probed for the effects of charged residues at the 432 position by substituting with either Aspartic acid (negative charge) or Lysine (positive charge) for Alanine in the wt protein (Figure 3.1.14). These amino acid exchanges displayed majorly altered protein expressions as well as channel properties. Glycosylation was basically restricted to core-glycosylation with a barely detectable highly-glycosylated protein (Figure 3.1.14 E). Surprisingly, both substitutions yielded channel that did not generate any measurable membrane currents following Ca^{2+} jumps (Figure 3.1.14 B and C) despite their clear cellular and membrane expression (Figure 3.1.14 E and F). The residual Ca^{2+} activated membrane currents reflected the current component already found in non-transfected HEK293 cells (see Figure 3.1.14 D).

The MHR domains are identified as four homology regions (MHR1-MHR4) based on the similarity of amino acid sequence in the TRPM subfamily while their functions are not yet known[12]. The published structure of TRPM4 reveals that a domain structure termed MHR1/MHR2 is formed by MHR1 and MHR2 regions. The MHR3 domain appears to serve as a bridge connecting the MHR1/2 and MHR4. The MHR3 and MHR4 domains are composed of α helices, which hook up to transmembrane domain to form interactions between the cytoplasmic domains and transmembrane domains through the S2-S3 linker[216]. The lower portion of MHR4 domain interacts with the TRP domain and the S2-S3 linker on one side and with the rib helix of C-terminal domain and MHR3 domain on the other side, indicating a possible cross interaction between the MHRs, C-terminal domain and the transmembrane domains.

Recent publications report the detailed 3D structure of the TRPM4 protein[210,211] and provide the first real structural model. Using such structural information, I modelled the immediate surroundings of position 432 and found that the mutations at this position indeed modified the compactness of the MHR3 domain (Figure 3.1.15). Position 432 locates within in MHR3 domain and the amino acid Alanine at this position forms interactions with the surrounding amino acids ((V401, P438 and F440). In contrast, I found that the substitute Threonine with a bulkier side chain forms additional interactions with surrounding amino acids (V401, R437, P438, F440, V441 and L444) suggesting a more compact and stable structure within the MHR3 domain. The Glycine at this position with the shortest possible side chain appears to induce more flexibility in this region and may thus regionally disrupt the α helix in the MHR3 domain to form a random coil. In the Valine substitution, an increased number of interactions among the regional residues may form a more compacted structure (similar to the A432T mutant) and stabilize the MHR3 domain. In contrast, in the A432D and A432K mutants, the bulkiness of Asp and Lys, strongly affects the flexibility of the surrounding helix and may in this way generate repulsion forces between helices to destabilize the MHR3 domain. The structure of the Ca^{2+} occupied TRPM4 protein appears to suggest that it is the cytoplasmic part of TRPM4 that is involved in the regulation of TRPM4´s gating behavior[216]. The cytosolic parts include the MHRs domains at N-terminus and the C-terminal domains (including helical 'ribs' and 'pole' helix). Based on the revealed structure, C-terminal domains span into the MHRs domains[210] and thus suggest that the position 432 in the MHR3 influences channel's gating characteristics by modulating the interactions between the N- and the C-terminus of TRPM4.

4.1.5 Possible interactions between N- and C-terminus to rescue TRPM4^{A432T}'s aberrant behavior

The C-terminal TRP domain plays an important role in regulating the functions of TRP channels[6,7,215,225-227]. The interaction between PIP_2 and the TRP domain regulates two fundamental properties of the TRPM8 channel: its activation and desensitization kinetics[215]. In the TRPV1 channel, the TRP domain appears essential for the channel's gating[226,227]. The interactions between the TRP box and the S4-S5 linker may control the open[6] and closed[214] state of the TRPV4 channel. For the

rat TRPM4 channel the requirement of a functional TRP domain for normal Ca^{2+} sensitivity was reported[228].

My data also provides evidence for a substantial functional interaction between the N- and C-terminus of the TRPM4 protein. This notion was majorly supported by my experiments in which I investigated the artificial amino acid substitution at position 1062 located in the TRP domain[61,229]. Nilius and coworkers described this interesting mutation in the TRP box, a R1062Q amino acid exchange, associated with an accelerated Ca^{2+}-dependent current deactivation[41]. I compared the wt protein with proteins carrying single (A432T or R1062Q) mutation or double mutations (A432T/R1062Q) and interestingly found that in the double mutant, aberrant alterations evoked by the single A432T mutation were largely counterbalanced by the R1062Q mutation with respect to basically all parameters studied (i.e. current density, activation and deactivation kinetics). I found that A432T and R1062Q displayed almost antagonistic effects on many of TRPM4´s properties suggesting that these two domains might indeed functionally interact in the intact tetrameric protein or at least influence the gating of the channel in a surprisingly antagonistic manner.

Recent structural data on TRPV1[230-232], TRPV2[52,230], TRPV6[232], TRPA1[233] and TRPP2[234-236] proposed that a short N-terminal α-helical domain upstream of TM1, the pre-S1 domain, may be involved in allosteric gating by directly interacting with the TRP-domain/TRP Box. However, in TRPM4 the corresponding amino acid sequence localizes to amino acid residues 672-689, considerably upstream of position 432. The structure of the human TRPM4 channel generated by electron cryo-microscopy[210,216] depicted that R11062 locates within the so called TRP helix which might directly interact with the S4-S5 linker and the MHR4 domain, suggesting that an interaction between the N- and the C-terminus might indeed modulate the gating of the TRPM4 channel[210,216].

4.1.6 Mutational spectrum of the TRPM4 channel in human cardiac conduction diseases

Cardiac conduction disturbances are common risk factors in cardiac diseases, thus the underlying mechanism and factors associated with the cardiac conduction system are important. Aberrant cardiac conduction caused by genetic defects may serve as disease

models to clarify the molecular and functional aspects of conduction impairment[94]. For most of the reports, original descriptions of penetrated family generations relate back many decades (e.g. see[91]) and describe these inherited cardiac conduction diseases such as progressive familial heart block (PFHB), but the underlying genetic cause and disease mechanism are elusive. Recently, mutations in the TRPM4 gene were suggested as the genetic cause for progressive familial heart block type I[59]. Since then, more and more TRPM4 mutations were identified in cardiac conduction diseases[61,92,93,233]. Some mutants' influences on TRPM4's behaviors are still unknown and wait to be further explored.

To evaluate the role of *TRPM4* gene in the development of inherited cardiac blocks, I employed the UV-flash assay to analysis the electrophysiological properties of nine additional TRPM4 mutants. I found that among these nine mutations (Q131H, D561A, T677I, G737R, Y790H, G844D, R892C, K914R and P970S), four of them (Q131H, D561A, R892C, P970S) did not change the TRPM4's properties, while five of them (T677I, G737R, Y790H, G844D and K914R) significantly altered the investigated properties. The nine mutations are summarized in Table 4.1.

Table 4.1 Properties of investigated TRPM4 mutations

Mutations	Current density	$K_{D,Ca}$	Activation	Deactivation
Q131H	n.s.	n.s.	n.s.	n.s.
D561A	n.s.	n.s.	n.s.	n.s.
T677I	Increase	Decrease	n.s.	Decrease
G737R	Increase	n.s.	n.s.	n.s.
Y790H	Increase	Decrease	n.s.	Decrease
G844D	Increase	n.s.	n.s.	Decrease
R892C	n.s.	n.s.	n.s.	n.s.
K914R	Increase	n.s.	Decrease	Deecrease
P970S	n.s.	n.s.	n.s.	n.s.

n.s: no significant difference when compared to the wt

TRPM4 is activated by intracellular Ca^{2+} via an -as of yet- unknown mechanism. Two possibilities for this appear likely: directly binding of Ca^{2+} to the protein or indirect activation by binding of Ca^{2+}-binding proteins to the channel. Well known Ca^{2+}-binding motifs such as the EF-hand, the C2 domain[234] or the 'Ca^{2+}-bowl' motif in BK potassium channels[235] have not been identified in the TRPM4 protein. However, five

Ca^{2+}-calmodulin binding sites were characterized and deletion of any of the three sites in the C-terminus strongly reduced the Ca^{2+} sensitivity of the resulting TRPM4 channels[40]. ATP, PKC-dependent phosphorylation and PIP_2 were reported to modify the Ca^{2+} sensitivity of TRPM4. In a recent study, a Ca^{2+} binding site comprising the side chains of Glu828 and Gln831 in S2 and Asn865 and Asp868 from S3 was suggested (Figure 4.1.5)[216].
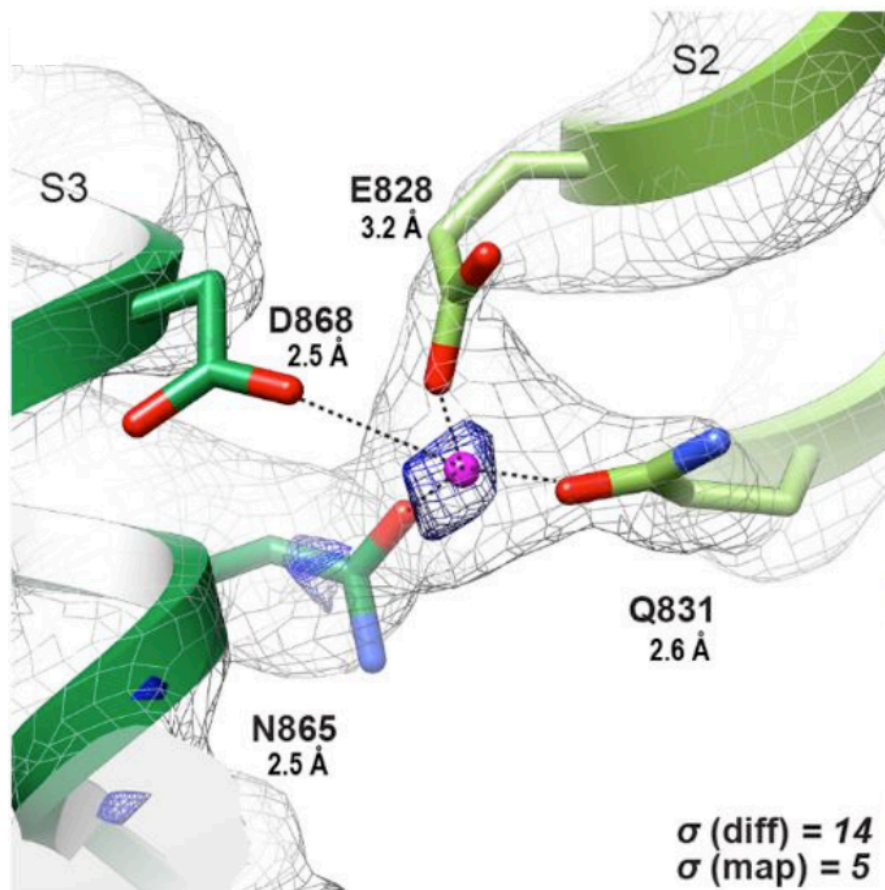
Figure 4.1.4 Ca^{2+} binding site.
Modified from reference[216].

In my experiment, I observed that both T677I and Y790H mutants increased the Ca^{2+} sensitivity of the TRPM4 channels. These findings represent the first reports that TRPM4's Ca^{2+} sensitivity is altered in human cardiac conduction block which might thus represent a new disease etiology. I also found that both mutants increased the maximal membrane current density of TRPM4 together with a slower deactivation but unaltered activation kinetics. So far, the underlying mechanisms are elusive and additional experiments are needed to uncover the molecular mechanisms.

The S4-S5 linker represents an important domain for the function of TRP channels[236]. In TRPV channels, it possibly interacts with PIP_2 to modulate the channel's gating properties[237]. In TRPM8, the S4-S5 linker plays a central role in voltage sensing and modulates the affinity of the menthol binding site[238]. Teng and coworkers' described that the S4-S5 linker of the TRPV4 protein regulates the kinetic properties including both open and closed gating[6,214]. A competing hydrophobic tug on L596 could unlock the S4-S5 linker's elbow to open the TRPV4 channel[6] and the S4-S5 linker also regulates TRPV4's closed and inactivated state by the L596-W733 interaction between the TRP box and the start of the S4-S5 linker. Disruption of this interaction by the L596P mutant increased channels' opening[214]. Replacing the conserved glycine residue in S4-S5 linker by a serine forced both TRPC4 and TRPC5 channels into an constitutively open state[8]. In recent years, more and more human mutants within the S4-S5 linker have been identified in TRPV3, TRPV4 and TRPA1 channelopathies[236]. Stallmyer *et al.* identified a mutant, K914R, within the S4-S5 linker of TRPM4. Nevertheless, the functional consequences of this mutation for the channel's properties are still elusive[94]. To answer this question, I performed a series of UV-flash experiments in HEK293 cells transiently expressing TRPM4^{K914R} mutant and found an increased membrane current density together with a slower activation and deactivation kinetics. The Ca^{2+} affinity for channel activation was not changed. Based on the published data and my results, I speculate that the S4-S5 linker of TRPM4 protein may also regulate the gating of TRPM4 channel through an unknown mechanism and more experiments need to be carried out in future studies.

The G844D mutant maps to the intracellular sequence between the second and third transmembrane segments of TRPM4. Functional analysis revealed a gain-of-function in TRPM4^{G844D} because of an impaired endocytosis, subsequently elevating TRPM4 channel's presence in the plasma membrane[61]. Furthermore, in my experiment I observed a slower deactivation in TRPM4^{G844D}, suggesting that position 844 might also be able to modulate channel gating.

In four mutations (Q131H, D561A, R892C and P970S) originally identified in patients with cardiac conduction diseases, I failed to reveal any alternations of TRPM4's electrophysiological properties. The Q131H mutant is located in a predicted calmodulin-binding site, but based on my results the Ca^{2+} sensitivity of TRPM4 was unchanged in

TRPM4^{Q131H}. The amino acid substitution P970S located in the pore-forming region of TRPM4 was speculated to affect the channel's open probability[94]. To testify this hypothesis, I carried out patch-clamp recordings and found that this mutation did not alter TRPM4's properties. The same also held true for mutations D561A and R892C. It thus remains unclear how these mutants are pathogenic in cardiac conduction diseases but in the end one might speculate that these mutations might indeed not be causative for the human pathology but only coincidental.

4.1.7 Summary & Conclusion

In summary, the gain-of-function mutation (A432T) in TRPM4 has been linked to life-threatening cardiac conduction disturbances in patients. For deeper insights, I employed an UV-flash assay and revealed that TRPM4^{A432T} mutation induced a 2-fold larger membrane current associated with less plasma membrane protein expression. Kinetic analysis unveiled a 4-fold slower deactivation which make a contribution to the increased membrane current progressively rising during human cardiac action potentials. Furthermore, by rational mutagenesis of TRPM4 at position 432, I found that the bulkiness of the residue was key to TRPM4^{A432T}'s aberrant gating. The charged residues at position 432 rendered TRPM4 channel non-functional. The slow deactivation caused by the substitution from alanine to the bulkier threonine at position 432 represents a key contributor to the gain-of-function in TRPM4^{A432T}. Besides, by modeling of TRPM4's structure revealed that the bulkiness of the residue at position 432 modulates the compactness of TRPM4's MHR3 domain and might thus alter the behaviors of ion channel. Interestingly, the aberrant functions of TRPM4^{A432T} mutation could be partial rescued by an artificial mutation R1062Q in the TRP box, suggesting a functional interaction between the N- and the C-terminus of TRPM4. These results suggest an important mechanism of TRPM4's mutation that its aberrant deactivation induced by altered compactness of MHR3 domain might substantially contribute membrane currents to human cardiac action potentials and represent possible disturbances for cardiac events.

A broader functional analysis of the mutational spectrum of TRPM4 identified in patients with cardiac conductance diseases depicted that mutations in the TRPM4 protein not only increased the membrane currents density but also altered the channel's Ca^{2+}

sensitivity and gating kinetics including both activation and deactivation. These findings broaden our understanding mechanistical aspects of TRPM4's regulation and might thus provide new targets for the treatment of inherited cardiac conduction diseases. In the end these findings may pave the way towards a less invasive therapy compared to the currently used approach of pace maker implantation.

4.2 TRPC1/TRPC4

4.2.1 Interaction between TRPC1 and TRPC4

Heterologously expressed TRPC1 proteins alone do not respond to muscarinic stimulation and are not able to form a functional homotetrameric channel, possibly because that homotetramers of TRPC1 are retained at the ER and failed to reach the plasma membrane[219]. Heteromerization with other TRPC channels, not only with TRPC4 and TRPC5 but also with the diacylglycerol-sensitive subfamily TRPC3, TRPC6 and TRPC7, TRPC1 successfully locates to the plasma membrane to form a receptor-operated heteromeric channel complex that modulates the Ca^{2+} entry[110]. The substitutions of glutamate by glutamine at positions 581 and 582 in the putative pore-forming region of TRPC1 decreased the Ca^{2+} influx through the heteromeric channel complex, suggesting that TRPC1 indeed directly contributes to pore formation rather than acting as an accessory subunit[110].

In agreement with that, I also observed that when expressed in HEK293 cells alone TRPC1 failed to respond to a stimulation through the M_2R agonist Carbachol. In the heteromeric channel complex, I found that TRPC1/TRPC4 hetermeric channels induced more Ca^{2+} entry than TRPC4 homotetramers under basal conditions, supporting the notion that TRPC4/TRPC1 may work as a background Ca^{2+} entry pathway[20]. TRPC4 is activated by stimulation of $G\alpha_{i2}$ through a direct interaction between $G\alpha_{i2}$ and the conserved C-terminal SESTD motif of TRPC4[157]. When co-expressed with M_2R, TRPC4 could be activated by Carbachol and generated a double rectifying membrane current, as shown in Figure 3.2.3 A. While TRPC1's expression substantially altered the biophysical properties of TRPC4 currents from double rectification to outward rectification and dramatically reduced the Ca^{2+} influx measured by Mn^{2+} quench experiment. This suggests that TRPC1 plays an important role in modulating the electrophysiological and physical behaviors of the heteromeric TRPC4/TRPC1 channel complex.

It seems that TRPC1 exhibits two different roles when assembled with TRPC4. without any agonist stimulation, TRPC1/TRPC4 worked synergistically as a background Ca^{2+} entry pathway[20]. However, under the stimulation of Carbachol, TRPC1 hindered the Ca^{2+} influx in TRPC4/TRPC1 channel complexes in my experiment also see in

reference[110]. Considering the fact that $G\alpha_{i2}$ activates TRPC4 by its direct interaction with the conserved C-terminal SESTD motif (700-728 amino acid) in TRPC4[157] which also participates in the assembly of TRPC4/TRPC1 channel complex[191]. Besides, TRPC1 lacks the binding interface for TRPC4-$G\alpha_{i2}$[125], thus I speculate that maybe it is the binding between $G\alpha_{i2}$ and TRPC4 during Carbachol stimulation that interferes the interaction of TRPC1 and TRPC4, then resulting in the changes of Ca^{2+} permeation in TRPC4/TRPC1 channel complexes.

4.2.2 The TRPC1 pore region regulates Ca^{2+} entry in the TRPC4/TRPC1 channel complex

To clarify the role of TRPC1 in the heteromeric TRPC4/TRPC1 channel in greater detail, two chimeras were constructed, in one of them the pore region of TRPC1 was substituted by the TRPC4 pore region (TRPC1C4$_{Pore}$) and in another the pore region of TRPC4 was replaced by TRPC1 pore region (TRPC4C1$_{Pore}$).

My results indicated that when heteromerized with TRPC4, the channel complex TRPC4/TRPC1C4$_{Pore}$ displayed a double rectifying current with less inward and outward current, as well an increased Ca^{2+} entry when compared to TRPC4/TRPC1. Both properties resemble hallmarks of the TRPC4 channel, suggesting that the pore region of TRPC1 is an important determinant for these biophysical properties (e.g. rectifying and Ca^{2+} entry). Lacking the TRPC1 pore, the remainder of the TRPC1 protein failed to display the original TRPC4/TRPC1 channel characteristics such as the outward rectification and reduced Ca^{2+} entry following agonist stimulation. These data support the notion that the TRPC1 protein in the heteromeric channel (TRPC4/TRPC1) indeed directly contributes to the formation of the resulting channel pore.

Furthermore, in a sort of verse approach I substituted the TRPC4 pore by the TRPC1 pore region to form a TRPC4/TRPC4C1$_{Pore}$ channel complex. Surprisingly, these heteromeric channel complexes were indistinguishable from the TRPC4 homotetramers in both, current density and the I-V relationship following Carbarchol stimulation (Figure 3.2.9). Noteworthy, in Mn^{2+} quench experiments under resting conditions, the chimeric channel displayed enhanced background Ca^{2+} entry, which appears to resemble the properties of the TRPC4/TRPC1 channel complex, supporting the notion that TRPC1 might be important for the constitutive channel activity in its "background Ca^{2+} entry"

mode. When stimulated with Carbarchol (Figure 3.2.10 B) I revealed that the chimera's Mn^{2+} quench rate was reduced indicating less Ca^{2+} permeability. This again resembled the properties of the TRPC1 contribution, i.e. reduced Ca^{2+} entry in the heteromeric wt channel. In summary, these surprising data strongly suggest that even through the TRPC1 pore in the TRPC4 chimeric protein failed to modulate the membrane current properties with respect to rectification it was still potent in modifying the TRP channel's Ca^{2+} permeability. These findings strongly suggest novel and distinct roles of the TRPC1 pore for gating and ion selectivity in the TRPC4/TRPC1 heteromeric channel protein.

4.2.3 S4-S5 linker of TRP channels modulates channel's function

In the Shaker potassium channel it was suggested, that the S4-S5 linker triggers the motion of S6 helices and thus modulates the channel's gating behavior in response to voltage changes[239]. A similar mechanism might also be present in the TRPC4 and TRPC5 channels. The G-S substitution mutant within the cytosolic S4-S5 linker in TRPC4 and TRPC5 rendered the channels consecutively open and abrogated any response to stimulation by G-protein coupled signaling. By rationally mutagenesis at the same site, it was shown that the simplicity and flexibility of the amino acid glycine modulates the channel's properties[8]. The corresponding conserved amino residue for TRPC1 was identified at site 623. As shown in Figure 3.2.12 and Figure 3.2.13, the G-S substitution in the S4-S5 linker increased inward currents and Ca^{2+} entry when co-expressed with TRPC4. Formerly, TRPC1 was identified as a heteromeric channel component inhibiting Ca^{2+} influx[110]. In contrast to that, my data demonstrated that the G-S mutation in TRPC1 relieved this inhibitory effect and indeed induced an increased Ca^{2+} entry, supporting the notion that the S4-S5 linker plays a crucial role in regulating the function of TRPC1 containing heterotetramers.

A plethora of additional single point mutations in or related to the S4-S5 linker of TRP channels have been reported to cause aberrant channel activities and may be related to several pathological phenotypes[240-242]. The G573S or G573C mutation of TRPV3 has been linked to Nh (non-hair) and Ht (hypotrichosis) in rodents[243]. In human TRPA1, two conserved residues (R852 and N855) in the S4-S5 linker appear crucial for stabilising the inter-subunit conformations, which is related to the channel's chemical

and voltage-induced gating[244]. Mutation K914R identified in the TRPM4 channel was identified in patients with cardiac conduction disorders[94] and my results indicated that this mutant alters both, the activation and deactivation kinetics of the TRPM4 channel. A disease related mutation in the S4-S5 linker of TRPC1 has not been reported as of now. It is therefore unclear whether mutations in the S4-S5 linker of TRPC1 are disease related or not although my results strongly suggest that the S4-S5 linker is indeed able to modulate the properties of TRPC1 channels.

The four amino acid motifs, pre-S1, S4-S5 linker, distal S6 and TRP-helix, define a unique signature in almost all TRP channels[236]. The S4-S5 linker reportedly regulates channel's gating by different mechanisms[214,230]. In TRPV4, the hydrophobic tug on L596 located within the S4-S5 linker allows channel opening by unlatching the S4-S5 linker elbow from the TRP helix and stabilization of the channel's closed state by the L596-W733 bond between the S4-S5 linker and the TRP box[6,214]. In TRPV1, the S4-S5 linker and S6 interacted through the hydrogen bond between D576 in the S4-S5 linker and M682 in S6. Loss of this hydrogen bridge causes a shift of the S4-S5 linker and promotes channel opening in the capsaicin-bound structure[230]. My results demonstrated that the G-S mutation in the S4-S5 linker of the TRPC1 channel modulates Ca^{2+} entry, although the underlying mechanism is still unclear.

4.2.4 Summary & Conclusion

In summary, I found that in TRPC4/TRPC1 heteromeric channel complexes, TRPC1 was responsible for generating outward rectifying membrane currents and for significantly decreasing the Ca^{2+} entry following activation by Carbachol. These findings are in agreement with previous reports[125]. In additional studies employing two novel chimeric proteins, $TRPC1C4_{Pore}$ and $TRPC4C1_{Pore}$, I was able to reveal that it is the pore region of TRPC1 that is crucial in TRPC4/TRPC1 channel complex for determining the channel's biophysical properties (current amplitude, I-V relationship and Ca^{2+} permeability). $TRPC1_{G-S}$ increased the inward currents without significantly altering the I-V relationships and partly increased the Ca^{2+} entry in $TRPC4/TRPC1_{G-S}$ heteromeric channel complex, displaying the important role of S4-S5 linker in modulating the channel's function. These findings make a contribution to understand the important

roles of the pore region and S4-S5 linker of TRPC1 in the function of TRPC4/TRPC1 heterotetramers.

Reference

1. Montell C, Rubin GM. Molecular characterization of the Drosophila trp locus: a putative integral membrane protein required for phototransduction. Neuron. 1989;2:1313–23.

2. Wu L-J, Sweet T-B, Clapham DE. International Union of Basic and Clinical Pharmacology. LXXVI. Current progress in the mammalian TRP ion channel family. Pharmacological Reviews. 2010;62:381–404.

3. Nilius B, Owsianik G. The transient receptor potential family of ion channels. Genome Biology. 2011;12:218–29.

4. Owsianik G, D'hoedt D, Voets T, Nilius B. Structure-function relationship of the TRP channel superfamily. Reviews of Physiology, Biochemistry and Pharmacology. 2006;156:61–90.

5. Erler I, Hirnet D, Wissenbach U, Flockerzi V, Niemeyer BA. Ca2+-selective transient receptor potential V channel architecture and function require a specific ankyrin repeat. Journal of Biological Chemistry. 2004;279:34456–63.

6. Teng J, Loukin SH, Anishkin A, Kung C. A competing hydrophobic tug on L596 to the membrane core unlatches S4-S5 linker elbow from TRP helix and allows TRPV4 channel to open. Proceedings of the National Academy of Sciences. 2016;113:11847–52.

7. Romero-Romero S, Gomez Lagunas F, Balleza D. Side chain flexibility and coupling between the S4-S5 linker and the TRP domain in thermo-sensitive TRP channels: Insights from protein modeling. Proteins. 2017;85:630–46.

8. Beck A, Speicher T, Stoerger C, Sell T, Dettmer V, Jusoh SA, et al. Conserved gating elements in TRPC4 and TRPC5 channels. Journal of Biological Chemistry. 2013;288:19471–83.

9. Moran MM, McAlexander MA, Bíró T, Szallasi A. Transient receptor potential channels as therapeutic targets. Nature Reviews Drug Discovery. 2011;10:601–20.

10. Zhu MX. Multiple roles of calmodulin and other Ca^{2+}-binding proteins in the functional regulation of TRP channels. Pflügers Archiv - European Journal of Physiology. 2005;451:105–15.

11. Nelson PL, Beck A, Cheng H. Transient receptor proteins illuminated: current views on TRPs and disease. The Veterinary Journal. 2011;187:153–64.

12. Clapham DE. TRP channels as cellular sensors. Nature. 2003;426:517–24.

13. Zhang Y, Hoon MA, Chandrashekar J, Mueller KL, Cook B, Wu D, et al. Coding of sweet, bitter, and umami tastes: different receptor cells sharing similar signaling pathways. Cell. 2003;112:293–301.

14. Talavera K. TRP Channels as Targets for Modulation of Taste Transduction. TRP Channels in Sensory Transduction. Cham: Springer International Publishing; 2015.

15. Marwaha L, Bansal Y, Singh R, Saroj P, Bhandari R, Kuhad A. TRP channels: potential drug target for neuropathic pain. Inflammopharmacology. 2016;24:305–17.

16. Julius D, Basbaum AI. Molecular mechanisms of nociception. Nature. 2001;413:203–10.

17. Caceres AI, Liu B, Jabba SV, Achanta S, Morris JB, Jordt S-E. Transient Receptor Potential Cation Channel Subfamily M Member 8 channels mediate the anti-inflammatory effects of eucalyptol. British Journal of Pharmacology. 2017;174:867–79.

18. Gouin O, L'Herondelle K, Lebonvallet N, Le Gall-Ianotto C, Sakka M, Buhé V, et al. TRPV1 and TRPA1 in cutaneous neurogenic and chronic inflammation: pro-inflammatory response induced by their activation and their sensitization. Protein Cell. 2017;8:644–61.

19. Abriel H, Syam N, Sottas V, Amarouch M-Y, Rougier J-S. TRPM4 channels in the cardiovascular system: Physiology, pathophysiology, and pharmacology. Biochemical Pharmacology. 2012;84:873–81.

20. Camacho-Londoño JE, Tian Q, Hammer K, Schröder L, Camacho Londoño J, Reil JC, et al. A background Ca^{2+} entry pathway mediated by TRPC1/TRPC4 is critical for development of pathological cardiac remodelling. European Heart Journal. 2015;36:2257–66.

21. Mathar I, Kecskes M, Van der Mieren G, Jacobs G, Camacho Londono JE, Uhl S, et al. Increased beta-adrenergic inotropy in ventricular myocardium from Trpm4-/- mice. Circulation Research. 2014;114:283–94.

22. Welsh DG, Morielli AD, Nelson MT, Brayden JE. Transient receptor potential channels regulate myogenic tone of resistance arteries. Circulation Research. 2002;90:248–50.

23. Kiselyov K, Chen J, Rbaibi Y, Oberdick D, Tjon-Kon-Sang S, Shcheynikov N, et al. TRP-ML1 is a lysosomal monovalent cation channel that undergoes proteolytic cleavage. Journal of Biological Chemistry. 2005;280:43218–23.

24. Dadon D, Minke B. Cellular functions of transient receptor potential channels. The International Journal of Biochemistry & Cell Biology. 2010;42:1430–45.

25. Alim I, Teves L, Li R, Mori Y, Tymianski M. Modulation of NMDAR subunit expression by TRPM2 channels regulates neuronal vulnerability to ischemic cell death. The Journal of Neuroscience. 2013;33:17264–77.

26. Manna PT, Munsey TS, Abuarab N, Li F, Asipu A, Howell G, et al. TRPM2-mediated intracellular Zn^{2+} release triggers pancreatic β-cell death. Biochemical Journal. 2015;466:537–46.

27. Minke B. The history of the Drosophila TRP channel: the birth of a new channel superfamily. Journal of Neurogenetics. 2010;24:216–33.

28. Duncan LM, Deeds J, Hunter J, Shao J, Holmgren LM, Woolf EA, et al. Down-regulation of the novel gene melastatin correlates with potential for melanoma metastasis. Cancer Research. 1998;58:1515–20.

29. Clapham DE. International Union of Pharmacology. XLIX. Nomenclature and Structure-Function Relationships of Transient Receptor Potential Channels. Pharmacological Reviews. 2005;57:427–50.

30. Fleig A, Penner R. The TRPM ion channel subfamily: molecular, biophysical and functional features. Trends in Pharmacological Sciences. 2004;25:633–9.

31. Simon F, Varela D, Cabello-Verrugio C. Oxidative stress-modulated TRPM ion channels in cell dysfunction and pathological conditions in humans. Cellular Signalling. 2013;25:1614–24.

32. Nilius B, Szallasi A. Transient receptor potential channels as drug targets: from the science of basic research to the art of medicine. Pharmacological Reviews. 2014;66:676–814.

33. Ceylan GG, Önalan EE, Kuloğlu T, Aydoğ G, Keleş İ, Tonyali Ş, et al. Potential role of melastatin-related transient receptor potential cation channel subfamily M gene expression in the pathogenesis of urinary bladder cancer. Oncology Letters. 2016;12:5235–9.

34. Song K, Wang H, Kamm GB, Pohle J, Reis F de C, Heppenstall P, et al. The TRPM2 channel is a hypothalamic heat sensor that limits fever and can drive hypothermia. Science. 2016;353:1393–8.

35. Uchida K, Demirkhanyan L, Asuthkar S, Cohen A, Tominaga M, Zakharian E. Stimulation-dependent gating of TRPM3 channel in planar lipid bilayers. FASEB Journal. 2016;30:1306–16.

36. Venkatachalam K, Montell C. TRP channels. Annual Review of Biochemistry. 2007;76:387–417.

37. Nilius B, Prenen J, Droogmans G, Voets T, Vennekens R, Freichel M, et al. Voltage dependence of the Ca2+-activated cation channel TRPM4. Journal of Biological Chemistry. 2003;278:30813–20.

38. Mathar I, Jacobs G, Kecskés M, Menigoz A, Philippaert K, Vennekens R. TRPM4. Handbook of experimental pharmacology. 2014;222:461–87.

39. Constantine M, Liew CK, Lo V, Macmillan A, Cranfield CG, Sunde M, et al. Heterologously-expressed and Liposome-reconstituted Human Transient Receptor Potential Melastatin 4 Channel (TRPM4) is a Functional Tetramer. Scientific Reports. 2016;6:19352–62.

40. Nilius B, Prenen J, Tang J, Wang C, Owsianik G, Janssens A, et al. Regulation of the Ca^{2+} Sensitivity of the Nonselective Cation Channel TRPM4. Journal of Biological Chemistry. 2005;280:6423–33.

41. Nilius B, Mahieu F, Prenen J, Janssens A, Owsianik G, Vennekens R, et al. The

Ca^{2+}-activated cation channel TRPM4 is regulated by phosphatidylinositol 4,5-biphosphate. EMBO Journal. 2006;25:467–78.

42. Hendriks G, Koudijs M, van Balkom BWM, Oorschot V, Klumperman J, Deen PMT, et al. Glycosylation is important for cell surface expression of the water channel aquaporin-2 but is not essential for tetramerization in the endoplasmic reticulum. Journal of Biological Chemistry. 2004;279:2975–83.

43. Petrecca K, Atanasiu R, Akhavan A, Shrier A. N-linked glycosylation sites determine HERG channel surface membrane expression. Journal of Physiology. 2004;515:41–8.

44. Much B, Wahl-Schott C, Zong X, Schneider A, Baumann L, Moosmang S, et al. Role of subunit heteromerization and N-linked glycosylation in the formation of functional hyperpolarization-activated cyclic nucleotide-gated channels. Journal of Biological Chemistry. 2003;278:43781–6.

45. Syam N, Rougier J-S, Abriel H. Glycosylation of TRPM4 and TRPM5 channels: molecular determinants and functional aspects. Frontiers in Cellular Neuroscience. 2014;8:52.

46. Woo SK, Kwon MS, Ivanov A, Geng Z, Gerzanich V, Simard JM. Complex N-glycosylation stabilizes surface expression of transient receptor potential melastatin 4b protein. Journal of Biological Chemistry. 2013;288:36409–17.

47. Levitan IB. Modulation of ion channels by protein phosphorylation and dephosphorylation. Annual Review of Physiology. 1994;56:193–212.

48. Cerda O, Cáceres M, Park K-S, Leiva-Salcedo E, Romero A, Varela D, et al. Casein kinase-mediated phosphorylation of serine 839 is necessary for basolateral localization of the Ca^{2+}-activated non-selective cation channel TRPM4. Pflügers Archiv - European Journal of Physiology. 2015;467:1723–32.

49. Crnich R, Amberg GC, Leo MD, Gonzales AL, Tamkun MM, Jaggar JH, et al. Vasoconstriction resulting from dynamic membrane trafficking of TRPM4 in vascular smooth muscle cells. American Journal of Physiology-Cell Physiology. 2010;299:C682–94.

50. Shigeto M, Ramracheya R, Tarasov AI, Cha CY, Chibalina MV, Hastoy B, et al. GLP-1 stimulates insulin secretion by PKC-dependent TRPM4 and TRPM5 activation. Journal of Clinical Investigation. 2015;125:4714–28.

51. Zhang Z, Okawa H, Wang Y, Liman ER. Phosphatidylinositol 4,5-bisphosphate rescues TRPM4 channels from desensitization. Journal of Biological Chemistry. 2005;280:39185–92.

52. Bousova K, Jirku M, Bumba L, Bednarova L, Sulc M, Franek M, et al. PIP2 and PIP3 interact with N-terminus region of TRPM4 channel. Biophysical Chemistry. 2015;205:24–32.

53. Park J-Y, Hwang EM, Yarishkin O, Seo J-H, Kim E, Yoo J, et al. TRPM4b channel suppresses store-operated Ca2+ entry by a novel protein–protein interaction with the TRPC3 channel. Biochemical and Biophysical Research Communications.

2008;368:677–83.

54. Sala-Rabanal M, Wang S, Nichols CG. On potential interactions between non-selective cation channel TRPM4 and sulfonylurea receptor SUR1. Journal of Biological Chemistry. 2012;287:8746–56.

55. Woo SK, Kwon MS, Ivanov A, Gerzanich V, Simard JM. The sulfonylurea receptor 1 (Sur1)-transient receptor potential melastatin 4 (Trpm4) channel. Journal of Biological Chemistry. 2013;288:3655–67.

56. Launay P, Fleig A, Perraud A-L, Scharenberg AM, Penner R, Kinet J-P. TRPM4 is a Ca2+-activated nonselective cation channel mediating cell membrane depolarization. Cell. 2002;109:397–407.

57. Murakami M, Xu F, Miyoshi I, Sato E, Ono K, Iijima T. Identification and characterization of the murine TRPM4 channel. Biochemical and Biophysical Research Communications. 2003;307:522–8.

58. Jang Y, Lee Y, Kim SM, Yang YD, Jung J, Oh U. Quantitative analysis of TRP channel genes in mouse organs. Archives of Pharmacal Research. 2012;35:1823–30.

59. Kruse M, Schulze-Bahr E, Corfield V, Beckmann A, Stallmeyer B, Kurtbay G, et al. Impaired endocytosis of the ion channel TRPM4 is associated with human progressive familial heart block type I. Journal of Clinical Investigation. 2009;119:2737–44.

60. Guinamard R, Chatelier A, Demion M, Potreau D, Patri S, Rahmati M, et al. Functional characterization of a Ca(2+)-activated non-selective cation channel in human atrial cardiomyocytes. Journal of Physiology. 2004;558:75–83.

61. Liu H, Zein El L, Kruse M, Guinamard R, Beckmann A, Bozio A, et al. Gain-of-function mutations in TRPM4 cause autosomal dominant isolated cardiac conduction disease. Circulation Cardiovascular Genetics. 2010;3:374–85.

62. Demion M, Bois P, Launay P, Guinamard R. TRPM4, a Ca2+-activated nonselective cation channel in mouse sino-atrial node cells. Cardiovascular Research. 2007;73:531–8.

63. Little SC, Mohler PJ. TRPM4 modulates sinus node diastolic depolarization. Heart Rhythm. 2013;10:1690–1.

64. DiFrancesco D. The role of the funny current in pacemaker activity. Circulation Research. 2010;106:434–46.

65. Monfredi O, Maltsev VA, Lakatta EG. Modern concepts concerning the origin of the heartbeat. Physiology. 2013;28:74–92.

66. Hof T, Simard C, Rouet R, Sallé L, Guinamard R. Implication of the TRPM4 nonselective cation channel in mammalian sinus rhythm. Heart Rhythm. 2013;10:1683–9.

67. Simard C, Hof T, Keddache Z, Launay P, Guinamard R. The TRPM4 non-selective cation channel contributes to the mammalian atrial action potential. Journal of Molecular

and Cellular Cardiology. 2013;59:11–9.

68. Demion M, Thireau J, Gueffier M, Finan A, Khoueiry Z, Cassan C, et al. Trpm4 Gene Invalidation Leads to Cardiac Hypertrophy and Electrophysiological Alterations. Bondarenko VE, editor. PLOS One. 2014;9:e115256–28.

69. Colquhoun D, Neher E, Reuter H, Stevens CF. Inward current channels activated by intracellular Ca in cultured cardiac cells. Nature. 1981;294:752–4.

70. Guinamard R, Demion M, Magaud C, Potreau D, Bois P. Functional expression of the TRPM4 cationic current in ventricular cardiomyocytes from spontaneously hypertensive rats. Hypertension. 2006;48:587–94.

71. Son M-J, Kim J-C, Kim SW, Chidipi B, Muniyandi J, Singh TD, et al. Shear stress activates monovalent cation channel transient receptor potential melastatin subfamily 4 in rat atrial myocytes via type 2 inositol 1,4,5-trisphosphate receptors and Ca^{2+} release. Journal of Physiology. 2016;594:2985–3004.

72. Hof T, Sallé L, Coulbault L, Richer R, Alexandre J, Rouet R, et al. TRPM4 non-selective cation channels influence action potentials in rabbit Purkinje fibres. Journal of Physiology. 2015;2:295–306.

73. Boukens BJ, Christoffels VM. Electrophysiological patterning of the heart. Pediatric Cardiology. 2012;33:900–6.

74. Michaëlsson M, Jonzon A, Riesenfeld T. Isolated congenital complete atrioventricular block in adult life. A prospective study. Circulation. 1995;92:442–9.

75. Vardas PE, Ovsyscher EI. Geographic differences of pacemaker implant rates in Europe. Journal of Cardiovascular Electrophysiology. 2002;13:S23–6.

76. Park DS, Fishman GI. The cardiac conduction system. Circulation. American Heart Association, 2011;123:904–15.

77. Ishikawa T, Tsuji Y, Makita N. Inherited bradyarrhythmia: A diverse genetic background. Journal of Arrhythmia. 2016;32:352–8.

78. Butters TD, Aslanidi OV, Inada S, Boyett MR, Hancox JC, Lei M, et al. Mechanistic links between Na+ channel (SCN5A) mutations and impaired cardiac pacemaking in sick sinus syndrome. American Heart Association, 2010;107:126–37.

79. Probst V, Kyndt F, Potet F, Trochu J-N, Mialet G, Demolombe S, et al. Haploinsufficiency in Combination With Aging Causes SCN5A-Linked Hereditary Lene`gre Disease. Journal of the American College of Cardiology. 2003;41:643–52.

80. Kyndt F, Probst V, Potet F, Demolombe S, Chevallier JC, Baro I, et al. Novel SCN5A mutation leading either to isolated cardiac conduction defect or Brugada syndrome in a large French family. Circulation. 2001;104:3081–6.

81. Rossenbacker T, Carroll SJ, Liu H, Kuipéri C, de Ravel TJL, Devriendt K, et al. Novel pore mutation in SCN5A manifests as a spectrum of phenotypes ranging from atrial flutter, conduction disease, and Brugada syndrome to sudden cardiac death. Heart

Rhythm. 2003;1:610–5.

82. Bezzina CR, Rook MB, Groenewegen WA, Herfst LJ, van der Wal AC, Lam J, et al. Compound Heterozygosity for Mutations (W156X and R225W) in SCN5AAssociated With Severe Cardiac Conduction Disturbances and Degenerative Changes in the Conduction System. Circulation Research. 2003;92:159–68.

83. Freyermuth F, Rau F, Kokunai Y, Linke T, Sellier C, Nakamori M, et al. Splicing misregulation of SCN5A contributes to cardiac-conduction delay and heart arrhythmia in myotonic dystrophy. Nature Communications. 2016;7:11067–80.

84. Isom LL. Sodium channel beta subunits: anything but auxiliary. The Neuroscientist. 2001;7:42–54.

85. Watanabe H, Koopmann TT, Le Scouarnec S, Yang T, Ingram CR, Schott J-J, et al. Sodium channel β1 subunit mutations associated with Brugada syndrome and cardiac conduction disease in humans. Journal of Clinical Investigation. 2008;118:2260–8.

86. Girard C, Duprat F, Terrenoire C, Tinel N, Fosset M, Romey G, et al. Genomic and functional characteristics of novel human pancreatic 2P domain K^+ channels. Biochemical and Biophysical Research Communications. 2001;282:249–56.

87. Morton MJ, Abohamed A, Sivaprasadarao A, Hunter M. pH sensing in the two-pore domain K^+ channel, TASK2. Proceedings of the National Academy of Sciences. 2005;102:16102–6.

88. Friedrich C, Rinné S, Zumhagen S, Kiper AK, Silbernagel N, Netter MF, et al. Gain-of-function mutation in TASK-4 channels and severe cardiac conduction disorder. EMBO Molecular Medicine. 2014;6:937–51.

89. Claycomb WC, Lanson NA, Stallworth BS, Egeland DB, Delcarpio JB, Bahinski A, et al. HL-1 cells: A cardiac muscle cell line that contracts and retains phenotypic characteristics of the adult cardiomyocyte. Proceedings of the National Academy of Sciences. National Academy of Sciences; 1998;95:2979–84.

90. Brink PA, Ferreira A, Moolman JC, Weymar HW, van der Merwe PL, Corfield VA. Gene for progressive familial heart block type I maps to chromosome 19q13. Circulation. 1995;91:1633–40.

91. Brink AJ, Torrington M. Progressive familial heart block--two types. South African Medical Journal. 1977;52:53–9.

92. Daumy X, Amarouch M-Y, Lindenbaum P, Bonnaud S, Charpentier E, Bianchi B, et al. Targeted resequencing identifies TRPM4 as a major gene predisposing to progressive familial heart block type I. International Journal of Cardiology. 2016;207:349–58.

93. Syam N, Chatel S, Ozhathil LC, Sottas V, Rougier J-S, Baruteau A, et al. Variants of Transient Receptor Potential Melastatin Member 4 in Childhood Atrioventricular Block. Journal of the American Heart Association. 2016;5.

94. Stallmeyer B, Zumhagen S, Denjoy I, Duthoit G, Hébert J-L, Ferrer X, et al.

Mutational spectrum in the Ca^{2+}-activated cation channel gene TRPM4 in patients with cardiac conductance disturbances. Human Mutation. 2012;33:109–17.

95. Kapplinger JD, Tester DJ, Alders M, Benito B, Berthet M, Brugada J, et al. An international compendium of mutations in the SCN5A-encoded cardiac sodium channel in patients referred for Brugada syndrome genetic testing. Heart Rhythm. 2010;7:33–46.

96. Burashnikov E, Pfeiffer R, Barajas-Martinez H, Delpón E, Hu D, Desai M, et al. Mutations in the cardiac L-type calcium channel associated with inherited J-wave syndromes and sudden cardiac death. Heart Rhythm. 2010;7:1872–82.

97. Giudicessi JR, Ye D, Tester DJ, Crotti L, Mugione A, Nesterenko VV, et al. Transient outward current (I_{to}) gain-of-function mutations in the KCND3-encoded Kv4.3 potassium channel and Brugada syndrome. Heart Rhythm. 2011;8:1024–32.

98. Riuró H, Beltrán-Álvarez P, Tarradas A, Selga E, Campuzano O, Vergés M, et al. A missense mutation in the sodium channel β2 subunit reveals SCN2B as a new candidate gene for Brugada syndrome. Human Mutation. 2013;34:961–6.

99. Liu H, Chatel S, Simard C, Syam N, Sallé L, Probst V, et al. Molecular genetics and functional anomalies in a series of 248 Brugada cases with 11 mutations in the TRPM4 channel. Aalto-Setala K, editor. PLOS One. 2013;8:54131–41.

100. Putney JW. Physiological mechanisms of TRPC activation. Pflügers Archiv - European Journal of Physiology. 2005;451:29–34.

101. Vannier B, Peyton M, Boulay G, Brown D, Qin N, Jiang M, et al. Mouse trp2, the homologue of the human trpc2 pseudogene, encodes mTrp2, a store depletion-activated capacitative Ca2+ entry channel. Proceedings of the National Academy of Sciences. 1999;96:2060–4.

102. Liman ER, Corey DP, Dulac C. TRP2: a candidate transduction channel for mammalian pheromone sensory signaling. Proceedings of the National Academy of Sciences. 1999;96:5791–6.

103. Hofmann T, Schaefer M, Schultz G, Gudermann T. Transient receptor potential channels as molecular substrates of receptor-mediated cation entry. Journal of Molecular Medicine. 2000;78:14–25.

104. Zitt C, Zobel A, Obukhov AG, Harteneck C, Kalkbrenner F, Lückhoff A, et al. Cloning and functional expression of a human Ca^{2+}-permeable cation channel activated by calcium store depletion. Neuron. 1996;16:1189–96.

105. Wes PD, Chevesich J, Jeromin A, Rosenberg C, Stetten G, Montell C. TRPC1, a human homolog of a Drosophila store-operated channel. Proceedings of the National Academy of Sciences. 1995;92:9652–6.

106. Singh BB, Liu X, Tang J, Zhu MX, Ambudkar IS. Calmodulin regulates Ca^{2+}-dependent feedback inhibition of store-operated Ca^{2+} influx by interaction with a site in the C terminus of TrpC1. Molecular Cell. 2002;9:739–50.

107. Ambudkar IS, de Souza LB, Ong HL. TRPC1, Orai1, and STIM1 in SOCE: Friends

in tight spaces. Cell Calcium. 2016;63:33–9.

108. Barrera NP, Shaifta Y, McFadzean I, Ward JP, Henderson RM, Edwardson JM. AFM imaging reveals the tetrameric structure of the TRPC1 channel. Biochemical and Biophysical Research Communications. 2007;358:1086–90.

109. Engelke M, Friedrich O, Budde P, Schäfer C, Niemann U, Zitt C, et al. Structural domains required for channel function of the mouse transient receptor potential protein homologue TRP1beta. FEBS Letters. 2002;523:193–9.

110. Storch U, Forst AL, Philipp M, Gudermann T, Schnitzler MMY. Transient Receptor Potential Channel 1 (TRPC1) Reduces Calcium Permeability in Heteromeric Channel Complexes. Journal of Biological Chemistry. 2012;287:3530–40.

111. Liu X, Singh BB, Ambudkar IS. TRPC1 is required for functional store-operated Ca^{2+} channels. Journal of Biological Chemistry. 2003;278:11337–43.

112. Beech DJ, Xu SZ, McHugh D, Flemming R. TRPC1 store-operated cationic channel subunit. Cell Calcium. 2003;33:433–40.

113. Hoth M, Penner R. Depletion of intracellular calcium stores activates a calcium current in mast cells. Nature. 1992;355:353–6.

114. Prakriya M, Feske S, Gwack Y, Srikanth S, Rao A, Hogan PG. Orai1 is an essential pore subunit of the CRAC channel. Nature. 2006;443:230–3.

115. Roos J, DiGregorio PJ, Yeromin AV, Ohlsen K, Lioudyno M, Zhang S, et al. STIM1, an essential and conserved component of store-operated Ca^{2+} channel function. The Journal of Cell Biology. 2005;169:435–45.

116. Hogan PG, Lewis RS, Rao A. Molecular basis of calcium signaling in lymphocytes: STIM and ORAI. Annual Review of Immunology. 2010;28:491–533.

117. Cheng KT, Liu X, Ong HL, Ambudkar IS. Functional requirement for Orai1 in store-operated TRPC1-STIM1 channels. Journal of Biological Chemistry. 2008;283:12935–40.

118. Huang GN, Zeng W, Kim JY, Yuan JP, Han L, Muallem S, et al. STIM1 carboxyl-terminus activates native SOC, Icrac and TRPC1 channels. Nature Cell Biology. 2006;8:1003–10.

119. Kim MS, Zeng W, Yuan JP, Shin DM, Worley PF, Muallem S. Native Store-operated Ca2+ Influx Requires the Channel Function of Orai1 and TRPC1. Journal of Biological Chemistry. 2009;284:9733–41.

120. Ong HL, Cheng KT, Liu X, Bandyopadhyay BC, Paria BC, Soboloff J, et al. Dynamic assembly of TRPC1-STIM1-Orai1 ternary complex is involved in store-operated calcium influx. Evidence for similarities in store-operated and calcium release-activated calcium channel components. Journal of Biological Chemistry. 2007;282:9105–16.

121. Schindl R, Fritsch R, Jardin I, Frischauf I, Kahr H, Muik M, et al. Canonical

Transient Receptor Potential (TRPC) 1 Acts as a Negative Regulator for Vanilloid TRPV6-mediated Ca^{2+} Influx. Journal of Biological Chemistry. 2012;287:35612–20.

122. Du J, Ma X, Shen B, Huang Y, Birnbaumer L, Yao X. TRPV4, TRPC1, and TRPP2 assemble to form a flow-sensitive heteromeric channel. FASEB Journal. 2014;28:4677–85.

123. Bai C-X, Giamarchi A, Rodat-Despoix L, Padilla F, Downs T, Tsiokas L, et al. Formation of a new receptor-operated channel by heteromeric assembly of TRPP2 and TRPC1 subunits. EMBO Reports. 2008;9:472–9.

124. Strubing C, Krapivinsky G, Krapivinsky L, Clapham DE. TRPC1 and TRPC5 form a novel cation channel in mammalian brain. Neuron. 2001;29:645–55.

125. Kim J, Kwak M, Jeon JP, Myeong J, Wie J, Hong C, et al. Isoform- and receptor-specific channel property of canonical transient receptor potential (TRPC)1/4 channels. Pflügers Archiv - European Journal of Physiology. 2014;466:491–504.

126. Chen J, Crossland RF, Noorani MMZ, Marrelli SP. Inhibition of TRPC1/TRPC3 by PKG contributes to NO-mediated vasorelaxation. American journal of physiology-Heart and circulatory physiology. 2009;297:H417–24.

127. Maroto R, Raso A, Wood TG, Kurosky A, Martinac B, Hamill OP. TRPC1 forms the stretch-activated cation channel in vertebrate cells. Nature Cell Biology. 2005;7:179–85.

128. Kerstein PC, Jacques-Fricke BT, Rengifo J, Mogen BJ, Williams JC, Gottlieb PA, et al. Mechanosensitive TRPC1 channels promote calpain proteolysis of talin to regulate spinal axon outgrowth. The Journal of Neuroscience. 2013;33:273–85.

129. Fabian A, Bertrand J, Lindemann O, Pap T, Schwab A. Transient receptor potential canonical channel 1 impacts on mechanosignaling during cell migration. Pflügers Archiv - European Journal of Physiology. 2012;464:623–30.

130. Ohba T, Watanabe H, Murakami M, Takahashi Y, Iino K, Kuromitsu S, et al. Upregulation of TRPC1 in the development of cardiac hypertrophy. Journal of Molecular and Cellular Cardiology. 2007;42:498–507.

131. Seth M, Zhang ZS, Mao L, Graham V, Burch J, Stiber J, et al. TRPC1 channels are critical for hypertrophic signaling in the heart. Circulation Research. 2009;105:1023–30.

132. Wu X, Eder P, Chang B, Molkentin JD. TRPC channels are necessary mediators of pathologic cardiac hypertrophy. Proceedings of the National Academy of Sciences. 2010;107:7000–5.

133. Caiozzo VJ. Plasticity of skeletal muscle phenotype: mechanical consequences. Muscle Nerve. 2002;26:740–68.

134. Berbey C, Weiss N, Legrand C, Allard B. Transient Receptor Potential Canonical Type 1 (TRPC1) Operates as a Sarcoplasmic Reticulum Calcium Leak Channel in Skeletal Muscle. Journal of Biological Chemistry. 2009;284:36387–94.

135. Zanou N, Shapovalov G, Louis M, Tajeddine N, Gallo C, Van Schoor M, et al. Role

of TRPC1 channel in skeletal muscle function. American Journal of Physiology-Cell Physiology. 2010;298:C149–62.

136. Zanou N, Schakman O, Louis P, Ruegg UT, Dietrich A, Birnbaumer L, et al. Trpc1 ion channel modulates phosphatidylinositol 3-kinase/Akt pathway during myoblast differentiation and muscle regeneration. Journal of Biological Chemistry. 2012;287:14524–34.

137. Liu X, Cheng KT, Bandyopadhyay BC, Pani B, Dietrich A, Paria BC, et al. Attenuation of store-operated Ca2+ current impairs salivary gland fluid secretion in TRPC1(-/-) mice. Proceedings of the National Academy of Sciences. National Acad Sciences; 2007;104:17542–7.

138. Sun Y, Birnbaumer L, Singh BB. TRPC1 regulates calcium-activated chloride channels in salivary gland cells. Journal of Cellular Physiology. 2015;230:2848–56.

139. Philipp S, Cavalie A, Freichel M, Wissenbach U, Zimmer S, Trost C, et al. A mammalian capacitative calcium entry channel homologous to Drosophila TRP and TRPL. EMBO Journal. European Molecular Biology Organization; 1996;15:6166–71.

140. McKay RR, Szymeczek-Seay CL, Lievremont JP, Bird GS, Zitt C, Jüngling E, et al. Cloning and expression of the human transient receptor potential 4 (TRP4) gene: localization and functional expression of human TRP4 and TRP3. Biochemical Journal. 2000;351(3):735–46.

141. Mizuno N, Kitayama S, Saishin Y, Shimada S, Morita K, Mitsuhata C, et al. Molecular cloning and characterization of rat trp homologues from brain. Molecular Brain Research. 1999;64:41–51.

142. Schaefer M, Plant TD, Stresow N, Albrecht N, Schultz G. Functional differences between TRPC4 splice variants. Journal of Biological Chemistry. 2002;277:3752–9.

143. Vazquez G, Wedel BJ, Aziz O, Trebak M, Putney JW. The mammalian TRPC cation channels. Biochimica et Biophysica Acta. 2004;1742:21–36.

144. Tang J, Lin Y, Zhang Z, Tikunova S, Birnbaumer L, Zhu MX. Identification of common binding sites for calmodulin and inositol 1,4,5-trisphosphate receptors on the carboxyl termini of trp channels. Journal of Biological Chemistry. 2001;276:21303–10.

145. Trost C, Bergs C, Himmerkus N, Flockerzi V. The transient receptor potential, TRP4, cation channel is a novel member of the family of calmodulin binding proteins. Biochemical Journal. 2001;355:663–70.

146. Mery L, Magnino F, Schmidt K, Krause KH, Dufour JF. Alternative splice variants of hTrp4 differentially interact with the C-terminal portion of the inositol 1,4,5-trisphosphate receptors. FEBS Letters. 2001;487:377–83.

147. Mery L, Strauss B, Dufour JF, Krause KH, Hoth M. The PDZ-interacting domain of TRPC4 controls its localization and surface expression in HEK293 cells. Journal of Cell Science. 2002;115:3497–508.

148. Myeong J, Kwak M, Hong C, Jeon J-H, So I. Identification of a membrane-targeting

domain of the transient receptor potential canonical (TRPC)4 channel unrelated to its formation of a tetrameric structure. Journal of Biological Chemistry. 2014;289:34990–5002.

149. Schaefer M, Plant TD, Obukhov AG, Hofmann T, Gudermann T, Schultz G. Receptor-mediated regulation of the nonselective cation channels TRPC4 and TRPC5. Journal of Biological Chemistry. 2000;275:17517–26.

150. Hofmann T, Obukhov AG, Schaefer M, Harteneck C, Gudermann T, Schultz G. Direct activation of human TRPC6 and TRPC3 channels by diacylglycerol. Nature. 1999;397:259–63.

151. Lemonnier L, Trebak M, Putney JW Jr. Complex regulation of the TRPC3, 6 and 7 channel subfamily by diacylglycerol and phosphatidylinositol-4,5-bisphosphate. Cell Calcium. 2008;43:506–14.

152. Storch U, Forst A-L, Pardatscher F, Erdogmus S, Philipp M, Gregoritza M, et al. Dynamic NHERF interaction with TRPC4/5 proteins is required for channel gating by diacylglycerol. Proceedings of the National Academy of Sciences. 2017;114:E37–E46.

153. Otsuguro K-I, Tang J, Tang Y, Xiao R, Freichel M, Tsvilovskyy V, et al. Isoform-specific Inhibition of TRPC4 Channel by Phosphatidylinositol 4,5-Bisphosphate. Journal of Biological Chemistry. 2008;283:10026–36.

154. Lee KP, Jun JY, Chang I-Y, Suh S-H, So I, Kim KW. TRPC4 is an essential component of the nonselective cation channel activated by muscarinic stimulation in mouse visceral smooth muscle cells. Molecules and Cells. 2005;20:435–41.

155. Zhu MH, Lee YM, Jin N, So I, Kim KW. The Transient Receptor Potential Protein Homologue TRPC4/5 as a Candidate for the Nonselective Cationic Channel Activated by Muscarinic Stimulation in the Murine Stomach. Neurophysiology. 2003;35:302–7.

156. Jeon JP, Lee KP, Park EJ, Sung TS, Kim BJ, Jeon JH, et al. The specific activation of TRPC4 by Gi protein subtype. Biochemical and Biophysical Research Communications. 2008;377:538–43.

157. Jeon JP, Hong C, Park EJ, Jeon JH, Cho NH, Kim IG, et al. Selective G alpha(i) Subunits as Novel Direct Activators of Transient Receptor Potential Canonical (TRPC) 4 and TRPC5 Channels. Journal of Biological Chemistry. 2012;287:17029–39.

158. Miehe S, Bieberstein A, Arnould I, Ihdene O, Rütten H, Strübing C. The phospholipid-binding protein SESTD1 is a novel regulator of the transient receptor potential channels TRPC4 and TRPC5. Journal of Biological Chemistry. 2010;285:12426–34.

159. Thakur DP, Tian J-B, Jeon J, Xiong J, Huang Y, Flockerzi V, et al. Critical roles of Gi/o proteins and phospholipase C-δ1 in the activation of receptor-operated TRPC4 channels. Proceedings of the National Academy of Sciences. 2016;113:1092–7.

160. Freichel M, Suh SH, Pfeifer A, Schweig U, Trost C, Weissgerber P, et al. Lack of an endothelial store-operated Ca^{2+} current impairs agonist-dependent vasorelaxation in TRP4-/- mice. Nature Cell Biology. 2001;3:121–7.

161. Tiruppathi C, Freichel M, Vogel SM, Paria BC, Mehta D, Flockerzi V, et al. Impairment of store-operated Ca^{2+} entry in TRPC4(-/-) mice interferes with increase in lung microvascular permeability. Circulation Research. 2002;91:70–6.

162. Yuan JP, Zeng W, Huang GN, Worley PF, Muallem S. STIM1 heteromultimerizes TRPC channels to determine their function as store-operated channels. Nature Cell Biology. 2007;9:636–45.

163. Sours-Brothers S, Ding M, Graham S, Ma R. Interaction between TRPC1/TRPC4 assembly and STIM1 contributes to store-operated Ca^{2+} entry in mesangial cells. Experimental Biology and Medicine. 2009;234:673–82.

164. Abdullaev IF, Bisaillon JM, Potier M, Gonzalez JC, Motiani RK, Trebak M. Stim1 and Orai1 mediate CRAC currents and store-operated calcium entry important for endothelial cell proliferation. Circulation Research. 2008;103:1289–99.

165. Plant TD, Schaefer M. TRPC4 and TRPC5: receptor-operated Ca^{2+}-permeable nonselective cation channels. Cell Calcium. 2003;33:441–50.

166. Lee KP, Yuan JP, Hong JH, So I, Worley PF, Muallem S. An endoplasmic reticulum/plasma membrane junction: STIM1/Orai1/TRPCs. FEBS Letters. 2010;584:2022–7.

167. Wakabayashi I, Marumo M, Graziani A, Poteser M, Groschner K. TRPC4 expression determines sensitivity of the platelet-type capacitative Ca^{2+} entry channel to intracellular alkalosis. Platelets. 2006;17:454–61.

168. Lindsey SH, Tribe RM, Songu-Mize E. Cyclic stretch decreases TRPC4 protein and capacitative calcium entry in rat vascular smooth muscle cells. Life Sciences. 2008;83:29–34.

169. Fatherazi S, Presland RB, Belton CM, Goodwin P, Al-Qutub M, Trbic Z, et al. Evidence that TRPC4 supports the calcium selective I(CRAC)-like current in human gingival keratinocytes. Pflügers Archiv - European Journal of Physiology. 2007;453:879–89.

170. Wang X, Pluznick JL, Wei P, Padanilam BJ, Sansom SC. TRPC4 forms store-operated Ca^{2+} channels in mouse mesangial cells. Cell Physiology. 2004;287:C357–64.

171. Sundivakkam PC, Freichel M, Singh V, Yuan JP, Vogel SM, Flockerzi V, et al. The Ca(2+) sensor stromal interaction molecule 1 (STIM1) is necessary and sufficient for the store-operated Ca(2+) entry function of transient receptor potential canonical (TRPC) 1 and 4 channels in endothelial cells. Molecular Pharmacology. 2012;81:510–26.

172. Makarewich CA, Zhang H, Davis J, Correll RN, Trappanese DM, Hoffman NE, et al. Transient receptor potential channels contribute to pathological structural and functional remodeling after myocardial infarction. Circulation Research. 2014;115:567–80.

173. Alzoubi A, Almalouf P, Toba M, O'Neill K, Qian X, Francis M, et al. TRPC4 inactivation confers a survival benefit in severe pulmonary arterial hypertension. American Journal of Pathology. 2013;183:1779–88.

174. Francis M, Xu N, Zhou C, Stevens T. Transient Receptor Potential Channel 4 Encodes a Vascular Permeability Defect and High-Frequency Ca^{2+} Transients in Severe Pulmonary Arterial Hypertension. American Journal of Pathology. 2016;186:1701–9.

175. Phelan KD, Mock MM, Kretz O, Shwe UT, Kozhemyakin M, Greenfield LJ, et al. Heteromeric canonical transient receptor potential 1 and 4 channels play a critical role in epileptiform burst firing and seizure-induced neurodegeneration. Molecular Pharmacology. 2012;81:384–92.

176. Munsch T, Freichel M, Flockerzi V, Pape H-C. Contribution of transient receptor potential channels to the control of GABA release from dendrites. Proceedings of the National Academy of Sciences. 2003;100:16065–70.

177. Schindl R, Frischauf I, Kahr H, Fritsch R, Krenn M, Derndl A, et al. The first ankyrin-like repeat is the minimum indispensable key structure for functional assembly of homo- and heteromeric TRPC4/TRPC5 channels. Cell Calcium. 2008;43:260–9.

178. Hofmann T, Schaefer M, Schultz G, Gudermann T. Subunit composition of mammalian transient receptor potential channels in living cells. Proceedings of the National Academy of Sciences. 2002;99:7461–6.

179. Hofmann T, Schaefer M, Schultz G, Gudermann T. Subunit composition of mammalian transient receptor potential channels in living cells. Proceedings of the National Academy of Sciences. 2002;99:7461–6.

180. Strübing C, Krapivinsky G, Krapivinsky L, Clapham DE. Formation of novel TRPC channels by complex subunit interactions in embryonic brain. Journal of Biological Chemistry. 2003;278:39014–9.

181. Zagranichnaya TK, Wu X, Villereal ML. Endogenous TRPC1, TRPC3, and TRPC7 proteins combine to form native store-operated channels in HEK-293 cells. Journal of Biological Chemistry. 2005;280:29559–69.

182. Liu X, Bandyopadhyay BC, Singh BB, Groschner K, Ambudkar IS. Molecular analysis of a store-operated and 2-acetyl-sn-glycerol-sensitive non-selective cation channel. Heteromeric assembly of TRPC1-TRPC3. Journal of Biological Chemistry. 2005;280:21600–6.

183. Wang Y, Wang Y, Li G-R. TRPC1/TRPC3 channels mediate lysophosphatidylcholine-induced apoptosis in cultured human coronary artery smooth muscles cells. Oncotarget. 2016;7:50937–51.

184. Bröker-Lai J, Kollewe A, Schindeldecker B, Pohle J, Nguyen Chi V, Mathar I, et al. Heteromeric channels formed by TRPC1, TRPC4 and TRPC5 define hippocampal synaptic transmission and working memory. EMBO Journal. 2017;36:2770–89.

185. Ma X, Qiu S, Luo J, Ma Y, Ngai C-Y, Shen B, et al. Functional role of vanilloid transient receptor potential 4-canonical transient receptor potential 1 complex in flow-induced Ca^{2+} influx. Arteriosclerosis, Thrombosis, and Vascular Biology. 2010;30:851–8.

186. Courjaret R, Hubrack S, Daalis A, Dib M, Machaca K. The Xenopus TRPV6

homolog encodes a Mg^{2+}-permeant channel that is inhibited by interaction with TRPC1. Journal of Cellular Physiology. 2013;228:2386–98.

187. Kobori T, Smith GD, Sandford R, Edwardson JM. The transient receptor potential channels TRPP2 and TRPC1 form a heterotetramer with a 2:2 stoichiometry and an alternating subunit arrangement. Journal of Biological Chemistry. 2009;284:35507–13.

188. Poteser M, Graziani A, Rosker C, Eder P, Derler I, Kahr H, et al. TRPC3 and TRPC4 associate to form a redox-sensitive cation channel. Evidence for expression of native TRPC3-TRPC4 heteromeric channels in endothelial cells. Journal of Biological Chemistry. 2006;281:13588–95.

189. Álvarez-Miguel I, Cidad P, Pérez-García MT, López-López JR. Differences in TRPC3 and TRPC6 channels assembly in mesenteric vascular smooth muscle cells in essential hypertension. Journal of Physiology. 2017;595:1497–513.

190. Maruyama Y, Nakanishi Y, Walsh EJ, Wilson DP, Welsh DG, Cole WC. Heteromultimeric TRPC6-TRPC7 channels contribute to arginine vasopressin-induced cation current of A7r5 vascular smooth muscle cells. Circulation Research. 2006;98:1520–7.

191. Myeong J, Ko J, Hong C, Yang D, Lee KP, Jeon J-H, et al. The interaction domains of transient receptor potential canonical (TRPC)1/4 and TRPC1/5 heteromultimeric channels. Biochemical and Biophysical Research Communications. 2016;474:476–81.

192. Hof T, Liu H, Sallé L, Schott J-J, Ducreux C, Millat G, et al. TRPM4 non-selective cation channel variants in long QT syndrome. BMC Medical Genetics. 2017;18:31–9.

193. Cheng H, Lederer WJ, Cannell MB. Calcium sparks: elementary events underlying excitation-contraction coupling in heart muscle. Science. 1993;262:740–4.

194. Vennekens R, Olausson J, Meissner M, Bloch W, Mathar I, Philipp SE, et al. Increased IgE-dependent mast cell activation and anaphylactic responses in mice lacking the calcium-activated nonselective cation channel TRPM4. Nature immunology. 2007;8:312–20.

195. Ullrich ND, Voets T, Prenen J, Vennekens R, Talavera K, Droogmans G, et al. Comparison of functional properties of the Ca2+-activated cation channels TRPM4 and TRPM5 from mice. Cell Calcium. 2004;37:267–78.

196. Prawitt D, Monteilh-Zoller MK, Brixel L, Spangenberg C, Zabel B, Fleig A, et al. TRPM5 is a transient Ca2+-activated cation channel responding to rapid changes in [Ca2+]i. Proceedings of the National Academy of Sciences. 2003;100:15166–71.

197. Kaplan JH, Ellis-Davies GC. Photolabile chelators for the rapid photorelease of divalent cations. Proceedings of the National Academy of Sciences. 1988;85:6571–5.

198. Ellis-Davies GC, Kaplan JH. Nitrophenyl-EGTA, a photolabile chelator that selectively binds Ca2+ with high affinity and releases it rapidly upon photolysis. Proceedings of the National Academy of Sciences. 1994;91:187–91.

199. Lipp P, Lüscher C, Niggli E. Photolysis of caged compounds characterized by ratiometric confocal microscopy: a new approach to homogeneously control and measure the calcium concentration in cardiac myocytes. Cell Calcium. 1996;19:255–66.

200. Neher E, Zucker RS. Multiple calcium-dependent processes related to secretion in bovine chromaffin cells. Neuron. 1993;10:21–30.

201. Kirillova J, Thomas P, Almers W. Two independently regulated secretory pathways in mast cells. Journal of Physiology. 1993;87:203–8.

202. Burgalossi A, Jung S, Man K-NM, Nair R, Jockusch WJ, Wojcik SM, et al. Analysis of neurotransmitter release mechanisms by photolysis of caged Ca^{2+} in an autaptic neuron culture system. 2012;7:1351–65.

203. Lipp P, Niggli E, Niggli E. Fundamental calcium release events revealed by two-photon excitation photolysis of caged calcium in Guinea-pig cardiac myocytes. Journal of Physiology. 1998;508 (3):801–9.

204. Lipp P, Niggli E. Sodium current-induced calcium signals in isolated guinea-pig ventricular myocytes. Journal of Physiology. 1994;474:439–46.

205. Gomez AM, Schwaller B, Porzig H, Vassort G. Increased exchange current but normal $Ca2+$ transport via Na^{+}-Ca^{2+} exchange during cardiac hypertrophy after myocardial infarction. Circulation. 2002.

206. Xian W, Hui X, Tian Q, Wang H, Moretti A, Laugwitz K-L, et al. Aberrant Deactivation-Induced Gain of Function in TRPM4 Mutant Is Associated with Human Cardiac Conduction Block. Cell Reports. 2018;24:724–31.

207. Chen Z, Xian W, Bellin M, Dorn T, Tian Q, Goedel A, et al. Subtype-specific promoter-driven action potential imaging for precise disease modelling and drug testing in hiPSC-derived cardiomyocytes. European Heart Journal. 2017;38:292–301.

208. Hui X, Reither G, Kaestner L, Lipp P. Targeted activation of conventional and novel protein kinases C through differential translocation patterns. Molecular and Cellular Biology. 2014;34:2370–81.

209. Leitner MG, Michel N, Behrendt M, Dierich M, Dembla S, Wilke BU, et al. Direct modulation of TRPM4 and TRPM3 channels by the phospholipase C inhibitor U73122. British Journal of Pharmacology. 2016;173:2555–69.

210. Winkler PA, Huang Y, Sun W, Du J, Lü W. Electron cryo-microscopy structure of a human TRPM4 channel. Nature. 2017;552:200–4.

211. Guo J, She J, Zeng W, Chen Q, Bai X-C, Jiang Y. Structures of the calcium-activated, non-selective cation channel TRPM4. Nature. 2017;552:205–9.

212. Ramsey IS, Delling M, Clapham DE. An introduction to TRP channels. Annual Review of Physiology. 2006;68:619–47.

213. Clapham DE, Montell C, Schultz G, Julius D, International Union of Pharmacology. International Union of Pharmacology. XLIII. Compendium of voltage-gated ion channels:

transient receptor potential channels. Pharmacological Reviews. 2003;55:591–6.

214. Teng J, Loukin SH, Anishkin A, Kung C. L596-W733 bond between the start of the S4-S5 linker and the TRP box stabilizes the closed state of TRPV4 channel. Proceedings of the National Academy of Sciences. 2015;112:3386–91.

215. Rohacs T, Lopes CMB, Michailidis I, Logothetis DE. PI(4,5)P2 regulates the activation and desensitization of TRPM8 channels through the TRP domain. Nature Neuroscience. 2005;8:626–34.

216. Autzen HE, Myasnikov AG, Campbell MG, Asarnow D, Julius D, Cheng Y. Structure of the human TRPM4 ion channel in a lipid nanodisc. Science. 2018;359:228–32.

217. Rychkov G, Barritt GJ. TRPC1 Ca^{2+}-permeable channels in animal cells. Handbook of experimental pharmacology. Berlin, Heidelberg: Springer Berlin Heidelberg; 2007;179:23–52.

218. Cheng KT, Ong HL, Liu X, Ambudkar IS. Contribution and regulation of TRPC channels in store-operated Ca^{2+} entry. Current Topics in Membranes. Elsevier; 2013;71:149–79.

219. Alfonso S, Benito O, Alicia S, Angélica Z, Patricia G, Diana K, et al. Regulation of the cellular localization and function of human transient receptor potential channel 1 by other members of the TRPC family. Cell Calcium. 2008;43:375–87.

220. FAST V. Simultaneous optical imaging of membrane potential and intracellular calcium. 2005;38:107–12.

221. Fast VG, Cheek ER, Pollard AE, Ideker RE. Effects of electrical shocks on Cai2+ and Vm in myocyte cultures. Circulation Research. 2004;94:1589–97.

222. Sobie EA, Kao JP, Lederer WJ. Novel approach to real-time flash photolysis and confocal Ca^{2+} imaging. Pflügers Archiv - European Journal of Physiology. 2007;454:663–73.

223. Bootman MD, Rietdorf K, Collins T, Walker S, Sanderson M. Ca^{2+}-Sensitive Fluorescent Dyes and Intracellular Ca^{2+} Imaging. Cold Spring Harbor Protocols 2013;3:83–99.

224. Cheng H, Beck A, Launay P, Gross SA, Stokes AJ, Kinet J-P, et al. TRPM4 controls insulin secretion in pancreatic beta-cells. Cell Calcium. 2007;41:51–61.

225. Hirschler-Laszkiewicz I, Tong Q, Waybill K, Conrad K, Keefer K, Zhang W, et al. The transient receptor potential (TRP) channel TRPC3 TRP domain and AMP-activated protein kinase binding site are required for TRPC3 activation by erythropoietin. Journal of Biological Chemistry. 2011;286:30636–46.

226. Gregorio-Teruel L, Valente P, Liu B, Fernández-Ballester G, Qin F, Ferrer-Montiel A. The Integrity of the TRP Domain Is Pivotal for Correct TRPV1 Channel Gating. Biophysical Journal. 2015;109:529–41.

227. García-Sanz N, Valente P, Gomis A, Fernández-Carvajal A, Fernández-Ballester G, Viana F, et al. A role of the transient receptor potential domain of vanilloid receptor I in channel gating. The Journal of Neuroscience. 2007;27:11641–50.

228. Yamaguchi S, Tanimoto A, Otsuguro K-I, Hibino H, Ito S. Negatively charged amino acids near and in transient receptor potential (TRP) domain of TRPM4 channel are one determinant of its Ca^{2+} sensitivity. Journal of Biological Chemistry. 2014;289:35265–82.

229. Kruse M, Pongs O. TRPM4 channels in the cardiovascular system. Current Opinion in Pharmacology. 2014;15:68–73.

230. Cao E, Liao M, Cheng Y, Julius D. TRPV1 structures in distinct conformations reveal activation mechanisms. Nature. 2013;504:113–8.

231. Gao Y, Cao E, Julius D, Cheng Y. TRPV1 structures in nanodiscs reveal mechanisms of ligand and lipid action. Nature. 2016;534:347–51.

232. Liao M, Cao E, Julius D, Cheng Y. Structure of the TRPV1 ion channel determined by electron cryo-microscopy. Nature. 2013;504:107–12.

233. Kruse M, Schulze-Bahr E, Corfield V, Beckmann A, Stallmeyer B, Kurtbay G, et al. Impaired endocytosis of the ion channel TRPM4 is associated with human progressive familial heart block type I. Journal of Clinical Investigation. 2009;119:2737–44.

234. Hartzell C, Putzier I, Arreola J. Calcium-activated chloride channels. Annual Review of Physiology. 2005;67:719–58.

235. Bao L, Kaldany C, Holmstrand EC, Cox DH. Mapping the BKCa channel's 'Ca^{2+} bowl': side-chains essential for Ca2+ sensing. The Journal of General Physiology. 2004;123:475–89.

236. Hofmann L, Wang H, Zheng W, Philipp SE, Hidalgo P, Cavalié A, et al. The S4––S5 linker – gearbox of TRP channel gating. Cell Calcium. 2017;67:156–65.

237. Brauchi S, Orta G, Mascayano C, Salazar M, Raddatz N, Urbina H, et al. Dissection of the components for PIP2 activation and thermosensation in TRP channels. Proceedings of the National Academy of Sciences. 2007;104:10246–51.

238. Voets T, Owsianik G, Janssens A, Talavera K, Nilius B. TRPM8 voltage sensor mutants reveal a mechanism for integrating thermal and chemical stimuli. Nature Chemical Biology. 2007;3:174–82.

239. Long SB, Tao X, Campbell EB, MacKinnon R. Atomic structure of a voltage-dependent K^{+} channel in a lipid membrane-like environment. Nature. 2007;450:376–82.

240. Grimm C, Cuajungco MP, van Aken AFJ, Schnee M, Jörs S, Kros CJ, et al. A helix-breaking mutation in TRPML3 leads to constitutive activity underlying deafness in the varitint-waddler mouse. Proceedings of the National Academy of Sciences. 2007;104:19583–8.

241. Lee KP, Nair AV, Grimm C, van Zeeland F, Heller S, Bindels RJM, et al. A helix-

breaking mutation in the epithelial Ca^{2+} channel TRPV5 leads to reduced Ca^{2+}-dependent inactivation. Cell Calcium. 2010;48:275–87.

242. Becker EBE, Oliver PL, Glitsch MD, Banks GT, Achilli F, Hardy A, et al. A point mutation in TRPC3 causes abnormal Purkinje cell development and cerebellar ataxia in moonwalker mice. Proceedings of the National Academy of Sciences. 2009;106:6706–11.

243. Asakawa M, Yoshioka T, Matsutani T, Hikita I, Suzuki M, Oshima I, et al. Association of a mutation in TRPV3 with defective hair growth in rodents. Journal of Investigative Dermatology. 2006;126:2664–72.

244. Zíma V, Witschas K, Hynkova A, Zímová L, Barvík I, Vlachova V. Structural modeling and patch-clamp analysis of pain-related mutation TRPA1-N855S reveal inter-subunit salt bridges stabilizing the channel open state. Neuropharmacology. 2015;93:294–307.

Appendix A: Publications

1.Wenying Xian, Xin Hui, Qinghai Tian, Alessandra Moretti, *et al.* Aberrant Deactivation-Induced Gain of Function in TRPM4 Mutant Is Associated with Human Cardiac Conduction Block. *Cell Reports*, 2018, *24*(3), 724–731.

2.Elisabeth Kaiser, Qinghai Tian, Michael Wagner, Monika Barth, Wenying Xian *et al*. DREADD technology reveals major impact of Gq signalling on cardiac electrophysiology. *Cardiovascular Research*, 2018

3.Zhifen Chen, Wenying Xian, Milena Bellin, *et al.*, Subtype-specific   promoter-driven action potential imaging for precise disease modelling and drug testing in hiPSC-derived cardiomyocytes. *European Heart Journal*, 2016, 38(4):292-301.

4.Lars Kaestner, Qinghai Tian, Elisabeth Kaiser, Wenying Xian, *et al*., Genetically Encoded Voltage Indicators in Circulation Research. *International Journal of Molecular Sciences*, 2015, 16(9):21626-21642.

Appendix B: Acknowledgment

I would like to express my special appreciation to my supervisor Prof. Dr. Peter Lipp. He is a tremendous mentor for me. He offered me this precious opportunity to be a PhD candidate in our lab. During my PhD study, he directly instructed my research work and gave me so many valuable suggestions. The encouragements from him inspired me a lot to get through the ups and downs in my studies. I also want to thank him for his generous time and efforts in my research articles and this dissertation. His patience, optimism, and cheerfulness impressed me and will energize me in my future academic carrier.

I would like to express my deep gratitude to Prof. Dr. Veit Flockerzi, I got the TRPC1 and TRPC4 plasmids and the HEK293 cell stably expressing M_2R or M_2R and TRPC4 channel from his lab. The human TRPM4^{wt} plasmid is also kindly provided by Prof. Dr. Veit Flockerzi. He is an expert of the TRP channels and offered me insightful advices about my TRP channel experiments.

I would like to thank Prof. Dr. Karl-Ludwig Laugwitz and Prof. Dr. Alessandra Moretti for providing the precious hiPS-CMs for my experiment and also offering me a great chance to learn the dissociation of hiPS-CMs in their lab.

I would like to thank Dr. Qinghai Tian, Dr. Xin Hui from my lab and Dr. Hongmei Wang from Prof. Dr. Veit Flockerzi's lab. They helped me a lot to finish this dissertation. Dr. Qinghai Tian and Dr. Xin Hui are two great teachers for me. Dr. Qinghai Tian taught me how to carry out the Ca^{2+} image experiments and also the data analysis with Matlab. Dr. Xin Hui guided me to learn the molecular cloning techniques. Besides, both of them offered me so many useful suggestions on the details of experiments and also guided me to become an independent scientist. Dr. Hongmei Wang's insights on the structure of TRPM4 proteins broaden my academic view. She helped me to generate a structural model to explain my electrophysiological results.

I am thankful for the assistance and friendships of all my dear lab mates. I would like to thank Dr. Lars Kaestner for his efforts to establish the set up for my UV-flash experiments. My appreciation also goes to Dr. Sandra Ruppenthal for her suggestions

on the molecular cloning. I deeply appreciated the generous help from the PhD candidates Katja Nitze and Julia Schweizer and Ms. Sabrina Henning. Especially in my first year in Germany, they helped me to get familiar with our lab as well as the experimental procedures in our lab and also helped me to handle some troubles in my daily life. I want to thank the PhD candidate Monika Barth for her help in my dissertation's writing. To Ms. Karin Schumacher and Ms. Cornelia Fess I feel grateful for their administrative supports and warm-hearted helps. To Ms Tanja Kuhn, I want to thank her for providing a lot support for my routine experiments, and also want to mention that jogging with her is a wonderful experience. To the PhD candidate Jia Guo, I want to thank him for his unselfish support and help during my experiments. Anyway, I want express my sincere gratitude to all my colleagues, some of them I did not mention above. They are all friendly and easy-going, without their constant support and help I couldn't have a comfortable and enjoyable life as a foreigner in Germany.

Besides I would like to thank all my lovely Chinese friends, with their companionships and supports, my life in Homburg becomes even easier and happier. Their comfort and kindness made me feeling less homesick and their successes and devotion in the academic research also inspired me to pursuit my own academic carrier.

Last but not least, I want to thank my family, especially my parents for their constant supports for my decisions. They raise me up and educate me to become a better person. They try their best to provide me good educational opportunities and never ask for any payback. From my hometown Chongqing to Nanjing, then from Nanjing to Homburg, I am more and more far away from them. Because of the long distance, I could not share the pressure they had to burden in their life, I might not take care of them when they were sick, but they never complained and always be supportive for my own desires. I am really grateful for all their supports, sacrifice and loving.